②

AD–A158 062

MODELING OF CONCRETE, SOIL, AND INTERFACES

Howard L. Schreyer

New Mexico Engineering Research Institute
University of New Mexico
Albuquerque, New Mexico 87131

June 1985

Final Report

Approved for public release; distribution unlimited.

DTIC
ELECTE
AUG 19 1985

S   D

B

AIR FORCE WEAPONS LABORATORY
Air Force Systems Command
Kirtland Air Force Base NM   87117-6008

85 · 8   15   020

This final report was prepared by the New Mexico Engineering Research Institute, University of New Mexico, Albuquerque, New Mexico, under Contract F29601-81-C-0013, Job Order 2302Y201 with the Air Force Weapons Laboratory, Kirtland Air Force Base, New Mexico. Dr Timothy J. Ross (NTES) was the Laboratory Project Officer-in-Charge.

When Government drawings, specifications, or other data are used for any purpose other than in connection with a definitely Government-related procurement, the United States Government incurs no responsibility or any obligation whatsoever. The fact that the Government may have formulated or in any way supplied the said drawings, specifications, or other data, is not to be regarded by implication, or otherwise in any manner construed as licensing the holder or any other person or corporation; or as conveying any rights or permission to manufacture, use or sell any patented invention that may in any way be related thereto.

This report has been authored by a contractor. Accordingly, the United States Government retains a nonexclusive, royalty-free license to publish or reproduce the material contained herein, or allow others to do so, for the United States Government purposes.

This report has been reviewed by the public Affairs Office and is releasable to the National Technical Information Services (NTIS). At NTIS, it will be available to the general public, including foreign nations.

If your address has changed, if you wish to be removed from our mailing list, or if your organization no longer employs the addressee, please notify AFWL/NTES, Kirtland AFB NM 87117-6008, to help us maintain a current mailing list.

This technical report has been reviewed and is approved for publication.
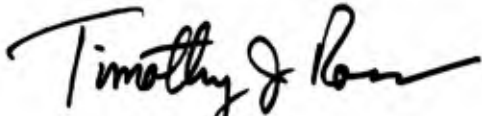
TIMOTHY J. ROSS
Project Officer

DAVID H. ARTMAN, JR
Major, USAF
Chief, Applications Branch

FOR THE COMMANDER
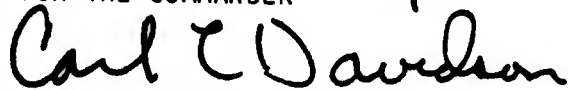
CARL L. DAVIDSON
Colonel, USAF
Chief, Civil Engineering Rsch Div

DO NOT RETURN COPIES OF THIS REPORT UNLESS CONTRACTUAL OBLIGATIONS OR NOTICE ON A SPECIFIC DOCUMENT REQUIRES THAT IT BE RETURNED.

REPORT DOCUMENTATION PAGE

1a. REPORT SECURITY CLASSIFICATION UNCLASSIFIED		1b. RESTRICTIVE MARKINGS		
2a. SECURITY CLASSIFICATION AUTHORITY		3. DISTRIBUTION/AVAILABILITY OF REPORT Approved for public release; distribution unlimited.		
2b. DECLASSIFICATION/DOWNGRADING SCHEDULE				
4. PERFORMING ORGANIZATION REPORT NUMBER(S) NMERI-8.13-TA8-80		5. MONITORING ORGANIZATION REPORT NUMBER(S) AFWL-TR-85-05		
6a. NAME OF PERFORMING ORGANIZATION New Mexico Engineering Research Institute	6b. OFFICE SYMBOL (If applicable)	7a. NAME OF MONITORING ORGANIZATION Air Force Weapons Laboratory		
6c. ADDRESS (City, State and ZIP Code) Box 25, University of New Mexico Albuquerque, New Mexico 87131		7b. ADDRESS (City, State and ZIP Code) Kirtland Air Force Base, New Mexico 87117		
8a. NAME OF FUNDING/SPONSORING ORGANIZATION	8b. OFFICE SYMBOL (If applicable)	9. PROCUREMENT INSTRUMENT IDENTIFICATION NUMBER F29601-81-C-0013		

8c. ADDRESS (City, State and ZIP Code)	10. SOURCE OF FUNDING NOS.			
	PROGRAM ELEMENT NO.	PROJECT NO.	TASK NO.	WORK UNIT NO.
11. TITLE (Include Security Classification) MODELING OF CONCRETE, SOIL, AND INTERFACES	61102F	2302	Y2	01

12. PERSONAL AUTHOR(S)
Howard L. Schreyer

13a. TYPE OF REPORT Final Report	13b. TIME COVERED FROM Nov 83 TO Oct 84	14. DATE OF REPORT (Yr., Mo., Day) 1985 June	15. PAGE COUNT 108

16. SUPPLEMENTARY NOTATION

Cont'd

17.	COSATI CODES		18. SUBJECT TERMS (Continue on reverse if necessary and identify by block number)
FIELD	GROUP	SUB. GR.	Viscoplasticity Strain Rate
11	02		Concrete Interface
08	07		Soils Strain Softening

19. ABSTRACT (Continue on reverse if necessary and identify by block number)

Experimental and theoretical developments on the modeling of concrete, soils, and interfaces are described. An improved relation for predicting the limit surface of concrete is given. The need for new devices and measurement techniques for rate effects in concrete and the response of unsaturated clay and silt is discussed. Preliminary data from existing experimental equipment are shown. The implications of strain softening are displayed with the use of a model problem.

Proposed work includes the use of a strain-softening model to represent interfaces, the extension of the viscoplastic model to represent anisotropic media, and the determination of rate effects in concrete for one- and two-dimensional experimental specimens.

20. DISTRIBUTION/AVAILABILITY OF ABSTRACT	21. ABSTRACT SECURITY CLASSIFICATION	
UNCLASSIFIED/UNLIMITED ☒ SAME AS RPT. ☐ OTIC USERS ☐	UNCLASSIFIED	
22a. NAME OF RESPONSIBLE INDIVIDUAL Dr Timothy J. Ross	22b. TELEPHONE NUMBER (Include Area Code) (505) 844-9087	22c. OFFICE SYMBOL NTES

DD FORM 1473, 83 APR   EDITION OF 1 JAN 73 IS OBSOLETE.

ACKNOWLEDGMENT

PREVIOUS PAGE
IS BLANK

CONTENTS

ILLUSTRATIONS

I. INTRODUCTION

The ability to predict the response of structures subjected to large, abrupt bursts of energy depends on a number of factors. These include load definition, the characteristics of the geological material in which the structure is embedded, the mechanism by which forces are transferred from the geological material to the structure, and the characteristics of the structure. The basic objective of the research project discussed here is to provide an improved understanding of the response of common geological and structural materials and of structure-media (concrete-soil) interfaces (SMI), to abrupt loading. For this purpose, engineering constitutive models have been developed, and appropriate experimental data are being used to validate the models.

A viscoplastic constitutive model for concrete and geological materials has continued to be used as the basis for investigations on the fundamental behavior of these materials. Although predictions of the limit stress are quite good for a wide range of materials, it has been observed that for mean pressures near zero, the results obtained for concrete were anomolous. To remedy this defect, the theory has been modified. The new form, which is described in Appendix A, appears to be general enough to include classical metal plasticity as one of the limiting cases. Although many details must still be investigated, the framework has been established for a constitutive equation that is relatively simple but much broader in scope than are existing constitutive relations.

For applications in which the complete energy-absorbing capabilities of materials are required, a model must also address postpeak behavior. If a material can display softening after the peak stress is reached in a structural element, then the softening will localize into a region that is small compared to the element. For a continuum, the region of localization will be a surface, a feature that is not observed experimentally. Instead, a band of softening is exhibited, and an additional feature must be incorporated into the constitutive equation to enable it to capture both the softening and the region of softening. One approach is to assume that the width of the band is known from the microstructure of the material. This procedure is described in Appendix B, which includes an application to reinforced concrete beams. An

alternative approach is given in Appendix C, where the stress is assumed to be a function of both strain and the gradient of strain. The resulting nonlocal constitutive relation is capable of predicting both softening and the zone of softening for a structural element.

A nonlocal constitutive relation with the ability to handle sharp gradients in strain may provide a convenient mechanism for modeling an interface between soil and concrete. The idea is proposed in somewhat more detail in Section II, with the suggestion that existing experimental data can be used for verification.

As described in Section III, experimental testing for rate effects in concrete has progressed beyond the conceptual stage to the point that a test device now exists. The initial suggestion that propellants might be suitable substances for providing forcing functions with short rise times appears to have been substantiated. Although the burning of propellants is not new, the use of propellants to provide a specific class of forcing functions in an enclosed environment requires some experimentation. In addition, the combination of high thermal and dynamic loads creates a need for the development of new instrumentation techniques. Meeting this need will be a major aspect of the research. Overall, the concept of rate-effect testing in concrete remains feasible.

Suction potential, which is a measure of the ability of fine-grained soils (silts, clays, and fine sands) to absorb water, may be a natural parameter for characterizing the strength and deformation behavior of these materials. To test the hypothesis, a small experimental program was initiated to obtain measures of suction potential and triaxial stress-strain data for unsaturated silts and clays, a class of geotechnical materials for which few data are available. As described in Section IV, two methods for measuring the suction potential were used, and the results were in good agreement. Consequently, the simpler of the two methods can now be used with confidence. The accuracy of the stress-strain data obtained from triaxial tests on cylindrical samples is another matter. Conventional methods relate the total force on the sample to the average strain, which is determined by dividing the axial shortening by the length of the specimen. Normally, lateral strains are not

measured; therefore, appropriate instrumentation had to be developed. Measurements based on photographs of the specimen at various stages of the loading process provided a means of obtaining lateral strain values. However, the lateral strain varied considerably with the longitudinal coordinate. This feature is merely a detailed display of the end effects that cause the barrel-shaped configuration commonly observed in cylindrical specimens. Because lateral strain varies considerably, it is highly probable that the longitudinal strain varies as well. To investigate this possibility, equally spaced staples were implanted along the specimen, and photographic measurements were made. The results indicate that a great deal of variation in longitudinal strain occurs. These improvements in measuring strain provide, for the first time, a means of obtaining stress-strain data that are suitable for the verification of constitutive models.

The primary focus for the continuation of this research project is summarized briefly in Section V. The effort will include the new approach to modeling soil-concrete interfaces, the continuation of experiments on rate effects in concrete, the possible incorporation of concepts from damage theory into the viscoplastic model, the theoretical study of unsaturated fine-grained soils, and the extension of the viscoplastic model to accommodate anisotropy.

II. INTERFACE MODELING

BACKGROUND

The use of computer-based techniques has spurred active research on the theoretical formulation of constitutive relations for the nonlinear response of materials. For interface or contact problems involving geological materials, such as problems dealing with soil-rock or soil-concrete interfaces, the available information is still sparse.

In the past, simple models based on Coulomb friction were commonly used in engineering and physics, and static tests were performed to determine friction coefficients for the SMI of interest. Experimental data indicate that these kinds of models may be inadequate. Because the friction phenomenon has not become a precise science, and much of its analytic description is based on empirical knowledge, the models for considering friction mechanisms cannot provide a satisfactory constitutive relation. Nevertheless, the simple friction approach has been used with either slide planes or thin finite elements to obtain a computational procedure.

This research is an attempt to find a new method for representing interface phenomena through the use of a nonlocal constitutive equation in which both theoretical and computational aspects are kept in mind. The idea used here is based on the observations that strain softening is accompanied by strain localization and that localization of deformation usually occurs adjacent to interface surfaces as illustrated in Figures 1 and 2. As Figure 1 shows, there is no unique stress-strain relation along a bar, even for a state of homogeneous stress. In fact, strain softening can occur anywhere, but a notch fixes the localization area at a given position. Similarly, the strain next to an interface is larger than the strain in other parts of the material. Thus, if strain softening and localization can be predicted simultaneously for a uniaxial stress specimen, the same model should also be suitable for representing interfaces. Adjusting constants in the model can provide the constitutive relation for interfaces at which two different types of materials meet.

4
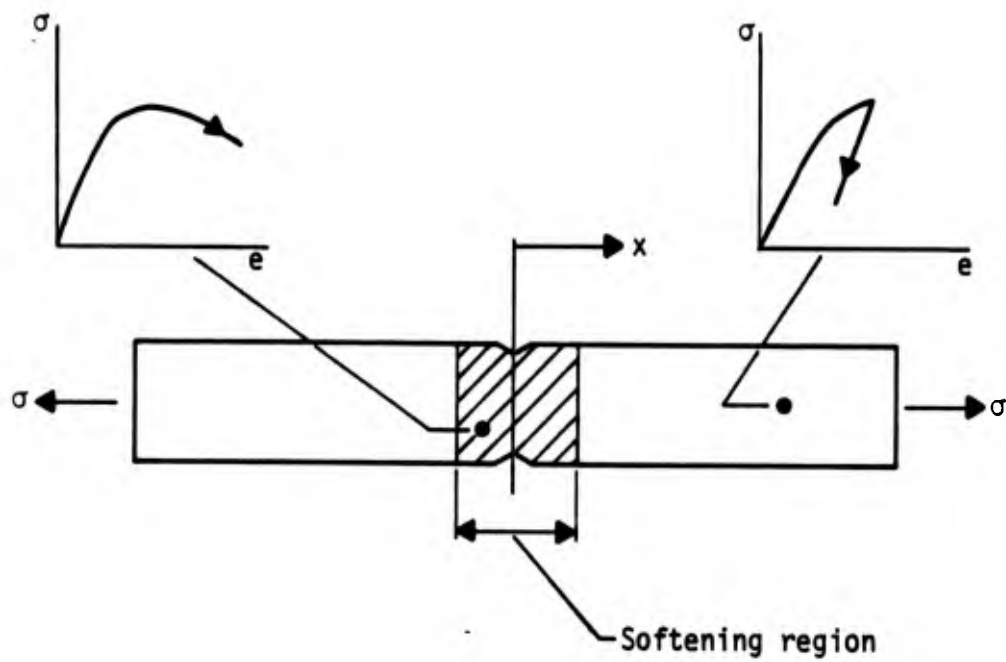
Figure 1.   Notched specimen under uniaxial stress.
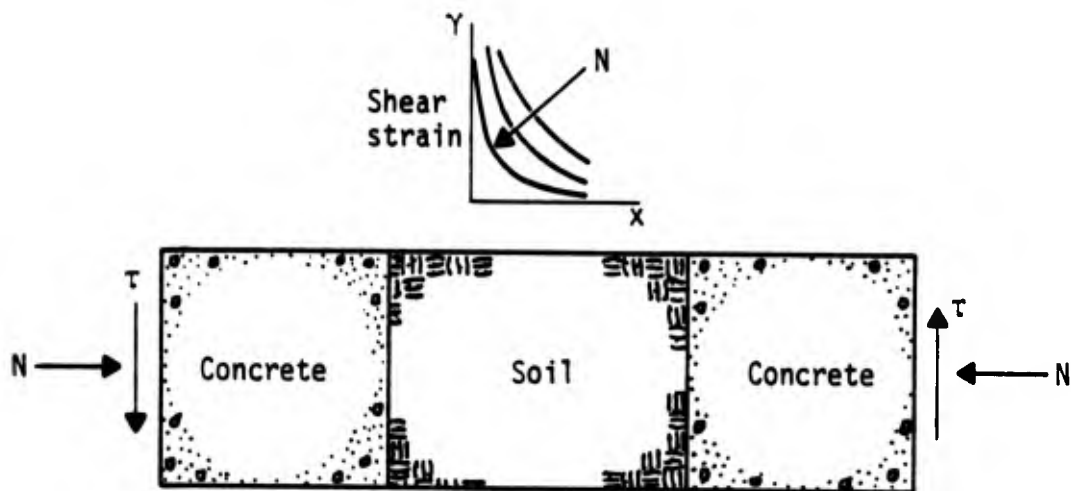
Figure 2.   Soil-concrete interface under pure shear.

LITERATURE REVIEW

Strain softening phenomena--Stief et al. (Ref. 1) studied the possibility
of strain localization into a shear band in the case of a metallic glass that
is modeled as a nonlinear viscoelastic solid. They derived an analytical
formula for the stress at localization in terms of physical parameters such as
the elastic shear modulus, initial free volume, and applied strain rate.
They point out that the weakening that initiates the shear band is due to the
stress concentration near microcracks when inhomogeneous flow occurs. As
a result, analytical expressions that predict values for stress at cata-
strophic softening agree closely with the values of stress at strain
localization calculated from the numerical solution of the full set of shear
band equations.

Li and Howard (Ref. 2) used the finite-element method to investigate the
growth of an initially spherical void embedded in a cylinder of elastic-
plastic material. The effects of various mean tensile stresses, equivalent
strains, and initial void volume fractions were included. Also studied were
void growth with and without softening, the effect of mean stress, and strain
softening. This study provides a logical connection between the macro- and
microresponse of the material, i.e., between the average response of a consti-
tutive model and the pointwise variables of a material.

Bazant and Oh (Ref. 3) studied several aspects of strain localization
including instability, ductility, and the size effect of concrete structures.
A finite-element crack band model, in which cracking was assumed to be uni-
formly distributed throughout the finite element, was set up, and the material
was described by a three-dimensional constitutive relation with tensile
strain-softening. Recently, the previously derived size effect law for blunt
fracture was exploited to determine the parameters of this finite-element
crack band model (Ref. 4). However, the assumed bilinear stress-strain rela-
tion is valid only for a certain element size, which corresponds to the repre-
sentative volume of the heterogeneous material, and to a certain width of the
cracking front. If a different element size must be used, the stress-strain
relation must be adjusted. Although so-called nonlinear, nonlocal material
models have been applied in finite-element analyses of dynamic failures caused
by strain softening, computer results indicate that these models are highly

6

susceptible to various instabilities, not only in the strain softening range but also in the elastic range. Bazant and Chang (Ref. 5) have addressed this problem in some detail.

Gopalaratnam and Shah (Ref. 6) have developed an analytical expression to describe the entire tensile response of concrete, i.e., a stress-displacement relation, by assuming a unique relationship between average stress and average crack wigth. Their tests showed that because of the localized nature of the postpeak deformations, no unique stress-strain relationship exists. The experimental results they obtained for the distribution of strain will be considered in the SMI research discussed in this section.

<u>Interface phenomena</u>--Huck et al. (Ref. 7) used a shear-loading computational code to research the static and dynamic responses of sand-concrete and clay-concrete interfaces under shear with high pressures. The analytical model is based on a frictional mechanism. They also obtained experimental data on shear stress-shear strain relations for the same types of interfaces.

De Beer (Ref. 8) has pointed out that the shearing strength of sand is a sensitive function of the density and varies with the mean normal pressure. It is expected that a similar phenomenon holds at interfaces.

Vermeer (Ref. 9) summarized several approaches for handling interfaces between granular materials and metal walls by considering the two friction angles associated with the powder and the interface, respectively. The first approach, that of using a nonassociated constitutive model and a fine mesh near the interface, showed that a thin shear band can develop. The second approach is to use special, thin interface elements, which are given a fictitious thickness. The slipping motion along the wall of a die can then be modeled. The third approach is to implement directly the frictional sliding as a mixed boundary condition. Vermeer also compared theoretical and experimental results for normal and shear stress distributions for a powder compaction apparatus. The comparison is qualitatively reasonable, but on a quantitative basis it is not satisfactory.

OUTLINE OF PROPOSED THEORY

It has been suggested that heterogeneous materials may be modeled by a nonlocal constitutive relation, where the stress at a certain point is a function of the strain and of the strain distribution over a certain representative volume of the material centered at that point. As is shown in Appendix C, one of the simplest forms for such a model, in which the effect of strains in the vicinity of a point may be captured, is based on the assumption that stress depends on both strain and strain gradients.

From the experimental data, it can be concluded that in the postpeak softening regime there is no unique stress-strain relationship and that failure localizes into a small region, the length of which varies with different materials for a given strain rate. On the other hand, it has been found that the interface of soil and concrete often initiates failure, which implies that the strength of the interface is different from that of adjacent points in the soil and concrete. To predict the distribution of stress and strain in the vicinity of an interface, an approach is proposed in which stress is a function of strain gradients as well as strain. As illustrated in Figure 3, the assumptions for a one-dimensional model are the following:

1. A simple hardening and softening relation exists in which the stress is given in terms of strain and a parameter identified as the peak stress; and

2. The peak stress decays linearly with the absolute value of the strain gradient.

A viscoplastic model, in which the limit state is affected by a norm of the strain gradient, will be used in an attempted generalization to three dimensions. The value of such an approach is purely speculative at this time.

VERIFICATION OF THEORY

Theoretical results of using the proposed one-dimensional model for representing an interface will be compared with experimental data from

8
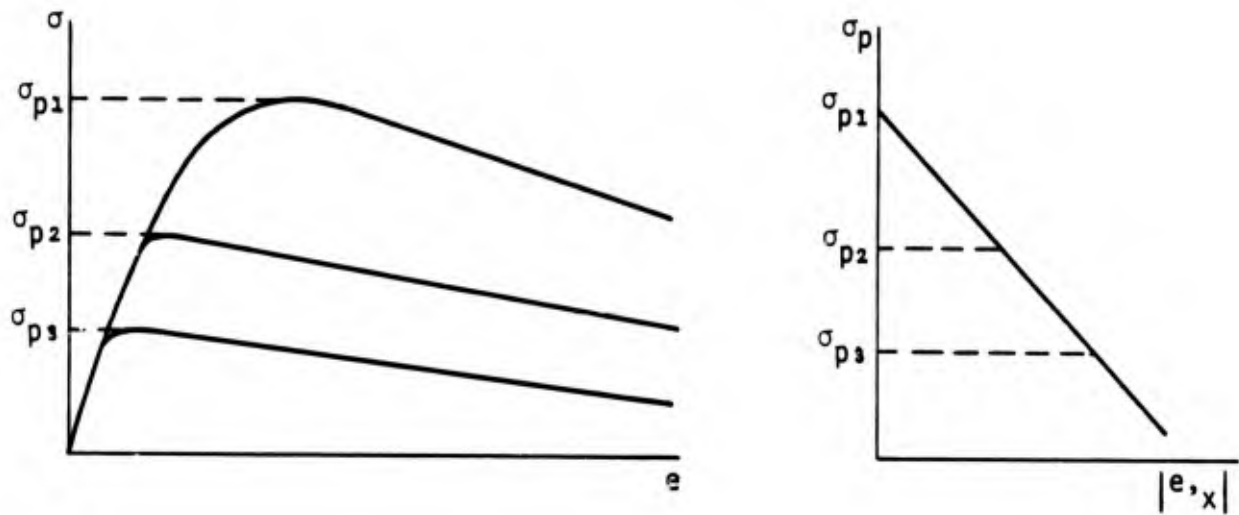
Figure 3. One-dimensional constitutive model.

sand-concrete and clay-concrete interfaces provided by Huck et al. (Ref. 7).
To evaluate the more general model, a two-dimensional problem will be ana-
lyzed. Strijbos and Vermeer (Ref. 10) have obtained experimental data on
boundary stresses by performing a one-sided die compaction of ferric oxide
powder. They also performed an analysis of the problem, but because of the
limitations of their computer program, they had to simulate an axisymmetric
problem by using a plane strain approach. The successful analysis of this
problem will provide credibility to the approach in which a nonlocal consti-
tutive equation is used to represent interfaces.

III. RATE EFFECTS IN CONCRETE

BACKGROUND

Many of the mechanical properties of concrete are affected by the rate at which the concrete is loaded. The extent to which a property is affected depends on the property being considered and the method used to prepare and test the concrete. As the first step in the investigation of strain rate effects in concrete, a literature survey was performed (Ref. 11). The survey revealed a basic lack of experimental data that could be used for material model development. Although data from uniaxial stress tests at various strain rates are available, significant pieces of information, such as lateral strains and static behavior, are often missing. Almost no data exist for any other stress path.

A two-pronged approach to closing the gap in the experimental data and providing adequate material models for frictional materials subjected to high rates of loading was then proposed in Reference 11. The experimental program was to be conducted in conjunction with the development of a third-invariant plasticity model. The program was scheduled to consist initially of uniaxial stress tests, but the technique to be used was one that could be developed later for performing multiaxial stress tests at high rates of loading. The results of these tests were then to be used to verify the material model and to identify areas requiring improvement.

To accomplish these goals, the following tasks were scheduled for this work phase: complete the design of the experimental testing device, construct the device, and begin the evaluation tests. The evaluation tests were to be used to develop needed instrumentation, operation procedures, and apparatus configurations that would provide the required data. If the evaluation tests were successfully completed, production tests were to be initiated. In this section, the progress made toward meeting these objectives is described.

DESCRIPTION OF APPARATUS

. Several designs for the testing device were considered. The final configuration consists of cylindrical segments bolted together with flanges.

10

Figure 4 is a schematic view of the device. The overall height of the apparatus is about 1 m. Two chambers are included to provide more control over the burning of the propellant used as the driving force in the tests.

The walls of the barrel are made from 4142 steel tubing with a 10.2-cm (4 in) inside diameter and a 16.5-cm (6.5 in) outside diameter. The flanges are standard 1500-lb flanges. A plate is inserted between the top two flanges to close off the upper chamber. This plate is 2.54 cm (1 in) thick and has two safety rupture disc devices. The discs are calibrated to rupture in case the pressure should rise above 68.9 MPa (10,000 lb/in^2). Another plate is inserted between the lower chamber and the upper chamber. In this plate, which is also 2.54 cm (1 in) thick, are venting holes that allow the pressure created by the burning propellant to escape into the lower chamber, where the load cell and specimen are located. The venting has two purposes: (1) to reduce the temperature load on the load cell, and (2) to provide some control over the rise time. The second purpose is of particular interest if a high-density or a fast-burning propellant is used. These types of charges will give a very fast rise time, and the venting plate can be used to reduce the rise time to the desired value. However, the charge currently in use is producing an appropriate rise time without the venting; therefore, the plate is used primarily to prevent the burning propellant from coming into contact with the load cell.

PROPELLANT CHARGE DESIGN

The Department of the Army has issued a propellant design handbook (Ref. 12) that includes an algorithm for determining the characteristics of burning propellants. The propellant parameters have been identified at arsenals where these propellants are in common use. The algorithm is coded to include a closed bomb configuration, which corresponds to rigid boundaries, and a configuration that permits displacements of the boundary based on the linear elastic constitutive properties of the material surrounding the propellant.

Pressure histories, which are particularly relevant for observing rate effects in concrete, can be obtained for various propellants. These histories indicate that the peak pressure in a chamber depends on the density of the propellant. Rise times depend on both the initial density and the propellant

11

Upper plate with rupture
disks

Upper chamber

Lower plate for venting
between chambers

Lower chamber

Specimen

Base plate bolted onto a
concrete slab
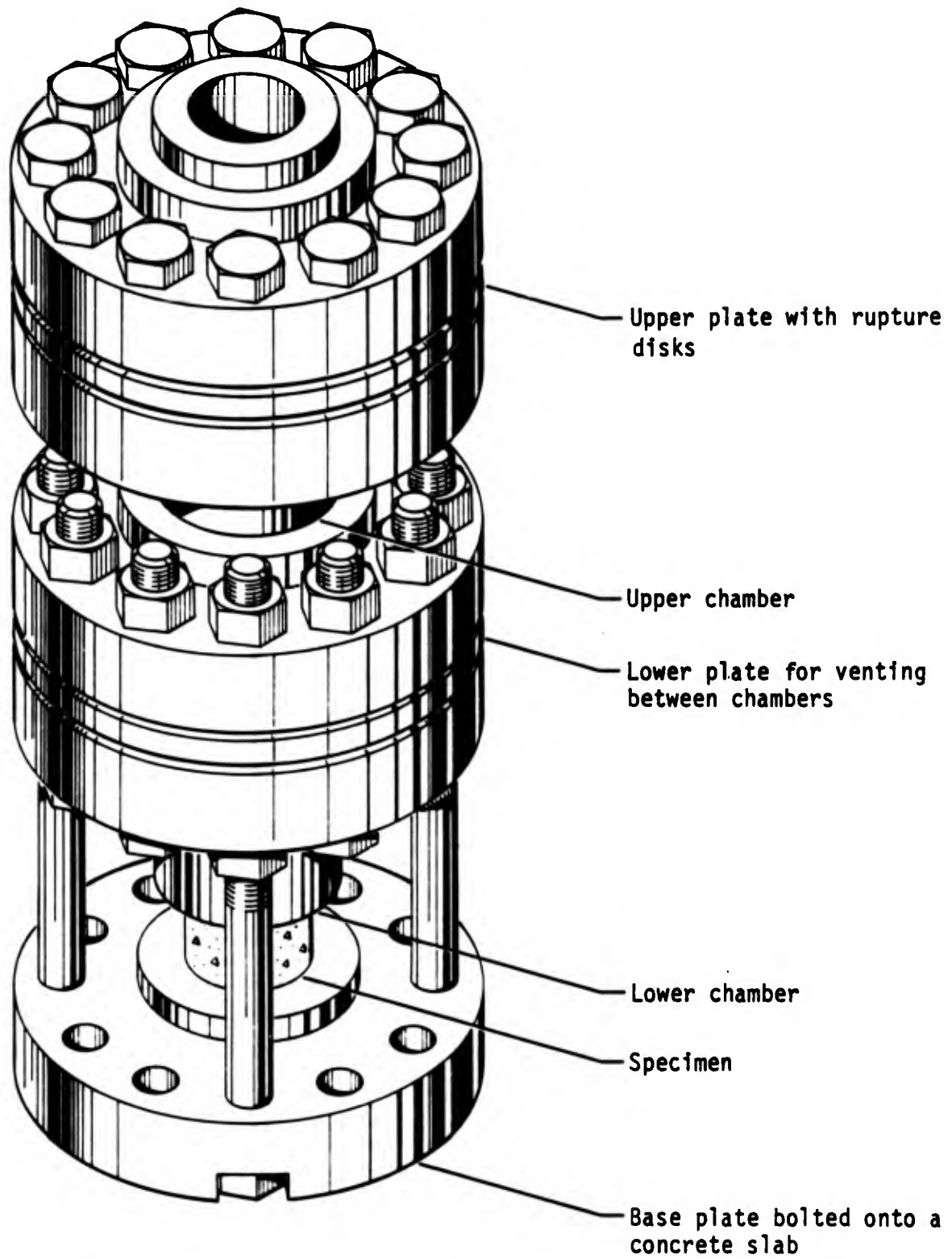
Figure 4.   Isometric drawing of a rapid loading device.

type. Higher initial loading densities give faster rise times and higher peaks. Iterating for different densities and propellants showed that for the desired pressure histories, a fast-burning propellant at a low density was required. The difficulty with low charge densities, however, is that the propellant may extinguish itself if any movement of the chamber boundaries occurs. This reaction is due to the interaction between pressures and burn rates for propellants. To ensure that the propellant would burn properly, a relatively high density (35 percent by weight) of a fairly large-grain, slow-burning propellant was used. This charge gave too high a peak pressure--over 138 MPa (20,000 lb/in^2)--and too short a rise time and caused some minor damage to the device. Once the device had been repaired, lower charge densities were tried to determine whether the charges could maintain their burn. A small charge at a 5-percent density was tried next. Only the lower chamber was used in this test. One continuous solid steel cylinder was used to simulate the load cell and specimen in order to avert a cavity expansion that could cause the propellant to stop burning. The results of this test were encouraging, except that the top of the solid steel cylinder was scorched by the burning propellant.

In an attempt to reduce the heat load on the load cell, a plate was introduced between the upper and lower chambers. Vent holes in the plate allow the high-pressure gas to vent to the lower chamber, where the load cell is located. Because the propellant actually burns in the upper chamber, away from the load cell, the load cell is not subjected to the intense, direct heat. The propellant density was increased gradually over the next few experiments to bring the peak pressure up to about 41.4 MPa (6000 lb/in^2). The shortcoming of the current setup is the occurrence of leakage, which prevents the pressure from increasing to its full potential and also causes the pressure to decay too rapidly. In the next set of tests, gaskets will be used to reduce or prevent leakage.

A summary of the propellant type and charge density for each test fired to date is provided in Table 1. The peak pressures achieved, as measured by the pressure gage for the lower chamber, are also included. Typical pressure and concrete strain history plots are shown in Figure 5. Because of a time shift between the concrete strain record and the record of pressure in the lower chamber, no pressure-strain curve is included.

13

TABLE 1. TEST SUMMARY

Test No.	Date	Propellant type	Charge density by volume, %	Total charge, kg (lb)	Specimen	Load cell	Peak pressure in lower chamber MPa (lb/in²)	Comments
1	6-29-84	M5	35	2.27 (5)	Steel	Aluminum	138 (>20,000)	Damaged device
2	8-3-84	M5	5	0.16 (0.35)	Steel	Steel	a___	Small chamber only
3	8-31-84	M5	4	0.32 (0.70)	Steel	Steel	28.3 (4,100)	Larger chamber with vent plate
4	9-6-84	Black powder	4	0.39 (0.85)	Steel	Steel	31.7 (4,595)	Larger chamber with vent plate
5	9-13-84	Black powder	5.2	0.39 (0.85)	Concrete	Aluminum	26.9 (3,900)	Larger chamber with vent plate
6	10-5-84	Black powder	6.2	0.45 (1.0)	Concrete	Aluminum	20 (2,900)	Larger chamber with vent plate

[a]Propellant burn test; peak pressures not available.
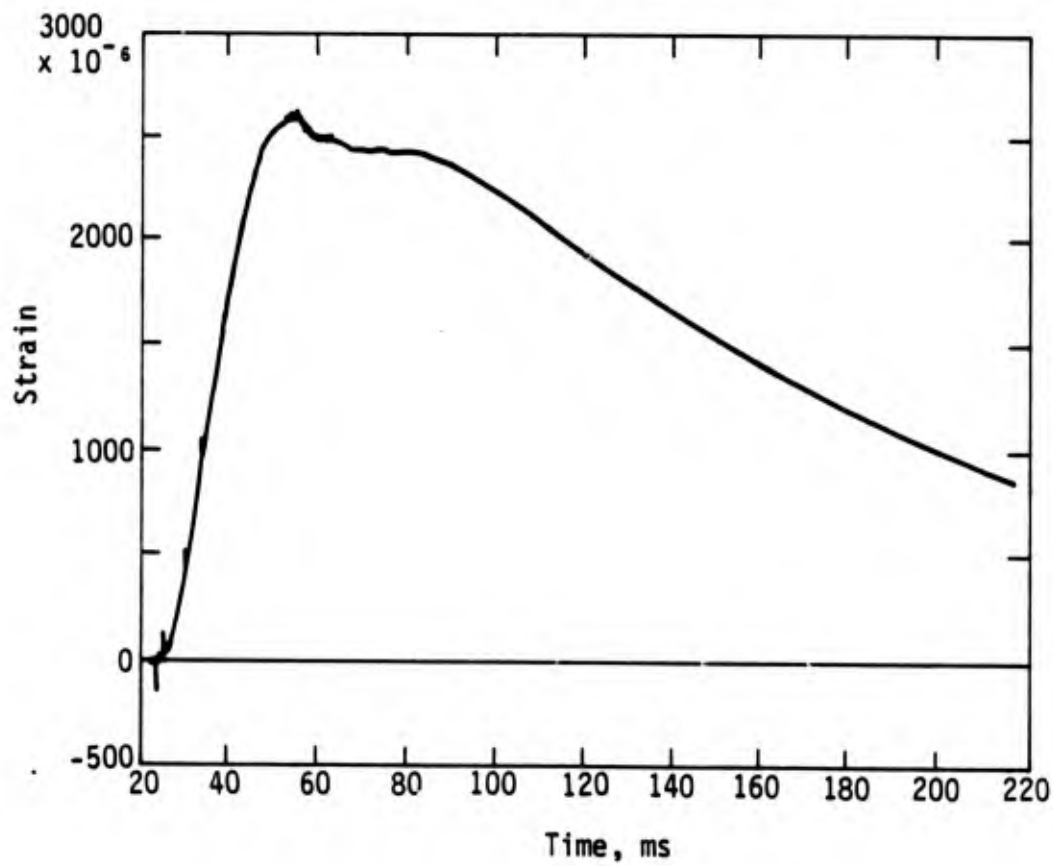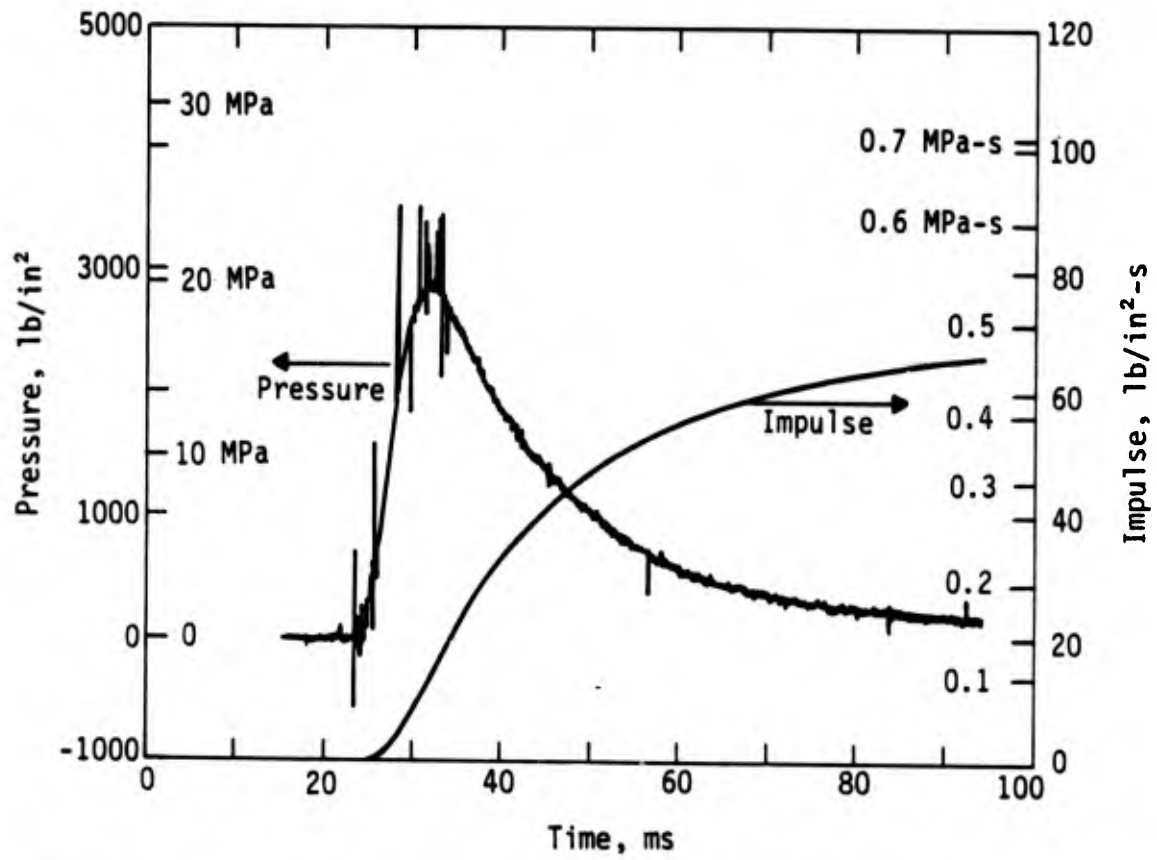
Figure 5. Typical pressure and concrete strain histories.

LOAD CELL DEVELOPMENT

Commercially manufactured load cells are not designed to be inserted into a closed chamber. Therefore, a special developmental effort was conducted. Specifications for the cell included the following: it had to be rugged enough to survive repeated tests; its physical dimensions were restricted; and it was required to provide linear response over the pressure range of interest.

The initial calibration tests indicated that this load cell was linear and reliable up to the desired force level. The cell was instrumented with two vertical and two horizontal semiconductor strain gages that would measure the Poisson effect. The full bridge provided temperature compensation and a good response. The difficulty with this load cell was that because the gages and wires were openly exposed to the heat, the gage survivability was poor.

To obtain better survivability, a second load cell was developed. On this load cell (Fig. 6) the strain gages are mounted in the interior of a hole drilled partway through the wall of the aluminum cylinder. A side exit is provided for the wires, and a steel pipe screwed into the exit protects the wires from the heat. The first of this type of load cell was instrumented with U-shaped strain gages that could not provide linear results because of the curvature of the hole. In the next model, a straight strain gage, which did not have to be curved around the hole, was used.

Gage survivability for this load cell seems to be good. Further tests will be conducted to verify the adequacy of the design. If further modifications are indicated, they will be implemented in future models.

EXTENSIONS

Because of the difficulty of developing an adequate load cell, production tests have not been accomplished. These tests will be made early in the new work phase, while a new device is being designed and built for biaxial testing. In addition to the experimental program, models will be developed from the data from the uniaxial stress tests and from biaxial stress data if available.

16
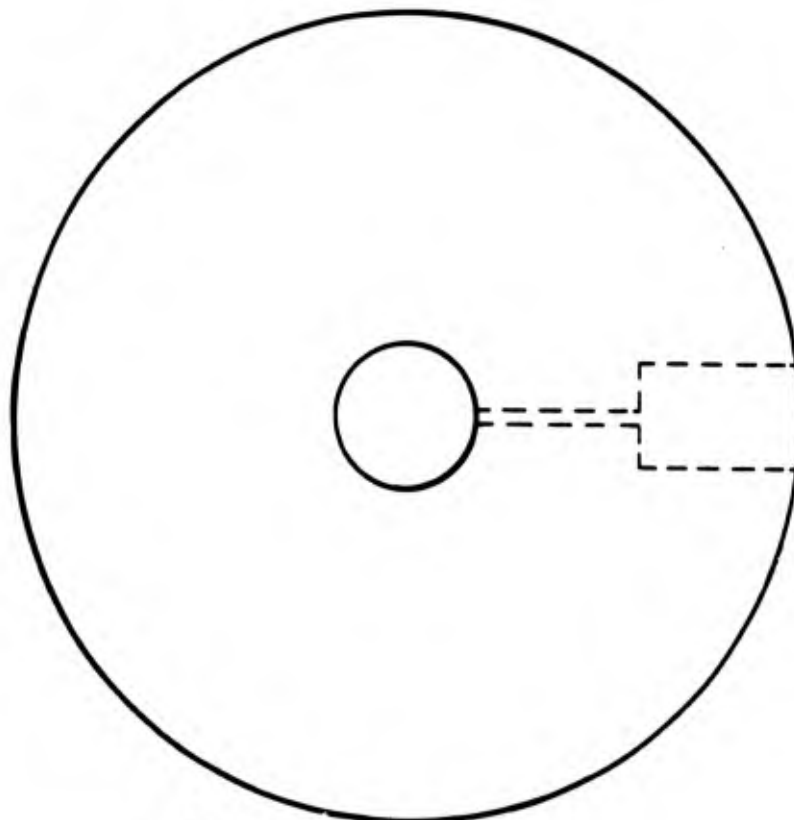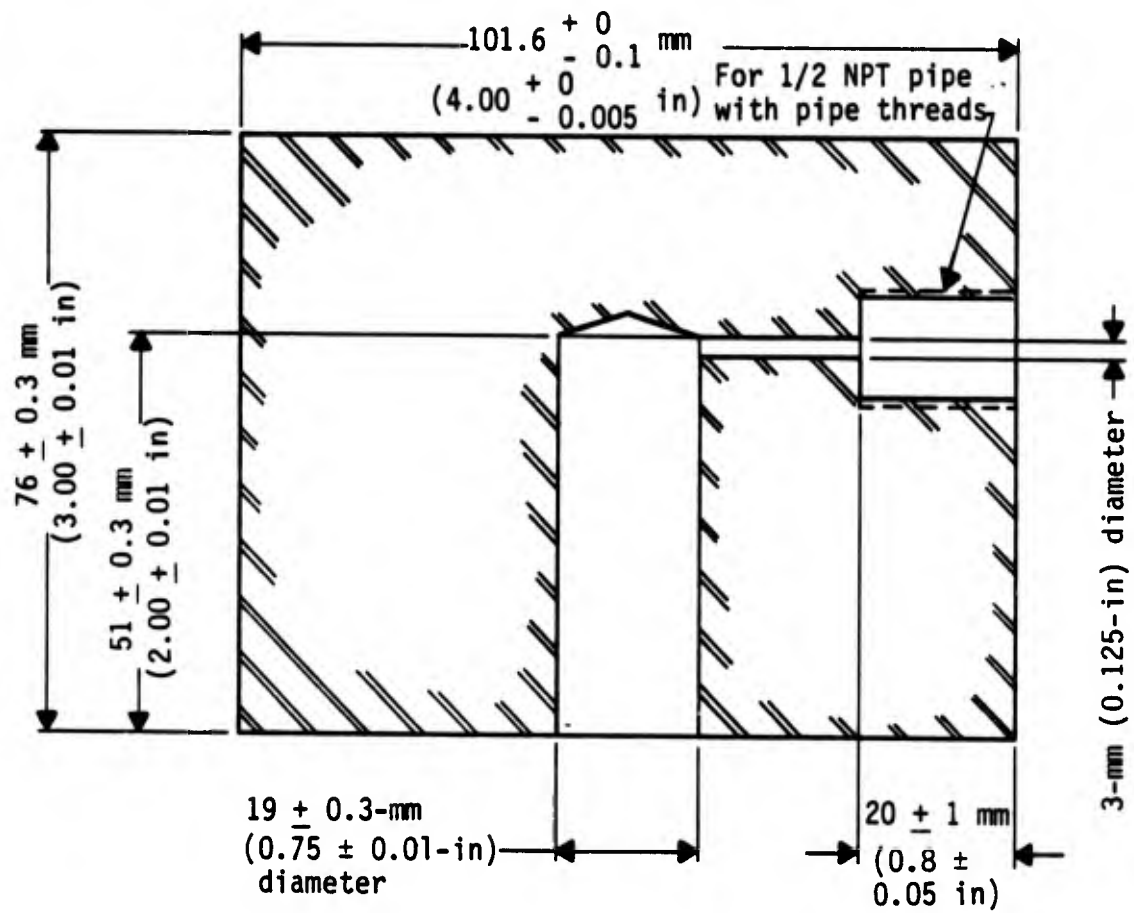
Figure 6. Load cell SB3.

The design for the biaxial testing device will be based on the latest
design for the uniaxial device. Essentially, two devices will be oriented to
load orthogonal axes of a cubical specimen. Several difficulties that are
immediately apparent include using a cylindrical barrel to load a square sur-
face, instrumenting three-dimensional concrete specimens, and firing two
devices simultaneously. These and other difficulties will be addressed as the
designing of the device progresses.

IV. BEHAVIOR OF UNSATURATED FINE-GRAINED SOILS

The prediction of the effect of stress waves in geological media requires the use of a numerical technique that includes a constitutive model. The conventional approach to modeling fine-grained soils is to assume that the medium is saturated and that rate effects can be ignored. Neither assumption is valid. The first phase of a comprehensive study of fine-grained soils consists of an investigation of the effect of moisture on the static response of clay and silt. It is postulated that suction, which is inversely related to moisture and tends to bind the soil particles together, is a parameter that could provide a unifying structure to the behavior of the complete class of fine-grained soils. Because the static behavior of these materials is not understood, it is premature to consider rate effects.

In order to develop procedures for studying the behavior of unsaturated fine-grained soils, several testing techniques were evaluated. The work consisted of classification tests, suction tests, and an evaluation of techniques for studying material behavior. The objectives were to select methods of measuring suction potential, to use suction in behavior studies, and to develop an experimental data base for investigating constitutive models of soil behavior.

CLASSIFICATION TESTS

Two materials were selected for study. The first, commonly called Vicksburg silt, was obtained from the U.S. Army Engineer Waterways Experiment Station (WES). The second is a clay obtained from a site in Oklahoma City. Results of standard classification tests on these soils, shown in Table 2, are typical values for these types of materials. All tests involved remolded materials. The specimens used in compression testing were prepared in a miniature compaction apparatus, which yielded specimens 3.6 cm (1.4 in) in diameter by 7.1 cm (2.8 in) high for the unconfined compression and the triaxial tests. A specimen size of 3.8 cm (1.5 in) in diameter by 7.6 cm (3.0 in) high was used in the stress path testing.

19

TABLE 2. RESULTS OF CLASSIFICATION TESTS

Property	Clay	Silt
Atterberg limits:		
Liquid, %	36	25
Plastic, %	23	20
Plasticity index, %	13	20
Activity	0.4	NA
Specific gravity	2.72	2.72
Passing no. 200 sieve, %	81.2	99.4
Finer than 0.002 mm, %	32.0	6.0
Unified Soil Classification	CL	ML-CL
Compaction test:[a]		
w, %	20.0	20.2
γ, kg/m^3	1706	1642

[a]Compactive effort = 86,684 J/m^3
(1810 [ft-lb]/ft^3) at 5 blows/layer.

SUCTION TESTING

In fine-grained soils, water is attracted predominately by the mechanisms of adsorption and capillary action, the former being most important for clays and the latter for silts. Water is attracted to or adsorbed by the particle surfaces because of negative charges resulting from charge imbalances and because of substitutions within the mineral structure of the particles. If the particles agglomerate to form clods, then capillary spaces, in which water is held by capillary forces, are also created.

Suction or suction potential is a measure of the free energy of water in a soil. Several methods of measurement are available. In this study two methods, called "energy methods," were used. These techniques require equilibration of the soil sample within a tightly closed container at constant temperature, followed by measurement of the relative humidity within the container (in equilibrium with the sample). The thermocouple psychrometer uses the wet-bulb, dry-bulb method, employing tiny thermocouples that serve as sensing elements. McKeen (Ref. 13) provides a detailed description of this

instrument as well as a historical review. The second method permits cali-
brated filter paper to reach moisture equilibrium with the soil. Determina-
tion of the water content of the filter paper and use of a calibration curve
then yields a suction value. Tests have demonstrated that the two methods
yield similar results when used on the same materials. The filter paper
method was used in the tests described here because it is capable of measuring
a wider range of suction values. Silt exhibits low suction values over normal
water content ranges, and clay exhibits high suction values over the same
ranges; therefore, this capability was important.

Measurements of suction were made at several water contents and after
compaction to various densities. These data are shown in Figures 7 and 8.
Lines were drawn through the data points to provide a representation of
expected average behavior. The curves for both types of soil in the range
tested have two distinct branches. Also, the energy change (suction) for a
given change in water content is much greater in clay than in silt. The
entire range of data for silt is in the capillary range $h < 33.2$ kPa. As the
water content increases from the dry state (point a in Fig. 8) in both mate-
rials, a point is reached (point b in Fig. 8) beyond which suction drops off
rapidly as the space available for water is filled. One would expect stress-
strain behavior to differ on the two branches as well as near the point of
saturation shown as point c in Figure 8.

STRAIN MEASUREMENT TECHNIQUE

To develop constitutive relations, it is essential that three-dimensional
stress-strain data be obtained for a variety of paths. A stress-path appa-
ratus was available for performing tests on compacted samples in a partially
saturated condition. Three sets of tests were performed on the cylindrical
samples. One set consisted of unconfined compression, which denotes the con-
dition of zero lateral stress and axial compressive stress. A second set
consisted of triaxial tests, where the lateral stress is a fixed compressive
value while the compressive axial stress increases in a monotonic manner. A
more general set, called stress-path tests, represents a class in which both
lateral and axial stresses are prescribed in a manner different from that used
for the first two sets.

21
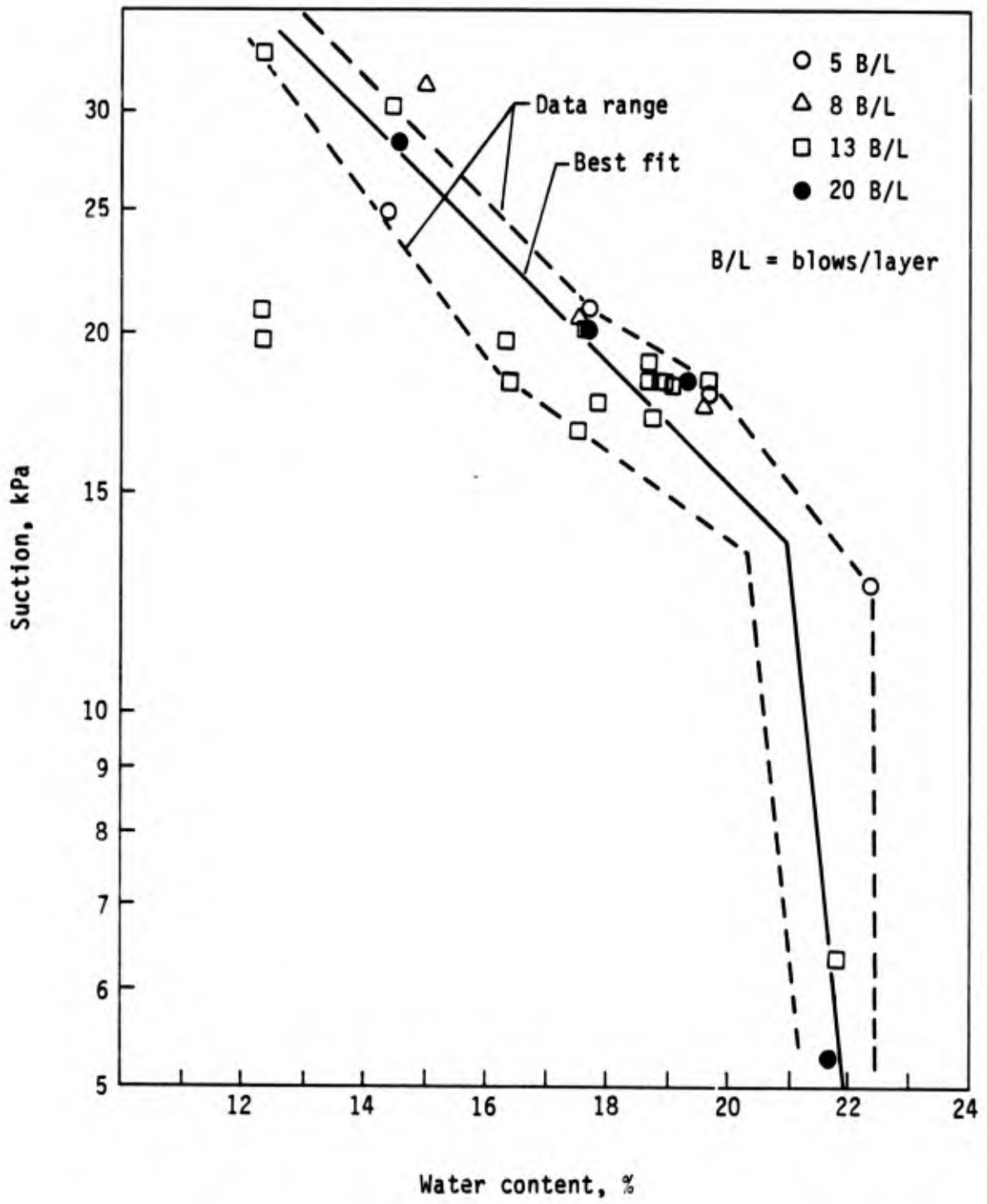
(a) Silt.

Figure 7. Suction-water content data.
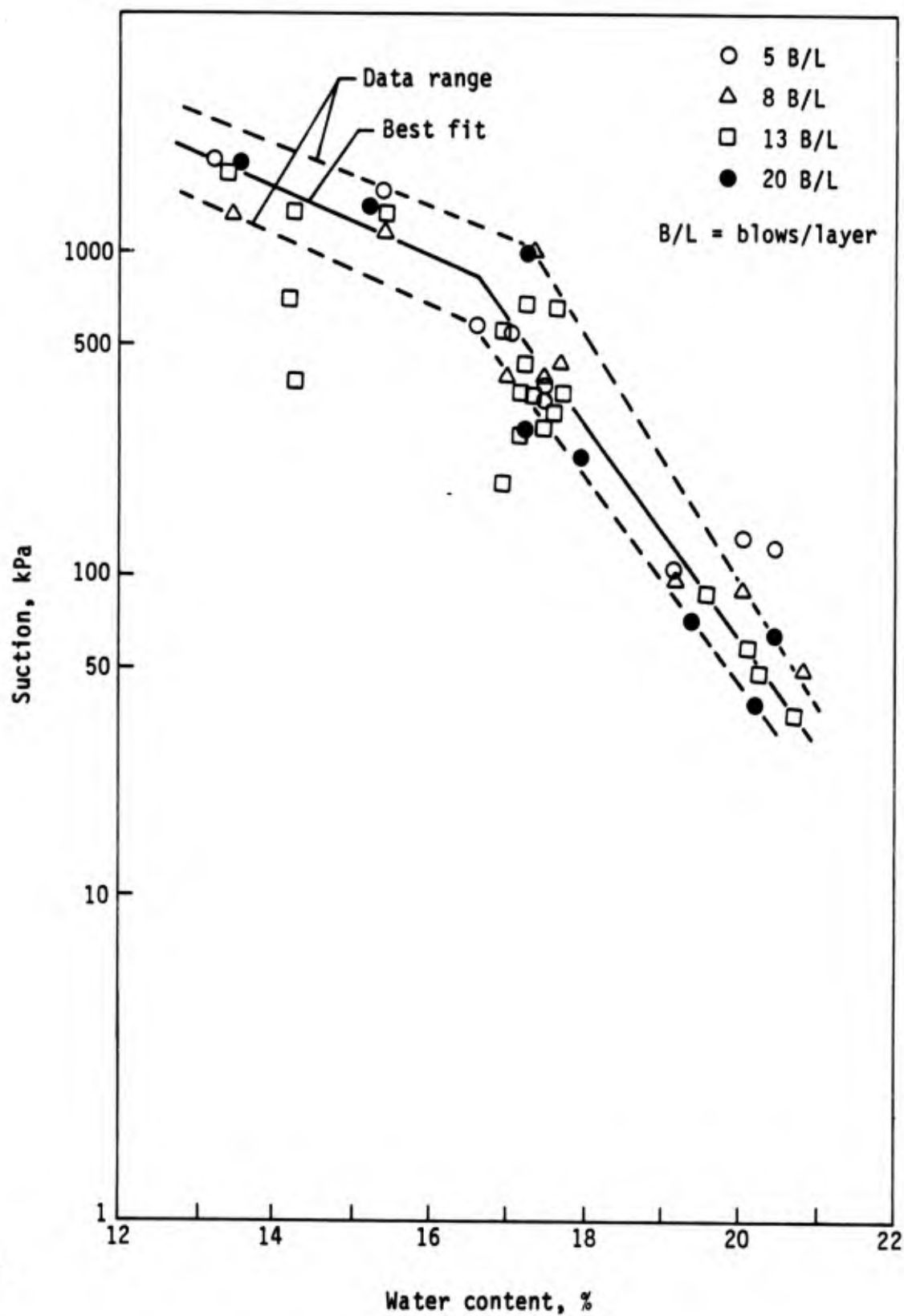
(b) Clay.

Figure 7. Concluded.

23
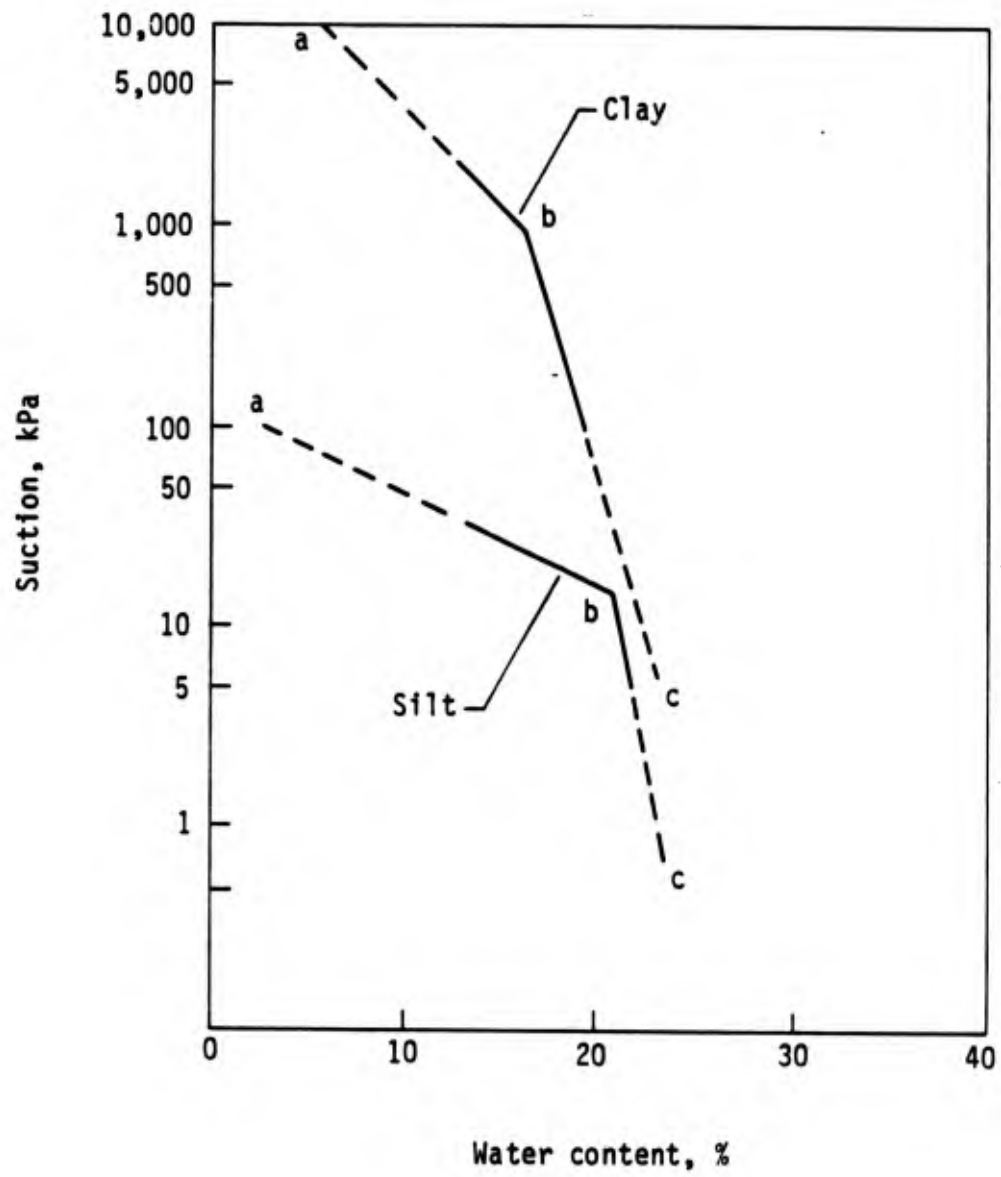
Figure 8. Suction-water content summary.

It is customary to use the relative displacements of the axial heads to obtain a measure of axial strain that is actually the average strain for the sample. Normally, volume changes for tests on soil specimens are obtained by measuring the amount of water that flows into, or out of, the specimen. Because the samples used in these tests were partially saturated, there was no flow of water; therefore, the standard technique for measuring volume change could not be used, and an alternate method of measuring lateral strains had to be devised.

The procedure adopted was that of photographing the specimen at various points along the loading path and measuring the width of the specimen with a parallax bar. This procedure is used to obtain coordinates of points in aerial photographs. After considerable effort had been made to reduce errors due to slack in the parallax bar and to obtain readings in a systematic manner, it was observed that the lateral strain varied by a considerable amount from one end of the specimen to the other, even for low values of stress. The implication of this observation was that the conventional method of using average strains would be unacceptable for obtaining data suitable for use in evaluating constitutive relations. Also, the possibility existed that the longitudinal or axial strain would vary as well. Therefore, it became imperative to measure the longitudinal or axial strain along the specimen rather than relying on the average strain.

After several alternative approaches had been evaluated, a system was adopted whereby staples were inserted in the specimen. The staples, which were visible through the rubber membrane that contained the specimen, served as reference points that could be used for making both longitudinal and lateral measurements on photographs. The following procedure was used:

1. Staples were inserted into the specimen (Fig. 9) as reference markers that divided the specimen into five vertical layers.

2. The specimen was placed in the triaxial cell as is normally done for any test.

3. Photographs were taken before the test began and at specified loads during the test. A Pentax 1000 camera with an f.2 lens and black and white Kodak film was used.

4. The photographs were processed to produce normal 3- by 5-in prints.

25
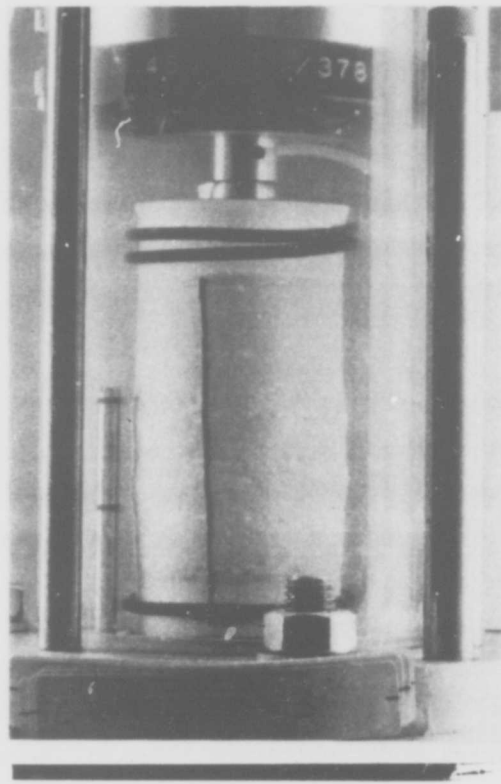
Figure 9. Triaxial test showing 25.4-mm reference rod.

5. The initial longitudinal and lateral dimensions of the layers were measured on the photographs and corrected for scale. A 25.4-mm reference rod placed next to the specimen was used for these measurements. With the parallax bar, distances were measured to within 0.01 mm (0.0004 in).

6. Similar measurements taken at subsequent times in the test provided data that could be used to determine changes in length and to calculate the strains that accompanied specific load changes.

The technique was calibrated by using the system to measure metal specimens machined to specified dimensions. The influence of the curved triaxial cell wall and the curvature induced by water in the test chamber was evaluated. The final step involved measuring differences in the positions of the staples at various times in the test, which cancelled the effects of the curvature features. The reference rod in the photographs was used to correct the data for any deviation in camera position that occurred during the tests.

26

UNCONFINED COMPRESSION TESTS

Three sets of unconfined compression tests were performed to provide data indicating the stress-strain response to variations in moisture condition, compactive effort, and rate of loading. First, tests were made at a constant displacement rate of 1.0 mm/min for six specimens with different water contents. All specimens were compacted at 13 blows per layer (B/L). The stress-strain responses of these specimens are shown in Figures 10a and 10b for silt and clay, respectively. The test numbers on the plots correspond to the parameters defined in Table 3. For the silt, test numbers 1, 2, 3, and 4 correspond to suctions that lie on branch a-b of the curve in Figure 8; test numbers 5 and 6 correspond to branch b-c. Figure 10a shows that for low suction (high water content), ductility is enhanced in comparison with the ductility displayed by curves associated with high suction (low moisture). Because of the limited amount of data, no conclusions can be drawn about peak stress. On the basis of the results shown in Figure 10b, a similar conclusion concerning ductility can be drawn for clay, with the additional feature that in this case the peak stress appears to decrease as the suction potential drops. Additional tests were conducted in which the displacement rate of the loading head was varied (0.1, 0.5, 1, 1.5, 2, and 4 mm/min) and the compactive effort was investigated (5, 8, 13, and 20 B/L). The stress-strain response curves were not affected significantly by these parameters.

TRIAXIAL TESTS

Unconsolidated, undrained triaxial tests at various confining pressures were performed on samples. Test results obtained for constant displacement rate include the typical data shown in Figures 11, 12, and 13. If σ_L and σ_a denote the lateral and axial stresses, respectively, then $q = (\sigma_a - \sigma_L)/2$ and $p = (\sigma_L + \sigma_a)/2$, where q denotes the shear and p is a measure of confining pressure. In Figure 12, σ represents the normal stress components, σ_a and σ_L. As expected, Figure 11 shows that the peak stress increases if the lateral stress is increased, and some softening is apparent. Figure 12 shows that a linear failure line is appropriate, and the effect of maximum shear stress on strain is illustrated in Figure 13.
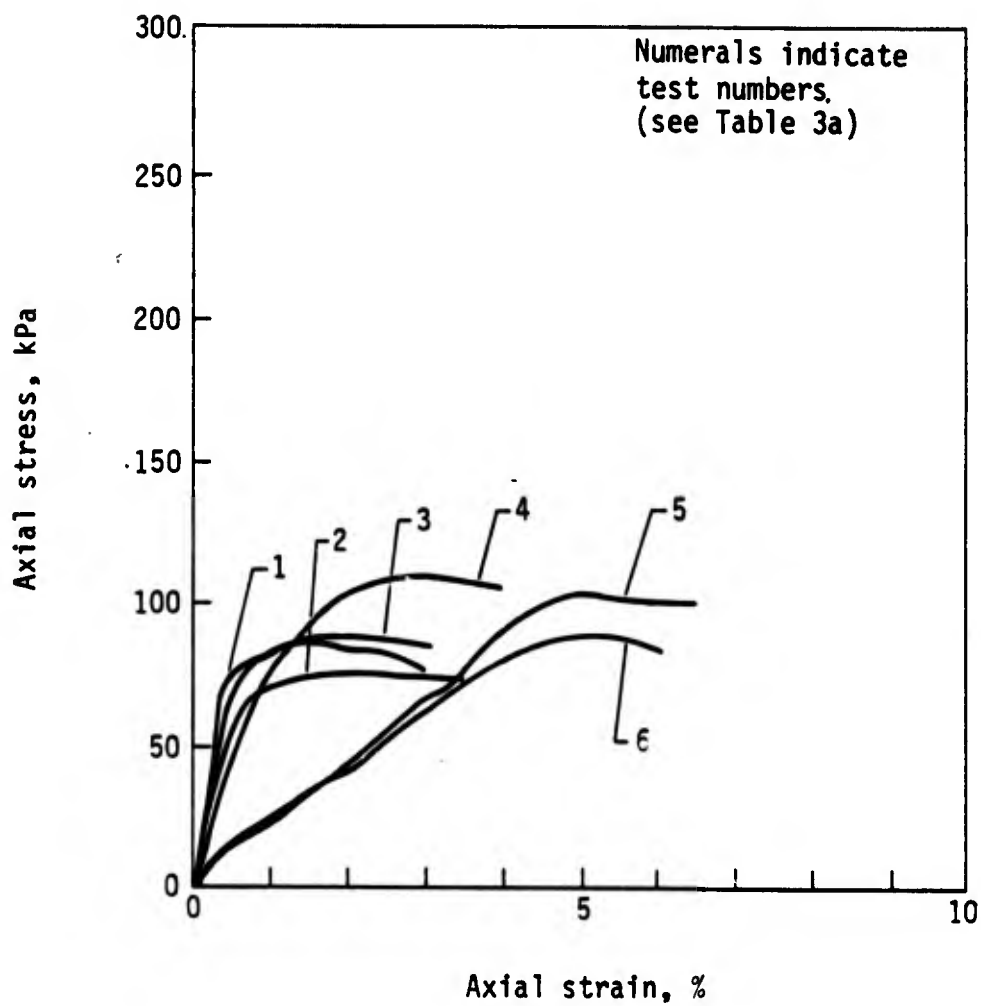
(a) Silt.

Figure 10. Stress-strain curves.

28
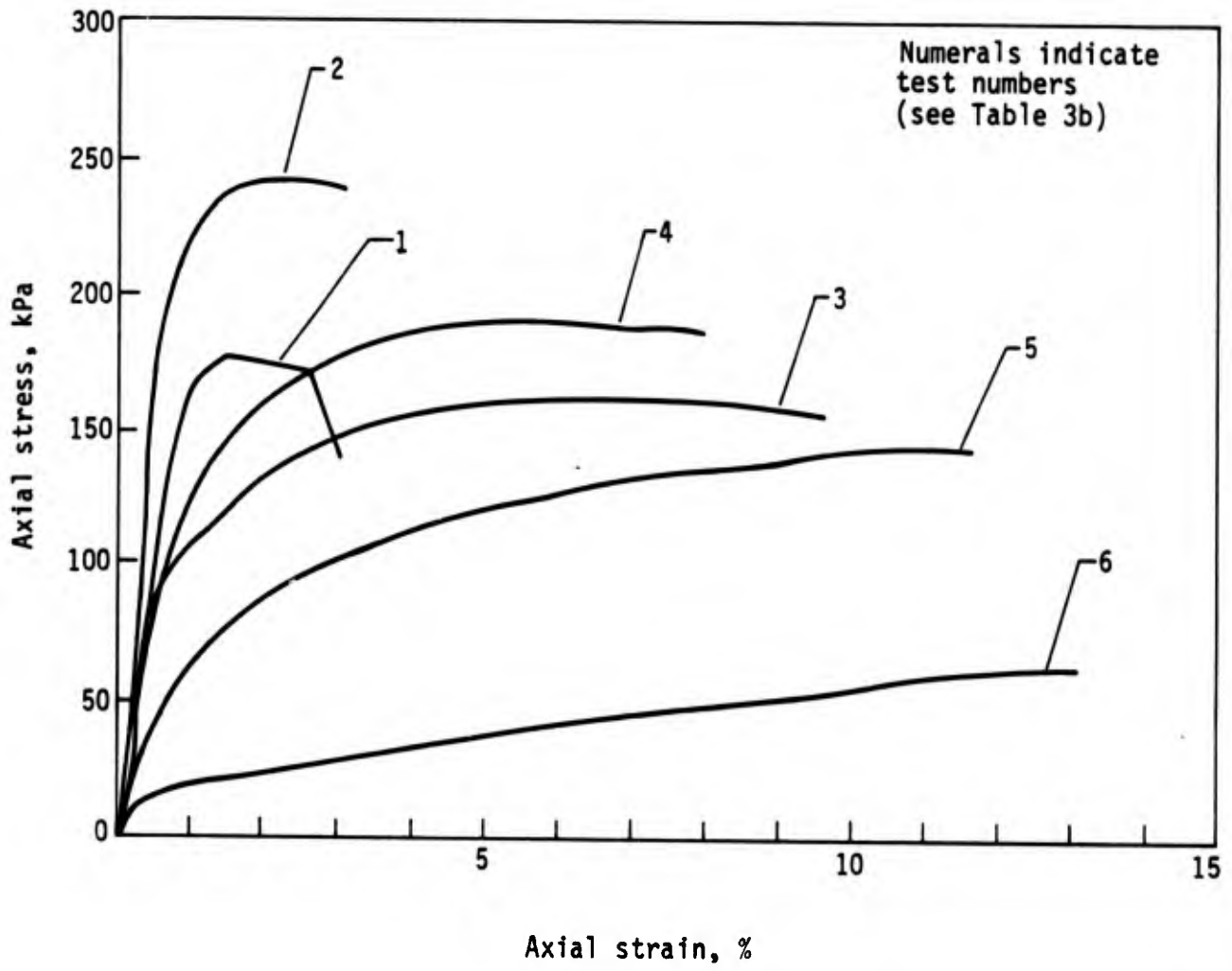
(b) Clay.

Figure 10. Concluded.

TABLE 3. STRESS-STRAIN DATA

(a) Silt

Test No.	w, %	γ_{dry}, kg/m³	σ_f, kPa	ε_f, %
1	15.4	1575.42	83.4	1.5
2	17.83	1600.09	73.1	2.1
3	19.03	1623.96	87.6	1.6
4	19.51	1643.66	109.0	2.85
5	21.13	1596.56	102.0	5.2
6	22.91	1577.98	85.5	5.0

(b) Clay

Test No.	w, %	γ_{dry}, kg/m³	σ_f, kPa	ε_f, %
1	14.1	1597.0	172.4	2.0
2	15.8	1632.3	237.9	1.5
3	17.7	1707.6	160.7	7.5
4	18.0	1696.4	188.2	6.0
5	19.8	1704.0	143.4	13.0
6	22.6	1625.9	64.8	17.0
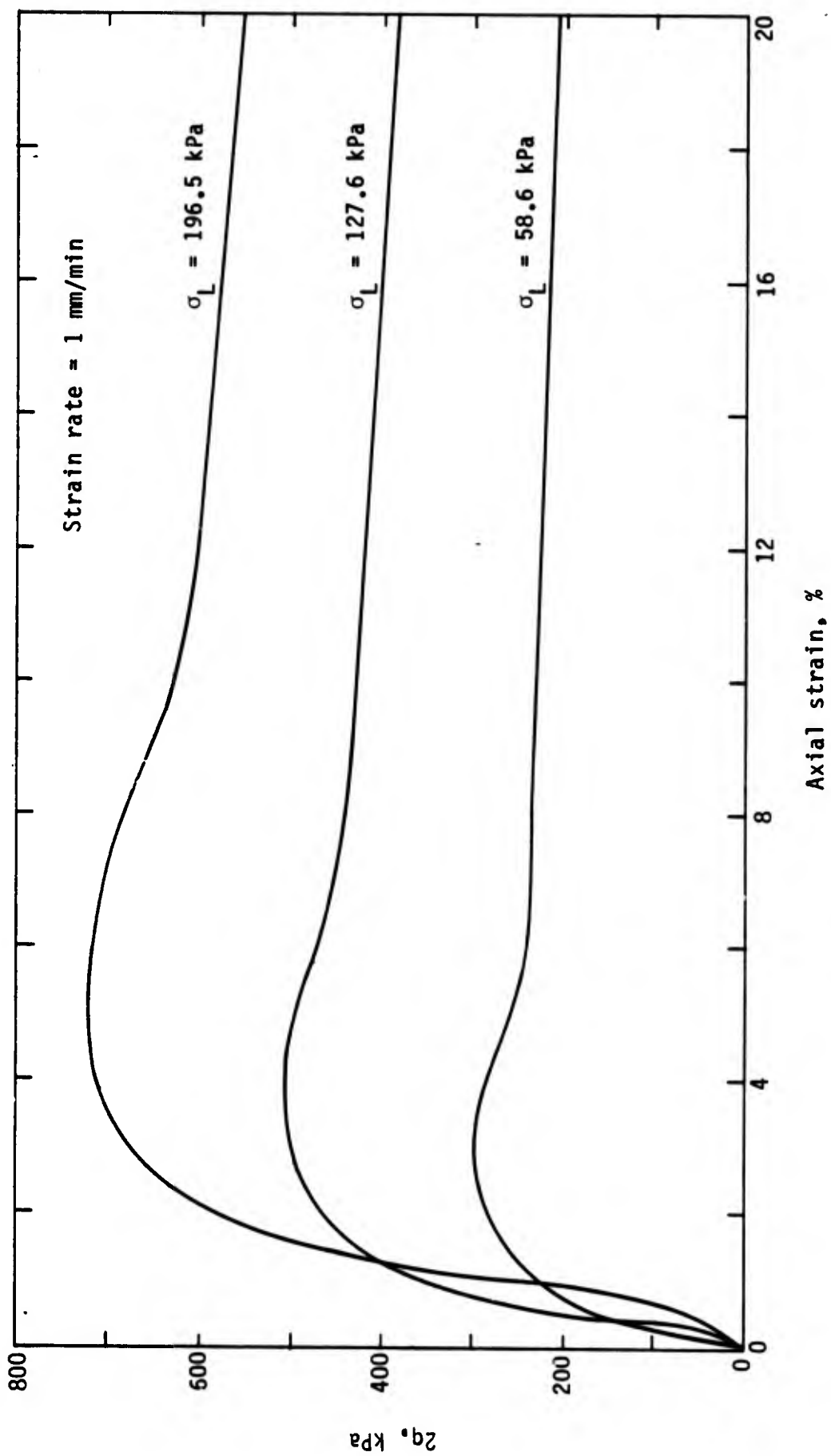
Figure 11. Principal stress difference versus axial strain for consolidated, undrained triaxial test.

31
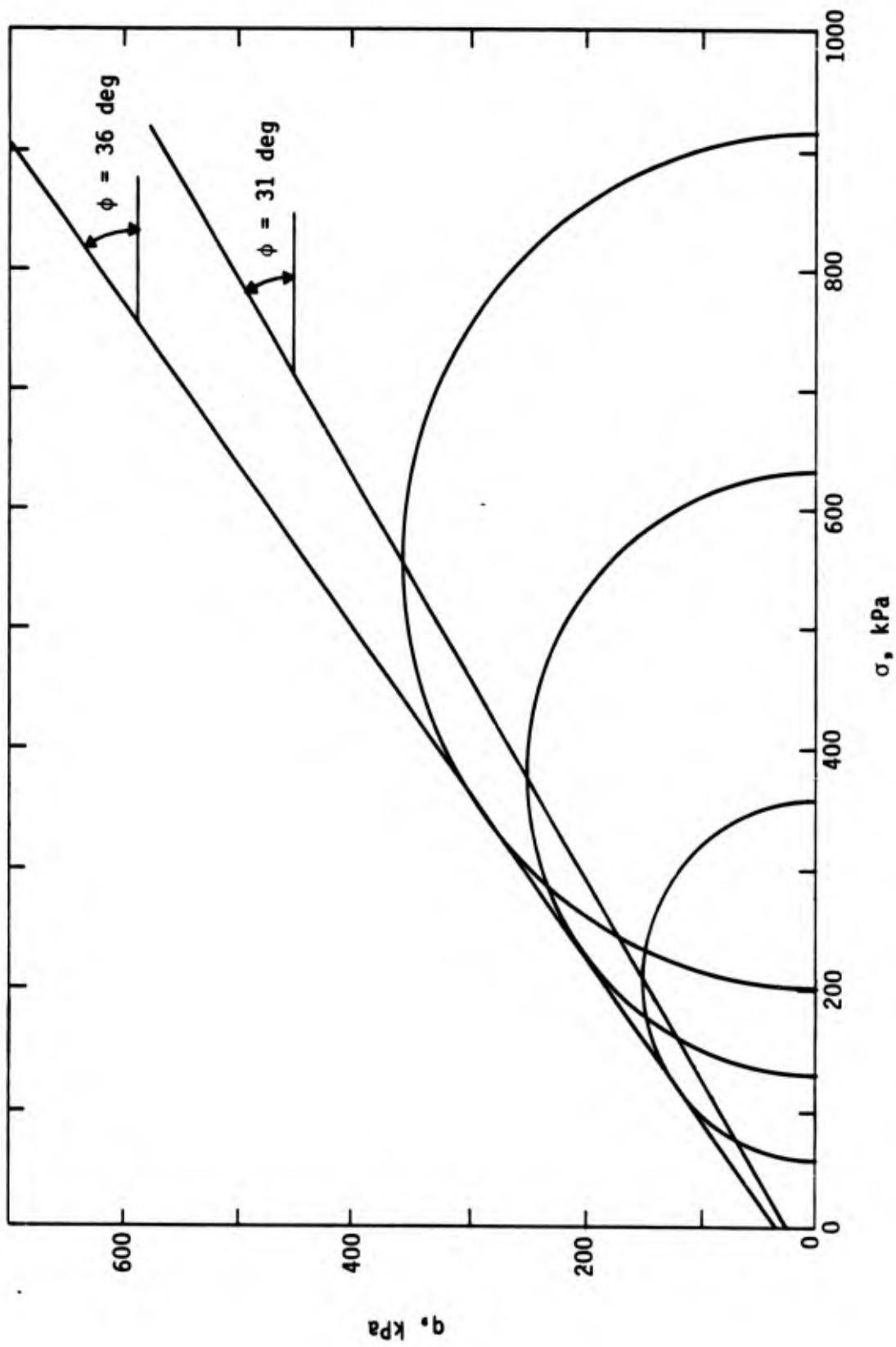
Figure 12. Mohr circles for triaxial test.
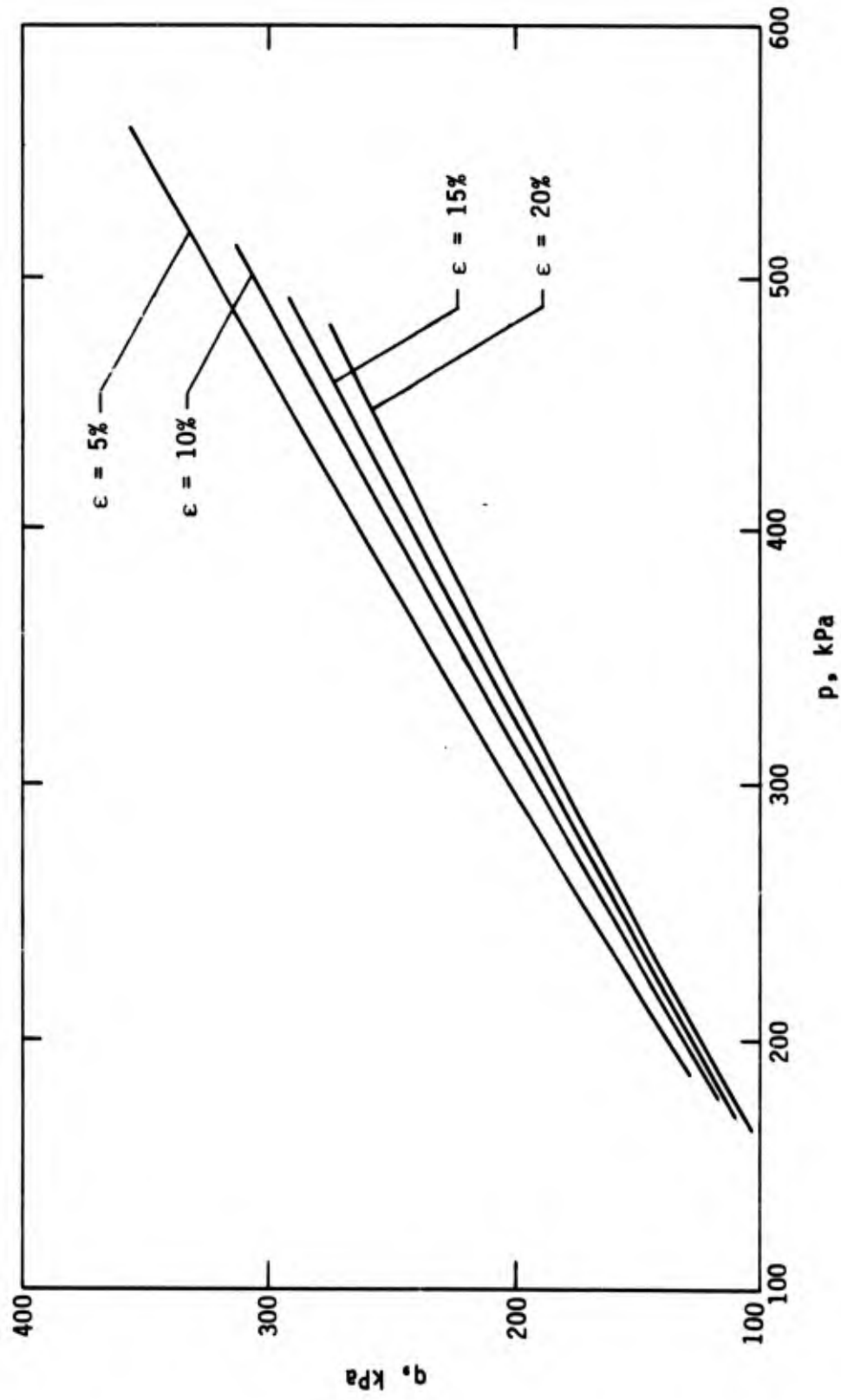
Figure 13. Lines of maximum shear for various values of axial strain from triaxial test.

STRESS PATH TESTS

A number of stress path tests were performed on compacted samples in the partially saturated condition. The stresses were changed manually in increments of 0.007 MPa/min. The tests were performed in such a way that drainage was not impeded. Because the samples were partially saturated, no water flow occurred. Axial stresses were obtained by dividing the axial force by the cross-sectional area, which was adjusted under the assumption that the sample maintained constant volume.

One object of the stress path testing was to obtain data that could be used to predict the change in axial strain that would occur in a given soil at a given moisture content when the sample was taken from one total stress condition to another. To accomplish this objective the following procedure was used:

1. The K_0 (consolidation) line was established. Because K_0 in terms of total stress was not known for this soil, a ratio of $\sigma_L/\sigma_a = 0.5$ was used. It was assumed at this stage of testing that the K_0 line represented the in situ stress condition for this particular soil at a given depth and moisture content.

2. The K_f (failure) line for the same soil was determined by starting at points on the K_0 curve and proceeding upward in the q-p plane until a limit state had been reached. In the first phase of the testing, the K_f line was determined by starting at two points on the K_0 line. From each point, three stress paths were followed, two at 45 deg and one vertical, as shown in Figure 14. These tests provided six points that could be used to establish the K_f line. However, it was found that the K_f line could be determined adequately by using only three vertical stress paths; consequently, only three paths were used for subsequent tests.

The results of the stress path testing on the Vicksburg silt are summarized in Figures 15, 16, and 17. The K_f lines for moisture contents of 19, 12.36, and 12.16 percent are plotted on Figure 15. Pertinent data and parameters taken from the K_f plots are shown in Table 4.

34
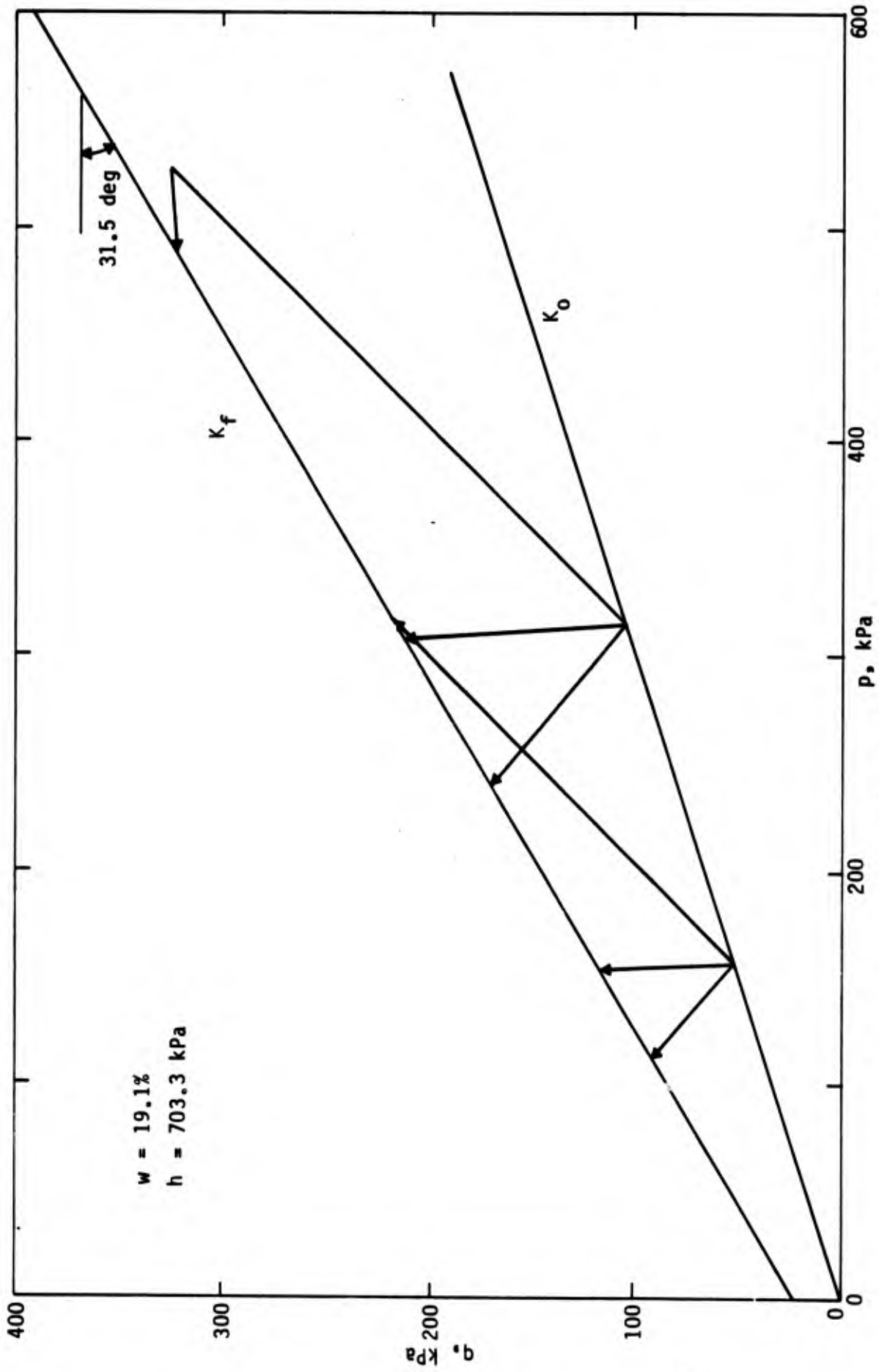
Figure 14. Lines of maximum shear determined by six stress paths from K_o line for Vicksburg silt.

35
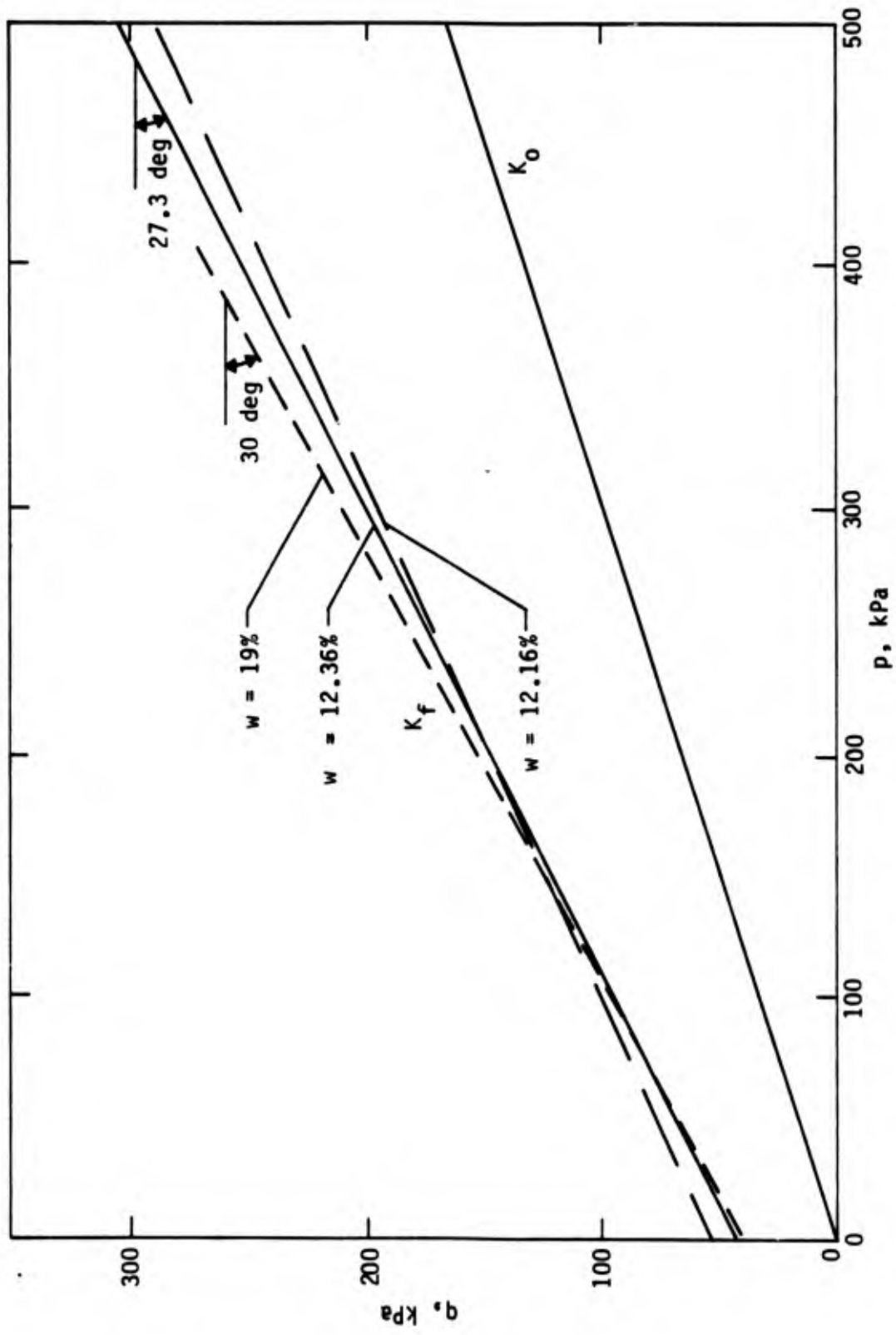
Figure 15. Lines of maximum shear for various moisture contents of Vicksburg silt.
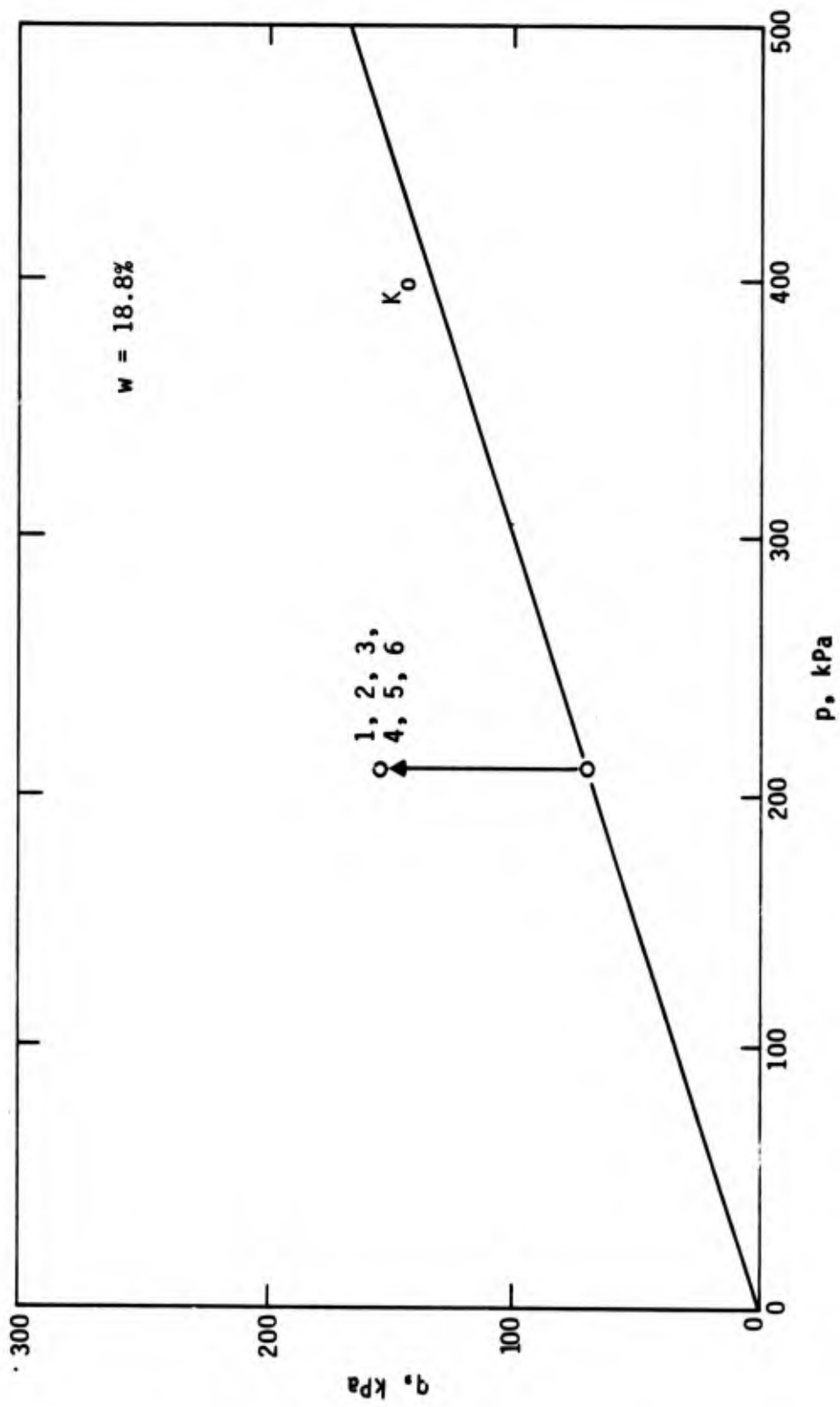
Figure 16. Results of six reproducibility tests for vertical stress paths.
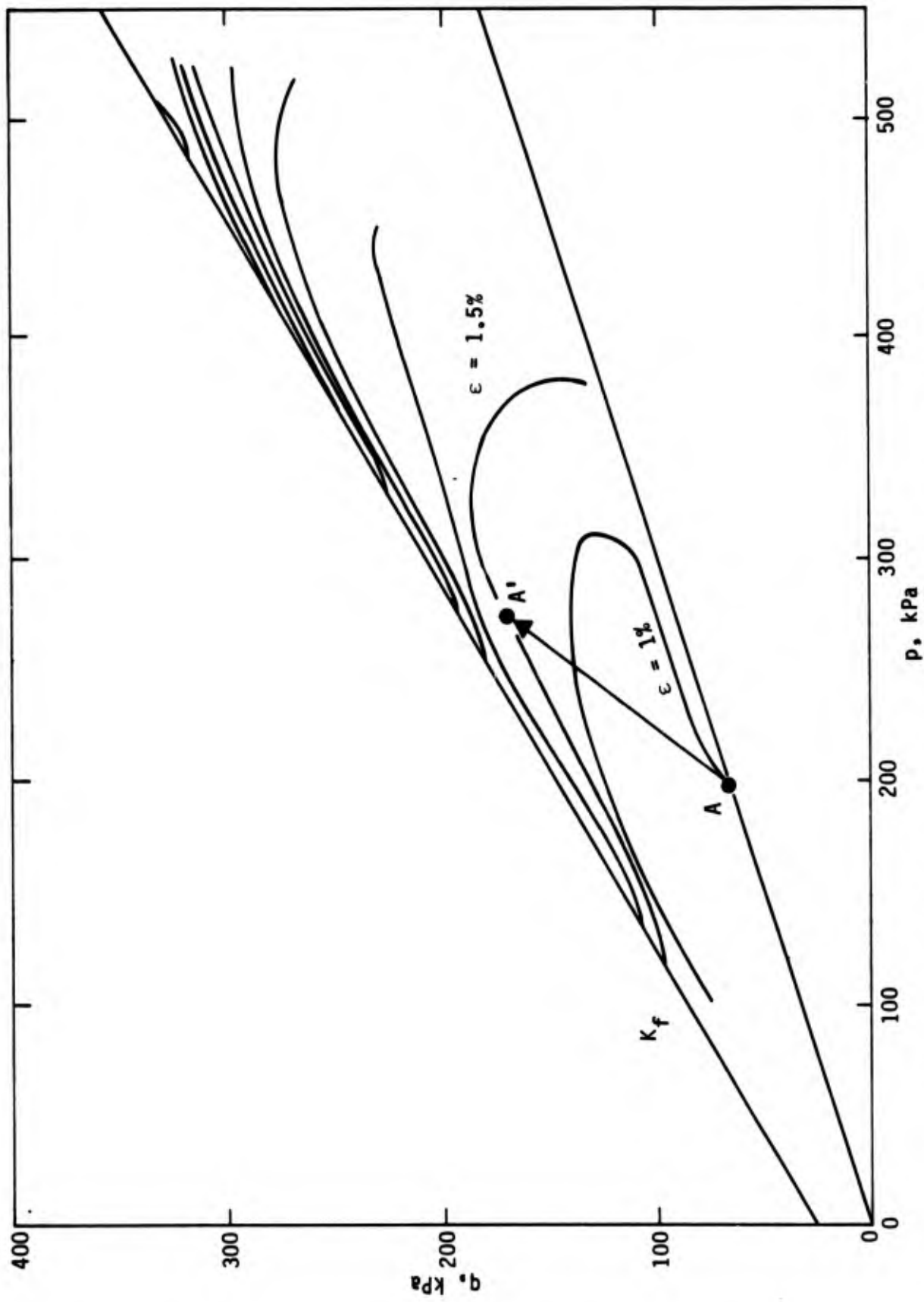
Figure 17. Contours of equal axial strain from stress path tests.

TABLE 4.   PARAMETERS FROM K_f LINES FOR VARIOUS
MOISTURE CONTENTS

w, %	β, deg	α, kPa	φ, deg	c, kPa
19	30	40.0	35.3	49.0
12.36	28	42.7	32.1	50.3
12.16	25	53.8	27.8	60.7

To check the reproducibility of the vertical stress paths, six tests were performed on samples at a moisture content of 18.8 percent. The results of these tests are shown in Table 5 and are plotted on Figure 16.

The K_f and K_0 lines shown on Figure 14 are repeated in Figure 17 along with contours of equal axial strains for points along the six stress paths. The use of this plot can be illustrated by considering point A, which represents soil consolidated at a specified condition, and point A', which represents a new state of stress. The axial strain that results from going from condition A to A' would be 0.5 percent. This strain would apply only for the soil and the moisture content for which the data were obtained.

CONCLUSION

A major result of this investigation is the discovery that conventional methods for measuring strains from triaxial tests on soil are not adequate for use in the development of constitutive models. Although no specific results are available, a promising method for measuring strains has been developed.

If average strains are used, the stress-strain curves of Figure 10 fall into two categories for both silt and clay. The two categories are defined by low and high values of axial strain at the peak stress. Low and high values of axial strain correspond to the upper and lower branches, respectively, of the suction potential curves shown in Figure 8. Another conclusion based on Figure 10 is that the limit values of stress may not depend on the suction potential, a finding that was unexpected. The correlation of strain and stress with suction potential will be extremely useful in the development of a constitutive model.

TABLE 5. RESULTS OF VERTICAL STRESS PATH TEST FOR REPRODUCIBILITY

Sample	w, %	p, kPa	q at failure, kPa	ε at failure, %	Suction, kPa	γ_{dry}, kg/m^3
1a	18.75	207	152	3.18	17.0	1626.0
1b	18.76	207	152	2.59	17.2	1625.1
1c	18.90	207	152	3.70	18.2	1626.0
2a	18.95	207	152	7.76	18.3	1618.3
2b	18.7	207	145	2.605	18.3	1632.8
2c	18.7	207	152	3.169	19.0	1628.9

V. PROPOSED WORK

The primary emphasis in this work phase has been on the development of an improved understanding of the behavior of concrete and geological materials and on the use of mathematical models to represent the observed response features. Advances in experimental observation have been made in the areas of rate effects in concrete, of suction potential in fine-grained soils, and of stress-strain data from triaxial tests. Significant improvements in modeling are reflected in strength predictions for concrete and in softening and strain localization phenomena. The work will be the basis for continued research on the fundamental behavior of concrete and soils.

The use of nonlocal constitutive relations holds great promise for problems involving strain localization, which is a characteristic associated with cracking, shear bands, and soil-concrete interfaces. Application of the theory to the latter case will be a significant aspect of the new work phase.

Development of the device for obtaining rate effects in concrete will continue until the proper type and amount of propellant can be specified routinely and the stress and strain components can be measured accurately under the specified thermal and dynamic environment. When this phase has been accomplished satisfactorily, a two-dimensional version of the device will be developed and will be used to obtain multiaxial stress-strain data.

Although limit stresses for concrete can be predicted accurately, the same is not true for strains at the limit state, where predictions may be in error by a much as 50 percent with the current version of the model. A concentrated effort will be made to investigate the source of this discrepancy. The damage theory proposed by Krajcinovic (Ref. 14) holds considerable promise. The essential idea is that an additional parameter, which at this stage of development may be a scalar, vector, or tensor, must be used to monitor the size and orientation of voids and microcracks. A description of the coalescence of voids and microcracks under three-dimensional states of stress is probably too ambitious to attempt, but it is possible that by merging damage theory with a viscoplastic model, one might obtain a useful engineering model. Preliminary investigations of this nature will be initiated by a comprehensive literature survey and an exploration of possible approaches.

41

Numerous data indicate the existence of anisotropic phenomena in concrete and soils. Anisotropy may stem from the basic structure of the material, such as that of conventional or fiber-reinforced concrete, or from the effect of a previous state of stress and strain. The scope of the existing viscoplastic model will be extended to incorporate anisotropic features, and theoretical and experimental data will be compared.

The experimental work on unsaturated fine-grained soils will be suspended temporarily with the conclusion of the present effort. The reason for the suspension is that the theoretical phase has not developed to a point at which a logical set of stress paths can be suggested for testing assumptions that are implicit in any model. Therefore, the focus of the next phase will be on using the experimental data that have been obtained so far to verify the use of the viscoplastic model for this class of soils.

Generally, the proposed work represents an effort to explore in more detail the fundamental response characteristics of concrete and soil. For each aspect that has been proposed, there is both a significant engineering need and very little, if any, corresponding effort by other research groups. Thus, this research can be considered both fundamental and of high potential value for technical applications.

REFERENCES

1. Steif, P. S., Spaepen, F., and Hutchinson, J. W., "Strain Localization in Amorphous Metals," **Acta Metallurgica,** Vol. 30, 1982, pp. 447-453.

2. Li, G. C., and Howard, I. C., "The Effect of Strain Softening in the Matrix Material During Void Growth," **Journal of the Mechanics and Physics of Solids,** Vol. 31, No. 1, 1983, pp. 85-102.

3. Bazant, Z. P., and Oh, B. H., "Crack Band Theory for Fracture of Concrete," **Materials and Structures,** (RILEM, Paris), Vol. 16, 1983, pp. 155-177.

4. Bazant, Z. P., "Determination of Nonlinear Fracture Parameters from Size Effect Tests," **Application of Fracture Mechanics to Cementitious Composites,** NATO Advanced Research Workshop, September 4-7, 1984, Northwestern University, Evanston, Illinois.

5. Bazant, Z. P., and Chang, Ta-Peng, "Instability of Nonlocal Continuum and Strain Averaging," **Journal of Engineering Mechanics,** Vol. 110, No. 10, 1984.

6. Gopalaratnam, V. S., and Shah, S. P., **Softening Response of Plain Concrete in Direct Tension,** The Technological Institute, Northwestern University, June 1984.

7. Huck, Peter J., et al., **Dynamic Response of Soil/Concrete Interfaces at High Pressure,** AFWL-TR-73-264, Air Force Weapons Laboratory, Kirtland Air Force Base, New Mexico, 1974.

8. De Beer, E., "Influence of the Mean Normal Stress on the Shearing Strength of Sand," **Proceedings of the 6th International Conference on Soil Mechanics and Foundation Engineering,** Montreal, Canada, September 8-15, 1965, Vol. I, pp. 165-169.

9. Vermeer, P A., "Frictional Slip and Nonassociated Plasticity," **Scandinavian Journal of Metalurgy,** Vol. 12, 1983, pp. 268-276.

10. Strijbos, S., and Vermeer, P. A., "Stress and Density Distributions in the Compaction of Powders," **Processing and Crystalline Ceramics** (Eds. H. Palmour, R. F. Davis, and T. M. Hare, Materials Science Research, Vol. II), Plenum Press, London, 1978, pp. 113-123.

11. Schreyer, H. L., **Development of a Third-Invariant Plasticity Theory for Concrete and Soils,** AFWL-TR-83-119, Air Force Weapons Laboratory, Kirtland Air Force Base, New Mexico, October 1984.

12. **Engineering Design Handbook: Propellant Actuated Devices,** AMCP 706-270, Department of the Army, U.S. Army Materiel Command, Alexandria, Virginia, 30 September 1975.

13. McKeen, R. G., **Design of Airport Pavements for Expansive Soils**, FAA-RD-81-25, Federal Aviation Administration, Washington, D.C., January 1981.

14. Krajcinovic, D., "Constitutive Equations for Damaging Materials," **Journal of Applied Mechanics**, Vol. 50, June 1983, pp. 355-360.

APPENDIX A*

LIMIT SURFACES FOR CONCRETE AND METALS

Howard L. Schreyer

.

Department of Mechanical Engineering and
The New Mexico Engineering Research Institute
University of New Mexico
Albuquerque, NM 87131

November 1984

----

*This appendix is a reproduction of a paper to be submitted for publication to the <u>Journal of Engineering Mechanics</u>. It is a self-contained document with its own internally consistent numbering system for equations, figures, and references.

INTRODUCTION

It has been generally assumed that, for metals, the surface defining the limit state is independent of mean pressure. One relation that has gained general acceptance because of its mathematical convenience and reasonably good agreement with experimental data is the surface obtained by setting the second invariant of the stress deviator equal to a constant. This surface is also known as the von Mises criterion. Recently, however, Casey and Jahedmotlagh (2) have emphasized the fact that at least some metals display a strength-differential effect, which is simply a manifestation of the dependence of the limit stress on mean pressure. This dependence is more commonly observed for concrete and geotechnical materials and is explicitly taken into account by Drucker and Prager (3), as a typical example.

Whether or not variations in pressure are included, the intersection of the von Mises surface and the deviatoric or pi plane is a circle. For many materials the experimentally determined shape is triangular rather than circular, and to represent theoretically the triangular shape, a third invariant of stress must be introduced. Criteria involving all three invariants (16) are quite successful because theoretical predictions based on these criteria agree well with experimental data.

Lade and Duncan (8) noticed that the limit state for a cohensionless soil could be represented adequately when only two invariants, the mean pressure and a particular combination of the three invariants of stress, were used. Lade (7) subsequently showed that concrete could be included in the theory. By considering a modification to Lade's approach, Schreyer (11) found that the limit surface could be transformed into a straight line, which offers some conceptual advantages for analyzing experimental data. These approaches have been used with some success as the basis for plasticity and viscoplasticity models (6, 12, 13).

In an attempt to apply the limit state criterion developed by Schreyer to a large amount of experimental data on concrete, Read (10) found a good correlation for data corresponding to large values of mean pressure and no correlation for those data associated with mean pressure close to zero. Read's

46

observation was the motivation for this study, with the result that the theory was modified through the use of a scaling factor on mean pressure. The scaling factor is significant near zero mean pressure and asymptotically approaches one for large mean pressure. Thus, the advantages of the theory have been retained and a deficiency has been removed.

An additional aspect of the newer formulation is that the parameters in the model can be given physical interpretations in a natural sense. For example, one parameter controls the shape of the intersection of the limit surface with the deviatoric plane so that both triangular and circular curves can be obtained. Pressure dependence can be conveniently adjusted, with the result that von Mises, Drucker-Prager, and more general surfaces are available with a single formulation. The theory is equally applicable to metals and concrete and perhaps will prove to be applicable to geotechnical materials, although the latter class is not considered in this paper.

DEVELOPMENT OF THE LIMIT SURFACE

In accordance with the development by Schreyer (11), define an invariant of the stress tensor, $\underset{\sim}{\sigma}$, by the relation

$$L = \frac{-[\det(\underset{\sim}{\sigma} - \underset{\sim S}{\sigma}) + \det \underset{\sim S}{\sigma}]^{1/3}}{\sigma 0} \tag{1}$$

in which det denotes the determinant, and the power of 1/3 is used so that the numerator has the dimension of stress. The reference stress σ_0 renders L dimensionless. With the assumption of isotropy,

$$\underset{\sim S}{\sigma} = \sigma_s \underset{\sim}{I} \tag{2}$$

where $\underset{\sim}{I}$ is the identity tensor, and σ_s is a material parameter.

It is instructive to develop alternate relations for L. In terms of the principal stresses σ_1, σ_2, and σ_3, and with the use of Eq. 2, the expression for L becomes

$$L = \frac{-[(\sigma_1 - \sigma_s)(\sigma_2 - \sigma_s)(\sigma_3 - \sigma_s) + \sigma^3]^{1/3}}{\sigma_0} \tag{3}$$

47

With the use of the mean pressure,

$$P = -1/3 \; tr \; \underline{\sigma} \tag{4}$$

where tr denotes the trace, the deviatoric stress tensor, $\underline{\sigma}^d$, is

$$\underline{\sigma}^d = \underline{\sigma} + P \; \underline{I} \tag{5}$$

Let the invariants of the stress deviator be

$$II^d = tr \; (\underline{\sigma}^d)^2$$

$$III^d = -det \; \underline{\sigma}^d \tag{6}$$

Then

$$L = \frac{[III^d - 0.5 \; (P + \sigma_s) \; II^d + (P + \sigma_s)^3 - \sigma_s^3]^{1/3}}{\sigma_0} \tag{7}$$

Postulate the existence of a unique surface that describes the limit state for all stress paths, and assume that this surface can be described by a general relation

$$L = f(P) \tag{8}$$

The implications of the assumption are that any single class of paths can be used to determine f and that the function will be equally valid for any other path. To be specific, consider paths for pure shear, which are defined as a hydrostatic state of stress followed by a simultaneous increase and decrease of two of the principal stresses; i.e., after the imposition of a hydrostatic stress, P, the principal stresses are given by

$$\sigma_1 = -P - S \quad \sigma_2 = -P + S \quad \sigma_3 = -P \tag{9}$$

for a monotonically increasing load parameter, S. Suppose the limit state in shear is given as a smooth function of P:

$$S = S_p \equiv S(P) \tag{10}$$

48

which may be determined from experimental data. If Eqs. 9 and 10 are substituted in Eq. 3, then Eq. 8 yields an expression for the general limit surface

$$f(P) = \frac{[(P + \sigma_s)^3 - S_p^2 (P + \sigma_s) - \sigma_s^3]^{1/3}}{\sigma_0} \tag{11}$$

For convenience, alternate variables are introduced. Let

$$S_0 = S_p(0) \tag{12}$$

and

$$L_0 \equiv f(0) = \frac{[-S_0^2 \sigma_s]^{1/3}}{\sigma_0} \tag{13}$$

Subtract L_0 from both sides of Eq. 8 and define a stretched parameter for mean pressure as follows:

$$P* = f(P) - L_0 \tag{14}$$

Then the limit surface defined by Eq. 8 becomes the linear relation

$$L = P* + L_0 \tag{15}$$

with the parameter σ_s and the parameters used to define S_p adjusted to optimize a fit to experimental data.

Suppose both sides of Eq. 15 are cubed. Then the use of Eqs. 7, 11, and 14 yields

$$III^d - (P + \sigma_s)\left(\frac{II^d}{2} - S_p^2\right) = 0 \tag{16}$$

For large values of $P + \sigma_s$, the limit surface reduces to

$$II^d = 2 S_p^2 \tag{17}$$

49

which is the criterion of Drucker and Prager (3) if S_p is linear in P. If S_p is constant, the von Mises criterion is obtained.

The shape of the intersection of the limit surface with the deviatoric or pi plane is frequently of interest. To obtain such a curve it is useful to employ coordinates q_1, q_2 in this plane and a third coordinate, q_3, perpendicular to the plane. One choice, which has been used previously (11) is

$$q_1 = \frac{(\sigma_1 - \sigma_2)}{\sqrt{2}}$$

$$q_2 = \frac{(2\sigma_3 - \sigma_1 - \sigma_2)}{\sqrt{6}}$$

$$q_3 = \frac{-(\sigma_1 + \sigma_2 + \sigma_3)}{\sqrt{3}} \qquad (18)$$

The inverse relations, in terms of principal stress and principal stress deviator components, are

$$\sigma_1 = \frac{1}{\sqrt{2}} q_1 - \frac{1}{\sqrt{6}} q_2 - \frac{1}{\sqrt{3}} q_3$$

$$\sigma_2 = \frac{-1}{\sqrt{2}} q_1 - \frac{1}{\sqrt{6}} q_2 - \frac{1}{\sqrt{3}} q_3$$

$$\sigma_3 = \frac{2}{\sqrt{6}} q_2 - \frac{1}{\sqrt{3}} q_3 \qquad (19)$$

and

$$\sigma_1^d = \frac{1}{\sqrt{2}} q_1 - \frac{1}{\sqrt{6}} q_2$$

$$\sigma_2^d = \frac{-1}{\sqrt{2}} q_1 - \frac{1}{\sqrt{6}} q_2$$

$$\sigma_3^d = \frac{2}{\sqrt{6}} q_2 \qquad (20)$$

respectively.

It follows that

$$II^d = q_1^2 + q_2^2$$

$$III^d = \frac{q_2}{3\sqrt{6}} (3q_1^2 - q_2^2) \tag{21}$$

which can be substituted in Eq. 16 to obtain an expression for the limit surface in q-space.

Typical limit curves in the q_1-q_2 plane are shown in Figure 1 for $S_p = 1$ and for various values of the sum $P + \sigma_s$. For small values of $P + \sigma_s$, a triangular shape is obtained. Because this shape is characteristic of limit surfaces for concrete and geotechnical materials at small values of mean pressure, these materials can be characterized by small values of σ_s. For large values of $P + \sigma_s$, the limit curve is circular. This behavior is consistent with experimental observations of concrete and geotechnical materials because the limit curve is generally believed to transition from a triangular to a circular shape as P increases. For metals, the circular shape is observed for all values of P; therefore, the correct behavior is obtained by choosing a large value for σ_s.

Thus, the parameter σ_s delineates the shape of the limit surface in the deviatoric plane, and the function S(P) describes the size of the surface as a function of mean pressure.

DEFINITION OF MATERIAL PARAMETERS

Uniaxial stress in compression is one path that is typically considered. Suppose the limit state is reached when

$$\sigma_1 = -f'_c \quad \sigma_2 = \sigma_3 = 0 \tag{22}$$

The mean pressure is $f'_c/3$. Let

$$S_c = S_p\left(\frac{f'_c}{3}\right) \tag{23}$$
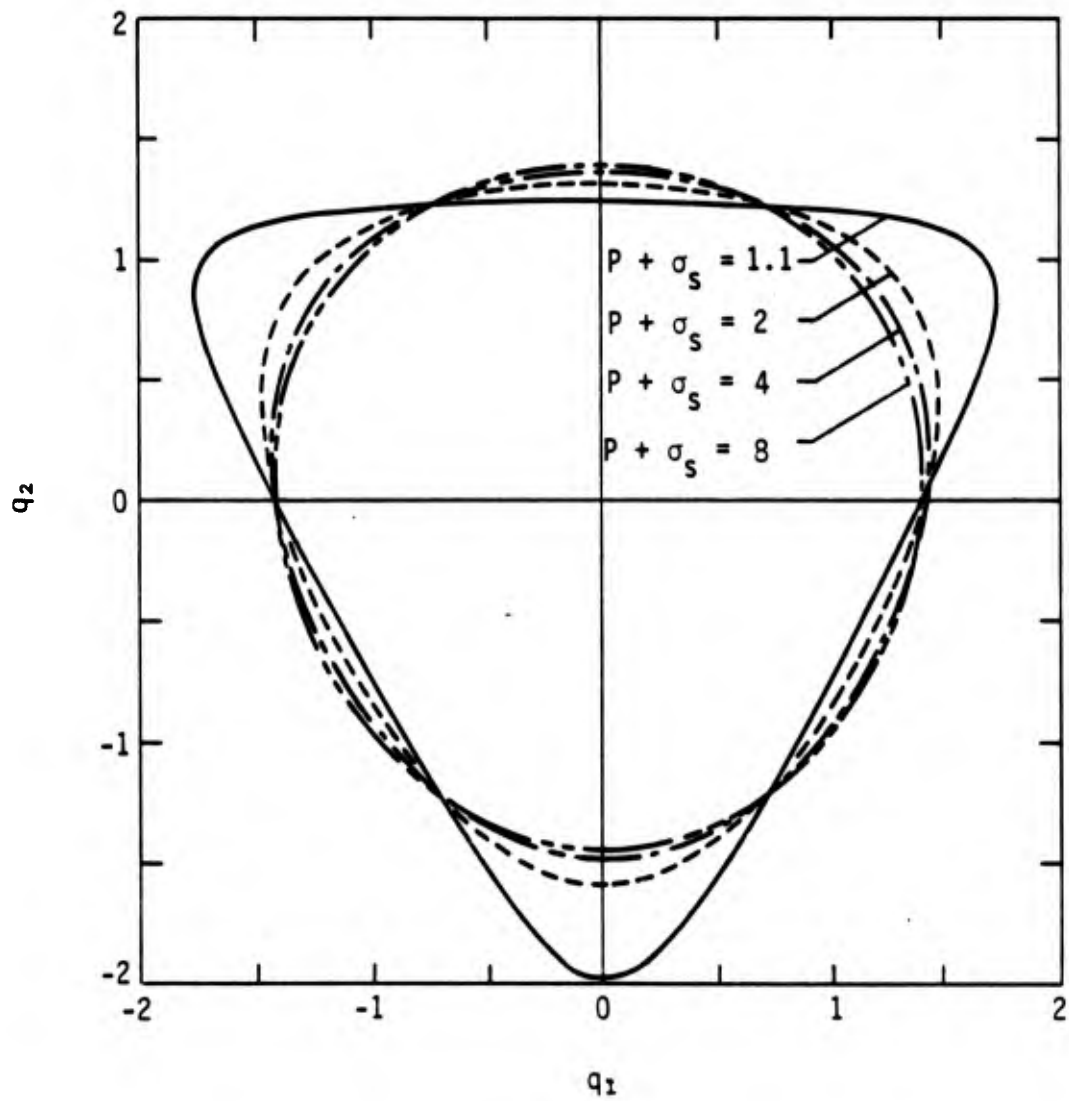
Figure A1. Typical limit curves in the q_1-q_2 plane for $S_p = 1$ and various values for the sum $P + \sigma_s$.

The use of Eq. 16 indicates that the material parameters must be related by the following expression:

$$\sigma_s = \frac{f_c'}{3} \frac{[S_c^2 - (f_c'/3)^2]}{(f_c'/\sqrt{3})^2 - S_c^2} \tag{24}$$

For example, if the simple shear-stress criterion, $S = f_c'/2$, is used, then $\sigma_s = 5/9 \, f_c'$. In general, σ_s can range from 0 to ∞, which implies that the function S_p must be chosen such that the value S_c satisfies the inequality

$$\frac{f_c'}{3} \leq S_c \leq \frac{f_c'}{\sqrt{3}} \tag{25}$$

In practice, Eq. 25 is not a severe constraint.

To be specific, it is assumed that S_p varies from a value of zero at $P = P_0$ (presumably negative) to a maximum vlaue S_m, which is asymptotically reached for large values of P. A function that provides this general feature is

$$S_p = S_m \left[1 - \exp\left(\frac{P_0 - P}{P_D}\right) \right] \qquad \begin{array}{l} P_D > 0 \\ P > P_0 \end{array} \tag{26}$$

where P_D controls the rate at which S_p approaches the value S_m. With the assumption of Eq. 26,

$$S_0 = S_m \left[1 - \exp\left(\frac{P_0}{P_D}\right) \right] \tag{27}$$

from which it follows that a cohesionless material defined by $S_0 = 0$ is modeled by choosing $P_0 = 0$.

An estimate for P_d can be obtained by using an inverted form of Eq. 26 as follows:

$$P_D = \frac{P - P_0}{\ln [S_m/(S_m - S_p)]} \tag{28}$$

and a data point that provides values for P and S_p.

DETERMINATION OF MATERIAL PARAMETERS

A personal computer and an interactive program were used to select material parameters for several materials. The procedure follows:

1. Select starting values for σ_s, S_m, P_0, and P_D. If the uniaxial compressive strength f'_c is the only convenient data point, the values $\sigma_s = 5/9\, f'_c$, $S_m = 2\, f'_c$, and $P_0 = -f'_c/10$ are often reasonable. With the assumption that $S_p\ (f'_c/3) = f'_c/2$, Eq. 28 yields $P_D = 0.43\, f'_c/\ln(4/3)$.

2. For each data point, and with $\sigma_0 = f'_c$, compute L and $P\ast$ from Eq. 1 or 3 and Eq. 14, respectively.

3. Determine the parameters α and β that provide the optimal fit of the straight line

$$L = \alpha P\ast + \beta \tag{29}$$

to the set of points obtained in step 2.

4. By trial and error, adjust the parameters σ_s, S_m, P_0, and P_D so that $\alpha = 1$, $\beta = L_0$, and the coefficient of correlation is as close to unity as possible. Experience indicates that the coefficient of correlation is most sensitive to σ_s, whereas α and β are most affected by S_m and P_0, respectively.

CORRELATION WITH EXPERIMENTAL DATA

Values of the material parameters are given in terms of f_c' in Table 1 for a large number of experimental data. For all cases, the coefficient of correlation is unity to within two significant figures. Those data obtained by Mills and Zimmerman (9), Bresler and Pister (1), and Goode and Henny (4) are labeled as MZ, BP, and GH, respectively. Groupings according to the values of f_c' are labeled A, B, etc., and follow those used by the original authors. The data from Goode and Henny (4) and Bresler and Pister (1) include pure torsion; therefore, it is apparent that the fit is now equally good in the region of small values of mean pressure. Typical results for data from Bresler and Pister and from Mills and Zimmerman are shown in the P*-L plane in Figure 2 and in the P-L plane in Figure 3. In the P-L plane, an extrapolation of data obtained for large values of P indicates a positive intercept of the L-axis, which is contrary to experimental observations. This discrepancy, observed by Read (10), illustrates the need for the stretched parameter P*.

Although the number of data points is limited, Green and Swanson (5) have provided typical data for high-strength concrete. The corresponding parameters are labeled GS in Table 1. A large number of data for a weak concrete was provided by Traina et al. (15), with some points involving tensile states of stress. Parameters for this concrete are labeled T and are also included in Table 1. Plots for the Traina data are not included because the limit state is a straight line for all cases. In fact, if $-L_0$, rather than f_c', is used for σ_0, the limit state for all these concretes consists of a single line.

Yield and limit states for high-strength steel may also display dependence on mean pressure. For the data provided by Spitzig et al. (14), the parameters that provide a fit to the limit state of AISI 4330 steel, expressed in MPa, are the following: $\sigma_s = 4480$, $S_m = 1380$, $P_0 = -2920$, and $P_D = 1000$. Corresponding parameters for a fit to the yield state are $\sigma_s = 3450$, $S_m = 1380$, $P_0 = -4030$, and $P_D = 2330$. The large values for σ_s indicate a circular shape for the intersection of the surfaces in the deviatoric plane. The appearance of the same value of S_m for both states is explained by the observation that the maximum value in shear for the yield state is reached at

55

TABLE A1. MATERIAL PARAMETERS FOR VARIOUS CONCRETES AND A STEEL

Source	f'_c, MPa	σ_s/f'_c	S_m/f'_c	P_0/f'_c	P_D/f'_c
MZ-A	24.1	2.0	2.0	-0.159	1.5
MZ-B	27.6	0.55	2.03	-0.0864	1.5
MZ-C	35.8	0.865	1.73	-0.219	1.5
BP-A	20.7	0.567	2.37	-0.0513	1.5
BP-B	29.3	0.353	2.24	-0.0517	1.5
BP-C	41.4	0.567	2.33	-0.0428	1.5
GH-A	35.9	0.558	2.50	-0.0267	1.5
GH-B	33.1	0.563	2.33	-0.0383	1.5
$GH-C_{12}$	30.0	0.552	2.37	-0.0446	1.5
$GH-C_3$	19.3	0.571	2.25	-0.0607	1.5
GH-DE	16.5	0.625	2.50	-0.0481	1.5
GS	48.3	0.56	1.80	-0.136	1.5
T	21.0	0.57	1.90	-0.0681	1.5
SSR-Y	1550	22.2	0.889	-2.60	1.5
SSR-L	2010	22.3	0.687	-1.46	0.5
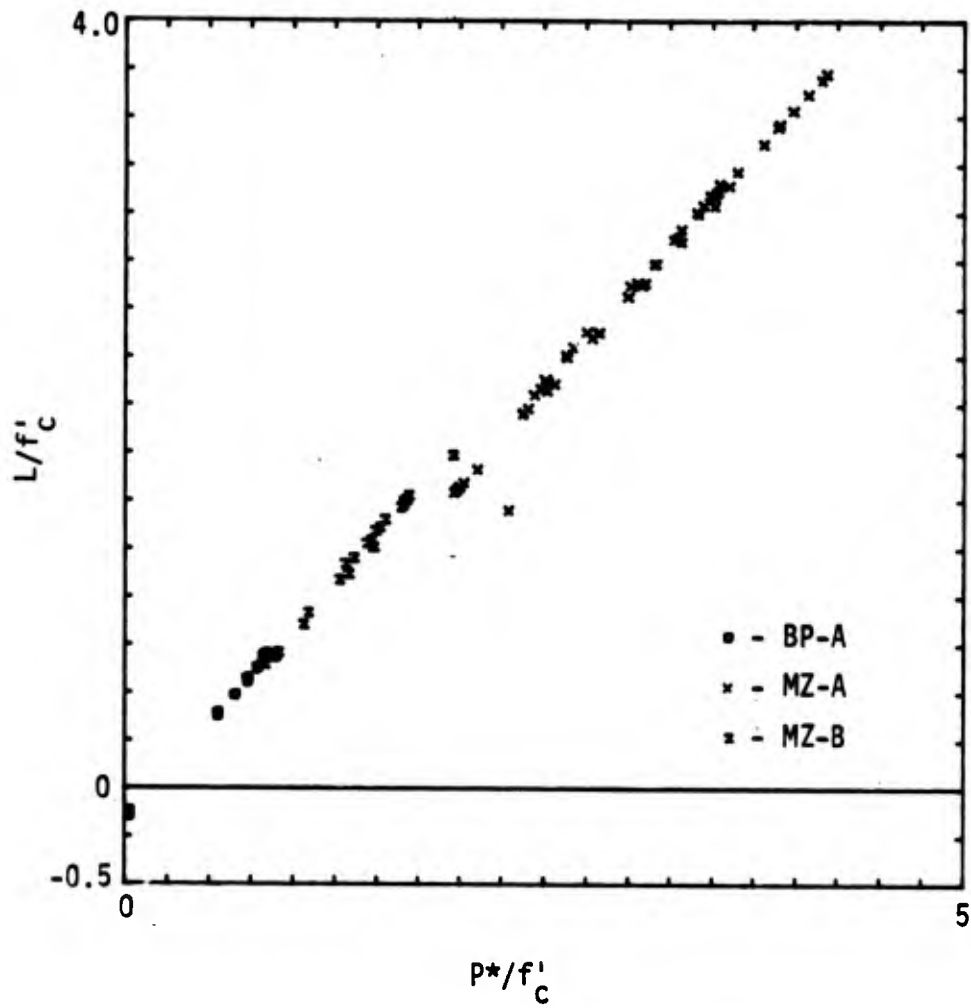
Figure A2. Typical results for the data from Bresler and Pister and from Mills and Zimmerman in the P*-L plane.

57
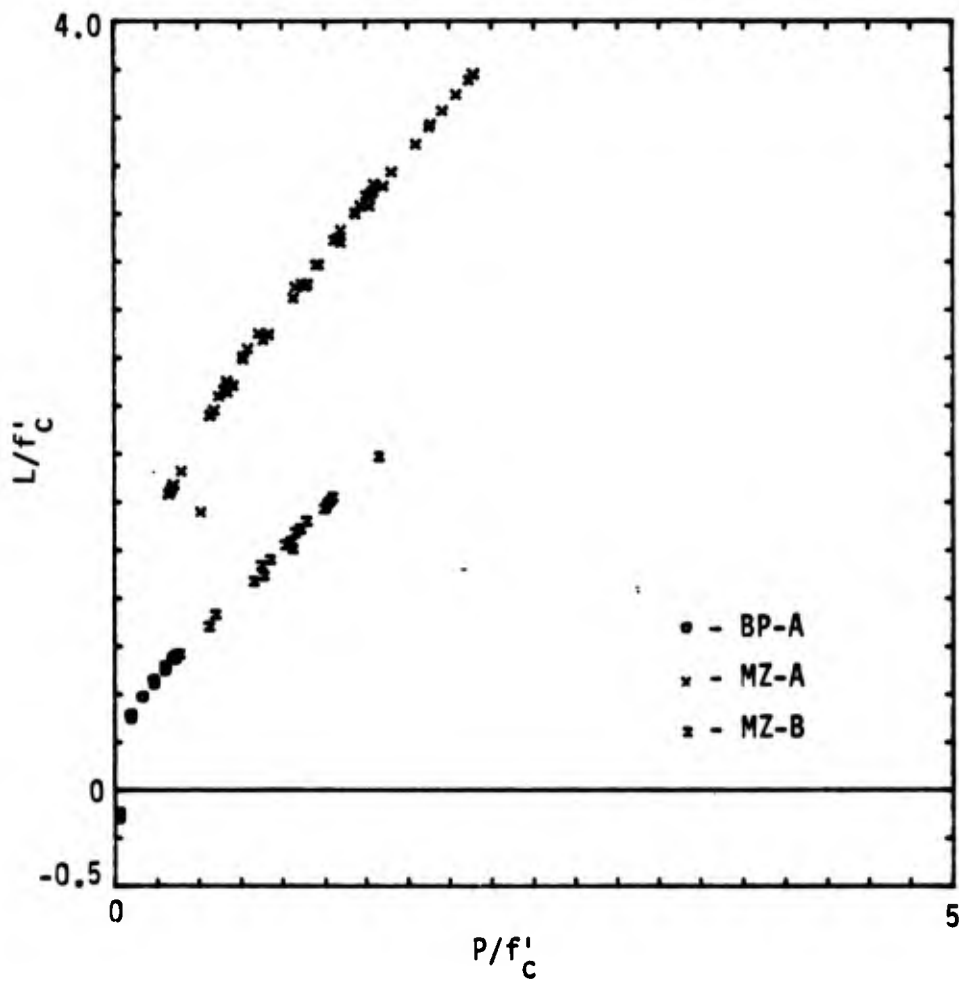
Figure A3. Typical results for the data from Bresler and Pister and from Mills and Zimmerman in the P-L plane.

a value of P_D that is much larger than the value of P_D for the limit state. For illustrative purposes, the parameters for steel at the yield and limit states are also included in Table 1 with the designations SSR-Y and SSR-L, respectively.

When the coefficients in the model are expressed in terms of the maximum stress in uniaxial compression, a consistent pattern appears. The ratio σ_s/f'_c is approximately 0.5 for concrete, which indicates a triangular shape in the deviatoric plane (a large value for steel denotes a circular shape). The maximum value for shear, S_m/f'_c, is of the order 2 for concrete and less than 1 for steel. The absolute value of P_0/f'_c is relatively small for concrete. The larger value for steel indicates the greater tensile carrying capacity of steel. The rate at which the maximum shear strength is attained with an increase in mean pressure, as exhibited by the parameter P_D/f'_c, shows that relatively more mean pressure is required for concrete than for steel to attain a maximum shear bearing capacity. All of these results are intuitively plausible and indicate that the model may be useful to engineers concerned with strength predictions.

CONCLUSION

A model containing parameters that have simple physical interpretations has been established for the limit state in stress. The parameter P_0 corresponds to a tensile cutoff expressed in terms of a mean stress. The maximum shear stress the material is capable of sustaining at high values of mean pressure is denoted by S_m. The shape of the limit surface in the deviatoric plane is governed by σ_s, and the parameter P_D governs the rate at which strength increases with mean pressure.

The model appears to be applicable to a large class of materials that includes concrete and metals. A good model for the limit state or the initial yield state is often the basis for a plasticity or viscoplasticity constitutive relation. The result of this study indicates that it may be feasible to use a single model for a much larger range of material behavior than has been considered until now.

59

APPENDIX - REFERENCES

1. Bresler, B. and Pister, K. S., "Strength of Concrete Under Combined Stress," _Journal of the American Concrete Institute_, Sept. 1958, pp. 321-345.

2. Casey, J. and Jahedmotlagh, H., "The Strength-Differential Effect in Plasticity," _International Journal of Solids and Structures_, Vol. 20, No. 4, 1984, pp. 377-393.

3. Drucker, D. C., and Prager, W., "Soil Mechanics and Plasticity Analysis of Limit Design," _Quarterly of Applied Mathematics_, Vol. 10, 1952, pp. 157-165.

4. Goode, C. D., and Henny, M. A., "The Strength of Concrete Under Combined Shear and Direct Stress," _Magazine of Concrete Research_, Vol. 19, No. 59, June 1967, pp. 105-112.

5. Green, S. J., and Swanson, S. R., _Static Constitutive Relations for Concrete_, AFWL-TR-72-244, Air Force Weapons Laboratory, Kirtland Air Force Base, New Mexico, 1973.

6. Lade, P. V., "Elasto-Plastic Stress-Strain Theory for Cohesionless Soil with Curved Yield Surfaces," _International Journal of Solids and Structures_, Vol. 13, 1977, pp. 1019-1035.

7. Lade, P. V., "Three Parameter Failure Criterion for Concrete," _Journal of the Engineering Mechanics Division_, ASCE, Vol. 108, 1982, pp. 850-863.8.

8. Lade, P. V., and Duncan, J. M., "Cubical Triaxial Tests on Cohensionless Soil," *Journal of Soil Mechanics Foundation Division*, ASCE, Vol. 99, 1973, pp. 793-812.

9. Mills, L. L., and Zimmerman, R. M., "Compressive Strength of Plain Concrete Under Multiaxial Loading Conditions," *Journal of the American Concrete Institute*, Oct. 1970, pp. 802-807.

10. Hegemier, G. A., Read, H. E., Murakami, H., Hageman, L. J., and Herrmann, R. G., *Development of Advanced Constitutive Model for Reinforced Concrete*, SSS-R-83-6112, Report submitted to Air Force Office of Scientific Research by S-Cubed, La Jolla, California, April 1983.

11. Schreyer, H. L., "A Third-Invariant Plasticity Theory for Frictional Materials," *Journal of Structural Mechanics*, Vol. 11, No. 2, 1983, pp. 177-186.

12. Schreyer, H. L., and Bean, J. E., "A Third-Invariant Viscoplasticity Theory for Rate-Dependent Soils," *Journal of Geotechnical Engineering*, Vol. 111, No. 2, February 1985, pp. 181-192.

13. Schreyer, H. L., and Babcock, S. M., "A Third-Invariant Plasticity Theory for Low-Strength Concrete," to appear in the *Journal of Engineering Mechanics*.

14. Spitzig, W. A., Sober, R. J., and Richmond, O., "Pressure Dependence of Yielding and Associated Volume Expansion in Tempered Martensite," *Acta Metallurgy*, Vol. 23, 1975, pp. 885-893.

15. Traina, L. A., Babcock, S. M., and Schreyer, H. L., *Reduced Experimental Stress-Strain Results for a Low-Strength Concrete Under Multiaxial States of Stress*, AFWL-TR-83-3, Air Force Weapons Laboratory, Kirtland Air Force Base, New Mexico, May 1983.

16. Willam, K. J., and Warnke, E. P., "Constitutive Model for the Triaxial Behavior of Concrete," <u>International Association of Bridges and Structures Subjected to Triaxial Stresses</u>, Paper III-1, Gergamo, Italy, May 17-19, 1974.

THE EFFECT OF LOCALIZATION ON THE SOFTENING
BEHAVIOR OF STRUCTURAL MEMBERS

This appendix is a reproduction of a paper presented at the American Society of Mechanical Engineers Annual Winter Meeting in New Orleans, 10-14 December 1984. The paper will appear in the proceedings of the Symposium on Constitutive Equations: Micro, Macro, and Computational Aspects. It is a self-contained document with its own internally consistent numbering system for equations, figures, and references.

THE EFFECT OF LOCALIZATION ON THE SOFTENING
BEHAVIOR OF STRUCTURAL MEMBERS

H. L. Schreyer
Z. Chen

Department of Mechanical Engineering and
New Mexico Engineering Research Institute
University of New Mexico
Albuquerque, NM 87131

ABSTRACT

Experimental results indicate that softening deformation is localized to a
relatively small region for segments of beams with constant bending moment. The
implication of this observation for the formulation of constitutive equations is
that a localization parameter must be incorporated into the model. For a simple
softening model, the effect of the magnitude of this parameter is investigated.
Results are given as load-displacement curves for beams.

If the parameter is small enough, or if a characteristic dimension of the
beam is large enough, the load-displacement curve can double back on itself.
The consequence of this feature is that even for displacement-controlled loading
devices the response may be unstable. Furthermore, if the possibility of
dynamic disturbances or stiffness imperfections is admitted, then the failure
load may be less than the limit load. This approach yields a nondimensional
failure load that decreases with the size of the structure and represents
another manifestation of the size effect. However, the lower limit of the fail-
ure load is not zero for realistic material parameters.

If the localization parameter is large, conventional softening behavior is
obtained and it becomes feasible to develop inversely moment-curvature relations
from load-displacement curves.

INTRODUCTION

If a structural member is loaded with a displacement-prescribed device, the
resulting load-displacement curve usually consists of a monotonically increasing
load up to the limit value and then a smooth reduction with a further increase
in displacement. The post-peak response, which is often called the strain-
softening regime, has recently come under intense scrutiny in an effort to make
designs less conservative. This attitude is appropriate for impulsive dynamic
loads and for static loads if there is a high degree of structural
indeterminacy.

Analyses that attempt to predict the post-peak response of beam structures
must involve a moment-curvature or constitutive relation that describes harden-
ing and softening at any point of each beam. Such moment-curvature relations

64

must be derived from a constitutive relation for the continuum or from experiments. However, even though load-deflection data are often available, it is not true that the corresponding moment-curvature relation is known. Consequently, the feasibility of obtaining moment-curvature functions indirectly from load-displacement experimental data for simple beam structures is questionable in light of the observation that in the softening regime, large strains are usually localized into small regions. This feature must be taken into account if correct moment-curvature relations are to be obtained.

Bazant [1] and Bazant and Panula [2] have discussed several aspects of strain localization including instability, ductility, and the size effect of concrete members. To a great extent, this paper can be viewed as an extension of these previous studies because it is assumed here, a priori, that strain localizes into a small but finite region. For beams, the measure of strain is taken to be the curvature; and although experimental evidence indicates that the region of localization decreases with increases in strain, the assumption is made that this region remains fixed. Such a restriction permits an investigation of the effect of the size of the localized softening region within the realm of elementary mechanics. Equilibrium paths can be established and the question of stability can be determined according to the nature of the loading system.

To illustrate the implication of localized softening in as simple a manner as possible, a symmetrically loaded four-point beam with simple supports is used as a model problem. For this geometry, the central region is one of uniform moment. Experimental evidence indicates that softening does not occur uniformly over this region if it is large enough; instead, softening is localized into a smaller region. For a given moment-curvature function, the extent of the area of localization can have a significant effect on the load-deflection relation. Naturally, a similar statement holds for the inverse problem. For a particular moment-curvature relation, analytical expressions are obtained that show the effect on the load-deflection relation of changes in the length of the localization region. An interesting result is that if the localization is severe enough, the load-deflection curve can turn back on itself after the peak load is reached, which implies that unstable states of equilibrium exist even for a displacement-controlled loading device. Furthermore, for small dynamic perturbations from the original stable loading path, or for imperfections in stiffness, it is possible to reach the unstable states with the consequence that the practical ultimate load can be much below the idealized ultimate load. The stability approach may be an alternate explanation for the size effect in the failure of beams composed of brittle materials, which has also been discussed recently by Bazant [3].

The theory is also applied to a more ductile case consisting of a reinforced concrete beam for which load-deflection data are available, and a moment-curvature relation is derived therefrom. If the localization length can be considered a legitimate material parameter, then the moment-curvature relation and the parameter can be used in the numerical analysis of more complex configurations in a procedure similar to that suggested by Riks [4] and Wempner [5].

PROBLEM AND SOLUTION TECHNIQUE

Consider a simply supported beam of length 2L loaded symmetrically with two concentrated loads of magnitude P. To allow for localized softening, one-half the beam is divided into the three regions shown in Fig. 1a. Because the problem is statically determinate, the moment diagram will always assume the form shown in Fig. 1b, where the peak moment is given by

$$M^* = PL_a \qquad (1)$$

and L_a denotes the distance between the simple support and the point of application of the load.

65
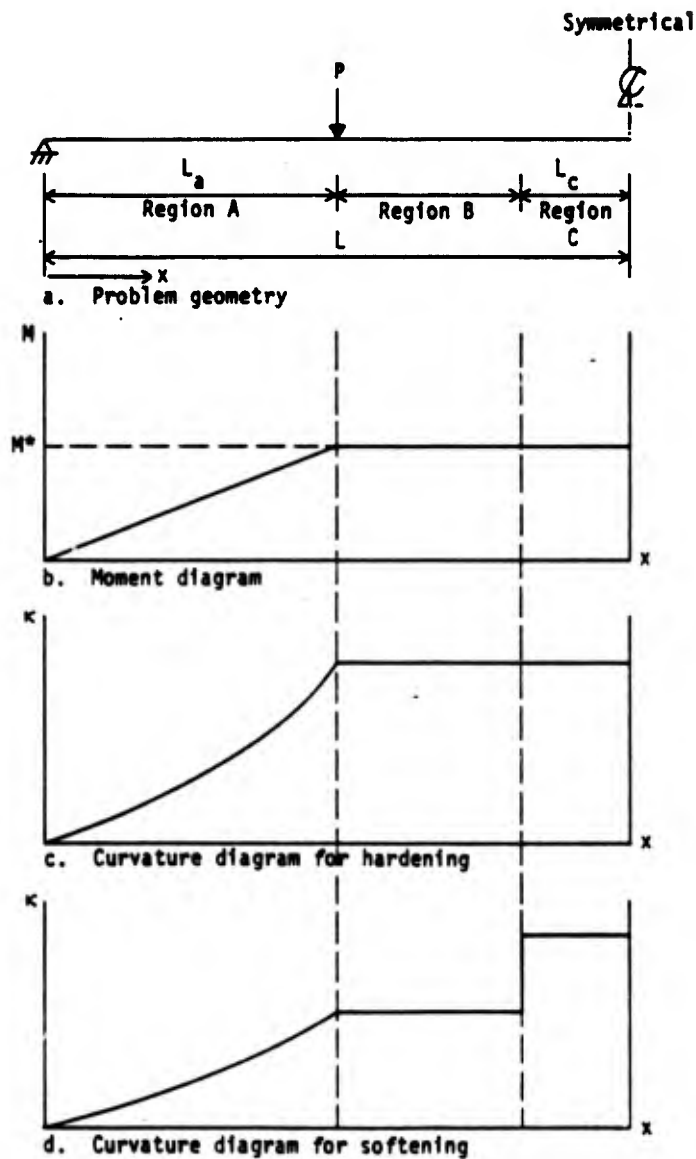
Figure B1.   Problem description

    A smooth hardening and softening behavior is assumed for the generic
moment-curvature (M-κ) relation illustrated in Fig. 2. Unloading occurs along
the straight line with slope E. This relation is assumed to hold everywhere,
except that in Region C, which is of length L_c, the peak moment is slightly less
than the value, M_0. The assumption forces softening to occur only in Region C.
The softening could exist anywhere between the applied forces and, indeed, most
experiments show that the softening region is located next to one of the loading
points. The choice of Region C forces symmetry, but it is believed that essen-
tial points will still be demonstrated. It is assumed further that in Region C
the curvature is constant and that L_c is a constant.
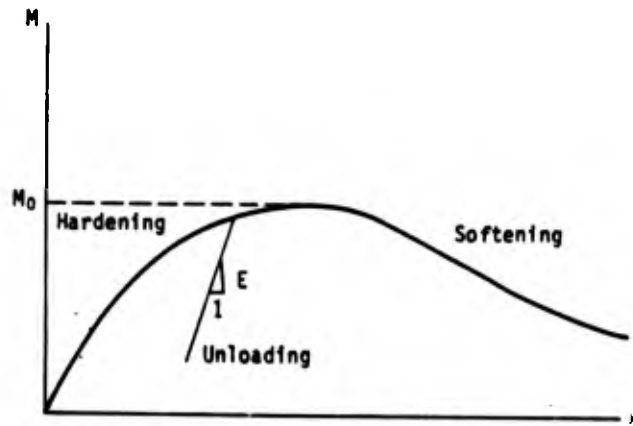
Figure B2. A generic moment-curvature relation

To obtain a load-deflection curve, suppose that the curvature in Region C is a monotonically increasing parameter. For a given increment in curvature, the moment-curvature diagram yields the increment in moment in Region C and consequently in Regions A and B as well. With due allowance for a loading or unloading condition, the increments in curvature in Regions A and B are also obtained from the moment-curvature relation. If all points in the beam are in the hardening regime, the curvature diagram will appear as shown in Fig. 1c; whereas if softening has occurred, there will be a discontinuity in curvature as shown in Fig. 1d.

If an increment in deflection, Δw, is taken to be positive downward in Fig. 1, an increment in curvature is given by

$$\Delta \kappa = -\Delta w,_{xx} \tag{2}$$

For Region A, the curvature and its increment are functions of x. Let

$$I_a(x) = \int_0^x \Delta \kappa(\hat{x}) d\hat{x} \tag{3}$$

so that the difference in slope between the ends of this region is

$$I = I_a(L_a) \tag{4}$$

Increments in curvature in Regions B and C are denoted by the constants $\Delta \kappa_b$ and $\Delta \kappa_c$, respectively. The integration of Eq. (2) and the imposition of continuity of deflection and slope, together with the boundary conditions of zero displacement at the left support and zero slope at the center line, yield

$$\Delta \delta = I L_a - J \pm \frac{\Delta \kappa_b}{2} (L - L_a - L_c) (L + L_a - L_c) + \frac{\Delta \kappa_c}{2} L_c (2L - L_c) \tag{5}$$

in which δ represents the deflection of the center point, and

$$J = \int_0^{L_a} I_a(x) dx \tag{6}$$

If increments in curvature are determined for each region by the use of equilibrium and Eq. (1), then Eq. (5) provides the corresponding increment in displacement.

67

ILLUSTRATIVE SOLUTIONS

Consider the piecewise linear moment-curvature relation shown in Fig. 3, which represents a crude approximation of the "exact" relation in Fig. 2. The hardening and softening parameters are designated by α and β, respectively. The corresponding load-deflection curve is represented symbolically in Fig. 4. The parameter n characterizes the softening portion of the load-deflection relation with a positive value representing the region to the right that is commonly seen in experiments. A vertical drop is denoted by $n = \pm\infty$, and the possibility of a solution doubling back from the peak values for P and δ is permitted through negative values of n.

In the hardening regime it is clear that increments in curvature are given by

$$\Delta\kappa_a = \frac{\Delta P}{\alpha E} x$$

$$\Delta\kappa_b = \Delta\kappa_c = \frac{\Delta P L_a}{\alpha E} \tag{7}$$

for an increment in force, ΔP. It follows from Eqs. (3), (5), and (6) that if

$$K = \frac{6E}{L_a(3L^2 - L_a^2)} \tag{8}$$

then

$$\frac{\Delta P}{\Delta\delta} = \alpha K \tag{9}$$

The softening regime is characterized by a negative value for ΔP and a positive value for $\Delta\kappa_c$. For linear unloading in Regions A and B, it follows that

$$\Delta\kappa_a = \frac{\Delta P}{E} x$$

$$\Delta\kappa_b = \frac{\Delta P}{E} L_a \tag{10}$$

$$\Delta\kappa_c = \frac{-\Delta P}{\beta E} L_a$$

and consequently that

$$\frac{\Delta P}{\Delta\delta} = -nK \tag{11}$$

where

$$n = \frac{-\ell_0^2}{\left[3\ell_c^2 - 6\ell_c + \ell_0^2\right]} \tag{12}$$

and

$$\ell_0^2 = \frac{\beta}{1 + \beta}\left(3 - \ell_a^2\right) \tag{13}$$

The dimensionless parameters

$$\ell_a = \frac{L_a}{L}; \qquad \ell_c = \frac{L_c}{L} \tag{14}$$

characterize the location of the load and the size of the localized softening region, respectively.
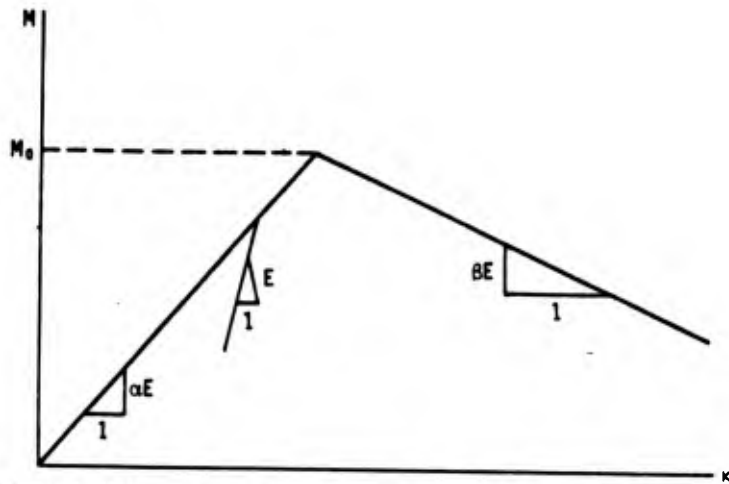
Figure B3. Approximate moment-curvature relation
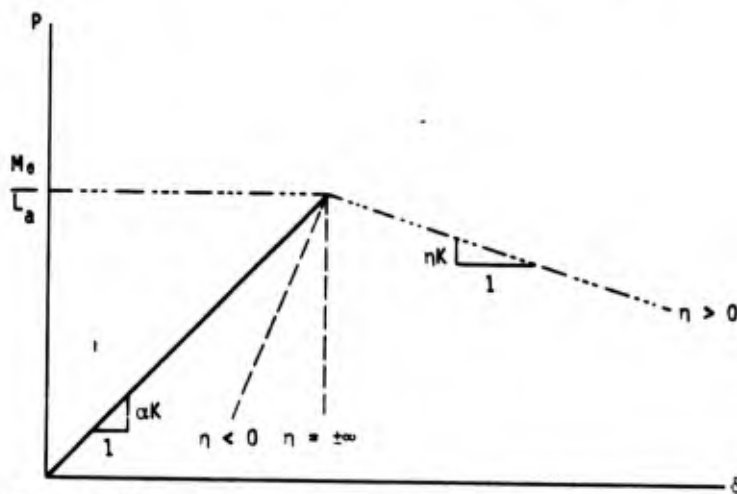
Figure B4. Possible equilibrium paths for a beam

The character of the response of the beam is reflected through the parameter n. As expected, if $\beta = 0$ then $n = 0$ for any value of ℓ_c. As the sketch in Fig. 5 shows, a complete spectrum of values for n is possible including the values of $\pm\infty$ when

$$\ell_c = \ell_c^* \equiv 1 - \left(1 - \frac{\ell_0^2}{3}\right)^{1/2} \tag{15}$$

The case given by Eq. (15) might be described as abrupt rupture, which holds for any value of β greater than zero. In particular, it is not necessary that $\beta = \infty$, which is the usual condition associated with rupture. It is more meaningful to consider two classes of problems: one for which $\ell_c > \ell_c^*$ and n is positive, and one for which $\ell_c < \ell_c^*$ and n is negative. The softening behavior for which n is positive can probably be handled by using existing computational techniques. An example is provided in the next section. For the moment, the possibility of negative values of n will be considered.
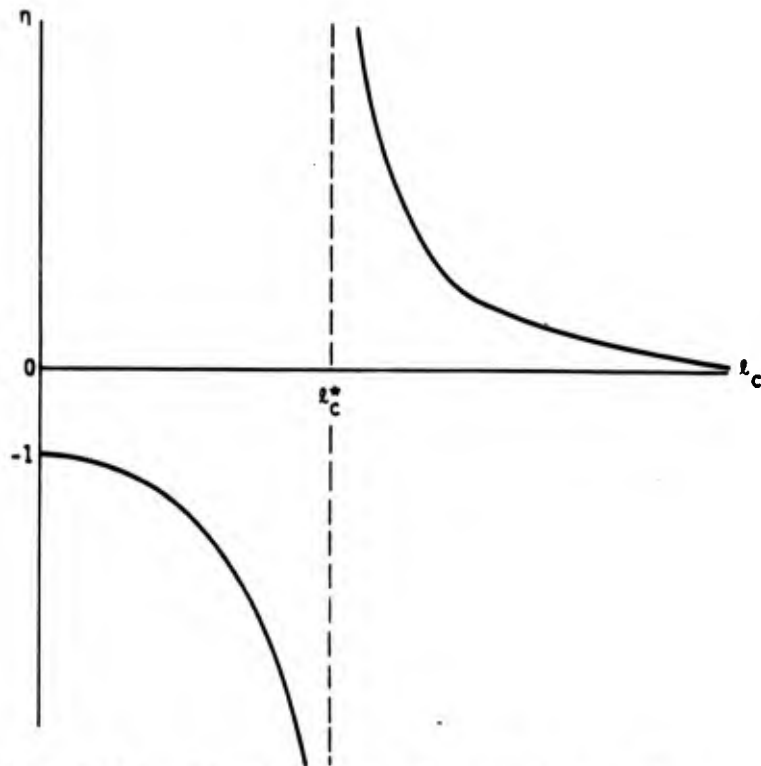
Figure B5. General behavior of n as a function of ℓ_c

If n is negative, it can be immediately concluded that once the limit load is reached, the structure is unstable even for a displacement-prescribed loading condition. An attempt to load the structure past the limit point will result in a sudden drop of the applied load to zero. Such a dynamic consequence would not occur if n were positive.

The span of negative values for n is $(-1, -\infty)$, where the first limit is obtained by setting $\ell_c = 0$ in Eq. (12). The closest branches of the stable and unstable equilibrium paths in the $P - \delta$ space have slopes of αK and K, respectively. For physically meaningful representations, α is between zero and one, where the lowest values are associated with ductile materials and values close to unity are associated with brittle materials. It follows that for brittle materials, the two equilibrium branches could be close. Suppose that static loading is accompanied by dynamic perturbations, which could be considered always present when a loading device is used and which are denoted symbolically as an additional deflection shown by the dotted line in Fig. 6. If adjacent points on the two equilibrium branches lie within the disturbance band, it is conceivable that the unstable branch could be reached and that failure would occur at a load less than the limit load. Specifically, let the nominal limit load be

$$P_0 = M_0/L_a \tag{16}$$

Then the center-point deflection at the limit state is $P_0/\alpha K$. For a dynamic disturbance of magnitude $\epsilon^* = \epsilon P_0/\alpha K$ under a displacement-prescribed load, geometrical arguments based on Fig. 6 show that the failure load is

$$
\begin{aligned}
P_F &= P_0 & n &> 0 \\
P_F &= P_0\left(1 - \frac{\epsilon}{1 + \frac{\alpha}{n}}\right) & -\infty &< n < -1
\end{aligned}
\tag{17}
$$

70
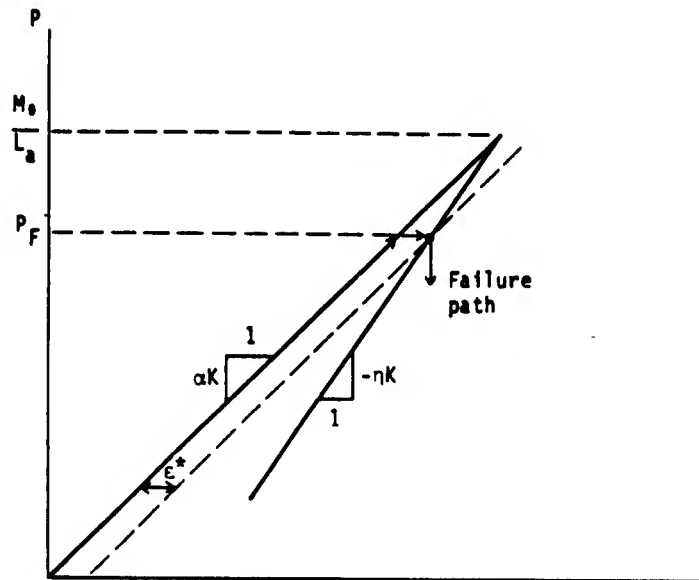
Figure B6.   Possible failure mode

One way to obtain a small value of ℓ_c is to allow L to grow. Thus, for a given value of ϵ, the dimensionless failure load will drop with L, which is a specific manifestation of the size effect discussed extensively by Bazant [3]. However, an implication of this theory is that for physically realistic values of α, β, and L_c, the reduction is limited to a value that depends on ϵ; that is, the failure load does not approach zero for large L. For example, suppose that $\epsilon = 0.01$. Then, for the worst case of $n = -1$ and for the small amount of ductility described by $\alpha = 0.98$, Eq. (16) implies that the failure load will be $P_F = P_0/2$.

Another implication of a negative value for n for more complex structures is that a computational method must be developed to determine whether an unstable equilibrium branch exists. The development of such a method will not be an easy task because most existing methods [6] are based on elasticity theory, for which additional displacement fields are generally not localized to the degree that they are for plastic softening.

APPLICATION TO A REINFORCED CONCRETE BEAM

Lane [7] performed several experiments for a beam geometry characterized by Fig. 1 but with the additional possibility of an axial load proportional to the lateral load. The nominal compressive strength (uniaxial stress) of the concrete was 34.5 MPa (5000 psi). The beam was 22.9 cm (9 in.) wide and 38.1 cm (15 in.) deep. Three reinforcing bars of diameter 1.9 cm (0.75 in.) were placed 6.4 cm (2.5 in.) from the bottom surface, and two reinforcing bars of diameter 0.6 cm (0.25 in.) were placed 3.8 cm (1.5 in.) from the top surface. Shear stirrups were placed at 15.2-cm (6-in.) intervals along the beam. For all cases, the beam span was 3.82 m (12.53 ft).

For the first series of experiments, that of immediate interest for this analysis, no axial load was applied. Experimental results were obtained for values of L_a equal to 96 cm, 130 cm, and 160 cm (37.5 in., 50 in., and 62.6 in.). On the basis of photographs of the failed specimens, the half-length of the softening regime, L_c, was selected somewhat subjectively to be 17 cm (6.7 in.).

71

The moment-curvature relation was assumed to be of the following form:

$$M = \alpha_1 \kappa \qquad\qquad 0 < \kappa < \kappa_1$$

$$M = M_0 + \frac{(\alpha_1 \kappa_1 - M_0)}{(\kappa_1 - \kappa_2)^2}(\kappa - \kappa_2)^2 \qquad \kappa_1 < \kappa < \kappa_2$$

$$M = M_0 + \frac{(M_3 - M_0)}{(\kappa_3 - \kappa_2)^2}(\kappa - \kappa_2)^2 \qquad \kappa_2 < \kappa < \kappa_3 \qquad (18)$$

$$M = M_3 + \beta_1 (\kappa - \kappa_3) \qquad\qquad \kappa_3 < \kappa$$

The experimental load-deflection curve for the center of the beam was used with Eq. (5) to determine the parameters of Eq. (18). The peak moment, M_0, is available from Eq. (16), and the other parameters were obtained by trial and error. The results are

$$M_0 = 2.67 \times 10^5 \text{ N·m} \qquad M_3 = 2.0 \times 10^5 \text{ N·m}$$
$$\alpha_1 = 2.04 \times 10^7 \text{ N·m}^2 \qquad \beta_1 = -2.0 \times 10^6 \text{ N·m}^2 \qquad (19)$$
$$\kappa_1 = 0.013/\text{m} \qquad \kappa_2 = 0.050/\text{m} \qquad \kappa_3 = 0.213/\text{m}$$

The unloading slope was taken to be equivalent to the tangent of the moment-curvature relation at the origin, i.e., α_1. The resulting moment-curvature relation is shown in Fig. 7, and the comparison with experimental load-deflection data for the three geometrical configurations is given in Fig. 8. The correlation between theoretical and experimental data indicates that the approach would be more than adequate for most computational purposes.

It must be emphasized that these fits were made under two restrictive assumptions: 1) the softening zone was fixed for the duration of the analysis, and 2) the deformation field was taken to be symmetric about the center line. Neither assumption is particularly valid, but each is considered appropriate for the purposes of illustrating features that may appear in structures that exhibit strain softening. Because the problem is nonlinear, there is no unique choice for the localization parameter and the moment-curvature relation. However, if the localization parameter can be established independently, the inverse procedure is a viable method for obtaining a beam constitutive equation.

CONCLUDING REMARKS

As the results of Krajcinovic [8] and Popelar and Hoagland [9] show, softening can be viewed as a natural consequence of the growth of microcracks or voids as reflected in a damage parameter. The resulting constitutive relation is useful for obtaining theoretical ultimate loads of structural members, but a more comprehensive approach requires the inclusion of the fact that softening tends to localize into a small region. As demonstrated by the analysis of the model problem, a spectrum of post-limit equilibrium paths is available in which each path is identified by a value of a parameter defined in terms of the length of the localization region and by a characteristic structure length. If dynamic perturbations or initial imperfections due to variations in structural stiffness are assumed to be always present, then a stability argument yields a theory that predicts a drop in the nondimensional failure load with either a decrease in the region of localization or an increase in the characteristic dimension of the structure. Although the nature of the decrease in the failure load is similar in many respects to that obtained by the assumption of a blunt fracture mechanism [3], the stability theory indicates that as the characteristic dimension increases, the failure load asymptotically approaches a finite value rather than a value of zero as indicated by the blunt fracture approach.
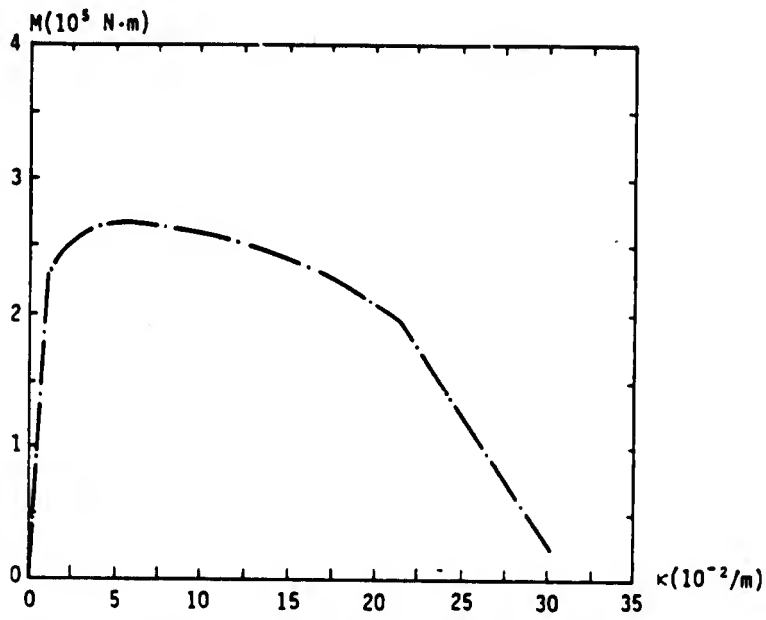
Figure B7. Moment-curvature relation for reinforced-concrete beam
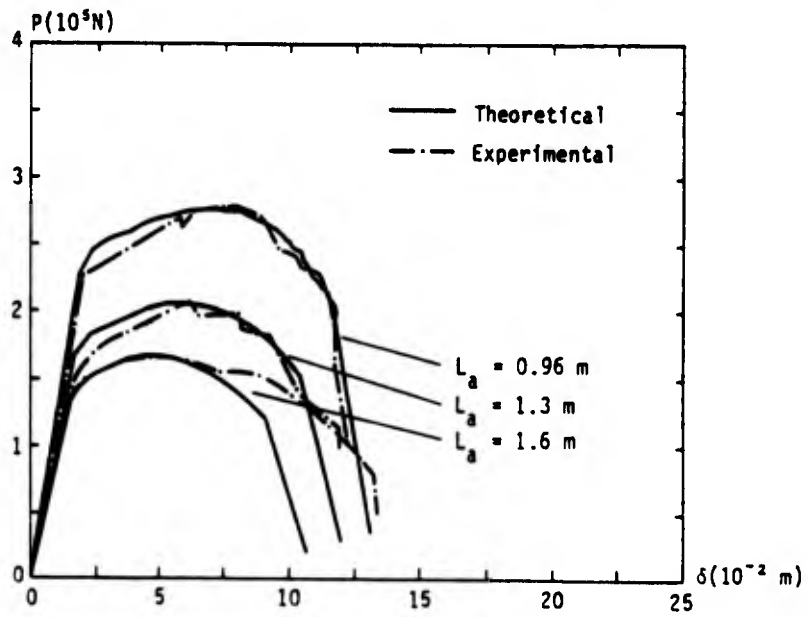
Figure B8. Comparison of experimental and theoretical load-deflection curves

73

The existence of unstable equilibrium paths provides a severe challenge for any numerical algorithm because these paths must be identified if a rigorous determination of a failure load is to be made. The fact that the source of the problem is localized could mean that approaches used for similar features in elastic problems may not be sufficiently robust, although recent developments look promising [10].

While this study has introduced no new concepts, it does show that the use of a simple beam as a model problem is helpful in illustrating some of the issues and problems associated with softening. A significant need remains for investigations of constitutive models and associated numerical algorithms.

ACKNOWLEDGMENT

REFERENCES

1. Bazant, Z. P., "Instability, Ductility, and Size Effect in Strain-Softening Concrete," Journal of the Engineering Mechanics Division, ASCE, Vol. 102, No. EM2, Proc. Paper 12042, April 1976, pp. 331-344.

2. Bazant, Z. P., and Panula, L., "Statistical Stability Effects in Concrete Failure," Journal of the Engineering Mechanics Division, ASCE, Vol. 104, No. EM5, Proc. Paper 14074, October 1978, pp. 1195-1212.

3. Bazant, Z. P., "Size Effect in Blunt Fracture: Concrete, Rock, Metal," Journal of Engineering Mechanics, Vol. 110, No. 4, April 1984, pp. 518-535.

4. Riks, E., "An Incremental Approach to the Solutions of Snapping and Buckling Problems," Int. J. Solids & Structures, Vol. 15, 1979, pp. 529-551.

5. Wempner, G. A., "Discrete Approximations Related to Nonlinear Theories of Solids," Int. J. Solids & Structures, Vol. 7, 1971, pp. 1581-1599.

6. Endo, T., Oden, J. T., Becker, E. B., and Miller, T., "A Numerical Analysis of Contact and Limit-Point Behavior in a Class of Problems of Finite Elastic Deformation," Computers & Structures, Vol. 18, No. 5, 1984, pp. 899-910.

7. Lane, G. E., Jr., Behavior of Reinforced Concrete Beams Under Combined Axial and Lateral Loading, AFWL-TR-76-130, Air Force Weapons Laboratory, Kirtland Air Force Base, New Mexico, May 1977.

8. Krajcinovic, D., "Distributed Damage Theory of Beams in Pure Bending," Journal of Applied Mechanics, Vol. 46, September 1979, pp. 592-596.

9. Popelar, C. H., and Hoagland, R. G., Fracture and Failure Instabilities in a Damaging Material, Personal Communication, Paper Submitted for Publication, May 1984.

10. de Borst, R., "Application of Advanced Solution Techniques to Concrete Cracking and Non-Associated Plasticity," Numerical Methods for Non-Linear Problems, Vol. 2, Proceedings of the International Conference held at Universidad Poltecnica de Barcelona, Spain, 9th-13th April, 1984, Pineridge Press, pp. 314-325.

APPENDIX C*

ONE-DIMENSIONAL SOFTENING WITH LOCALIZATION

Howard L. Schreyer

Zhen Chen

.

Department of Mechanical Engineering and
The New Mexico Engineering Research Institute
University of New Mexico
Albuquerque, NM 87131

November 1984

---

*This appendix is a reproduction of a paper to be submitted for publication to
the Journal of Applied Mechanics. It is a self-contained document with its
own internally consistent numbering system for equations, figures, and
references.

INTRODUCTION

Numerous computational codes contain numerical algorithms for strain-hardening plasticity. To develop a capability for predicting large deformations, strain softening must be incorporated. Strain softening is associated with localization, and if no precautions are taken, the region of localization will depend on the size of the mesh used for spatial discretization. This mesh-dependence is clearly unacceptable, and therefore an approach that can provide basic equations governing the phenomena of softening and localization is needed. Several studies concerning the conditions necessary for the onset of localization are available (Rudnicki and Rice, 1975; Vermeer, 1982; Prevost, 1984), but which procedure is optimal for predicting postlimit states is still not clear.

From a continuum point of view, Bazant (1976) has pointed out that the region of localization must condense to what might be considered a surface. However, such an idealization is rarely observed in experiments. On the other hand, there is no doubt that a region of localization exists and may consist of a band whose lateral dimension appears to depend on the physical characteristics of the materials. Because of the complexity of problems involving a material instability, a numerical technique such as the finite-element method has been used to obtain most solutions. Innerent in such a technique is the problem that a region of localization that is smaller than the element size cannot be accurately represented. In fact, the predicted response will generally depend on the element size, and this feature is unacceptable to analysts.

Recently, considerable effort has been made to obtain a suitable approach to handling strain softening and localization. A promising approach (Bazant, 1984; Pietruszczack & Mroz, 1981) involves the assumption that the size of the localization is fixed according to the material being studied. Softening characteristics can then be adjusted to take element size into account or to ensure that an appropriate amount of energy dissipation is provided. However, Willam (1984) suggests that in order to take into account what appear to be different modes of softening, a composite damage formulation is necessary. A motivation for the use of a nonlocal constitutive equation is that in this

way, the aspects discussed by Willam can perhaps be synthesized into one theory, although Bazant and Chang (1984) point out that certain precautions must be taken.

At least two aspects of strain softening and localization have not been addressed. First, the effect of initial imperfections is unknown; and second, the potential usefulness of a nonlocal constitutive relation has not been demonstrated conclusively. In this paper, the implications of softening, localization, and stiffness imperfections and the assumption that stress is a function of both strain and the gradient of strain are explored by means of a one-dimensional model problem. It is believed that the insight provided can be useful to the construction of more general theories to address the issues raised by Willam (1984).

MODEL PROBLEM

To simulate the softening phenomenon (Crisfield, 1982), consider a body of length $L = a + b$ and a unit cross-sectional area as shown in Figure 1. This body can be considered a bar or, in a more general sense, a structural member or even a finite element of a continuum. The element is considered to be composed of two segments described by similar constitutive equations, the only difference being that the limit stress for segment B is slightly less than that for segment A. If the stress on the element is such that the strain in region B exceeds the value at the limit state, then softening will be exhibited. It is assumed that softening occurs uniformly over region B and that parameter b is the dimension of the localized softening region. It is also assumed that the length of the element is greater than that of the softening regime, i.e., $L > b$.

For simplicity, the constitutive relation for both regions is considered to be bilinear. The slopes of the loading and softening segments are αE and $-\beta E$, respectively. If unloading occurs, a line with slope E is followed so that if $\alpha < 1$, the effect of strain hardening can be simulated in an approximate sense. The limit stress for region A, denoted by σ_a, is assumed to be infinitesimally larger than the limit stress for region B, denoted by σ_0. These details are sketched in Figure 2.

77
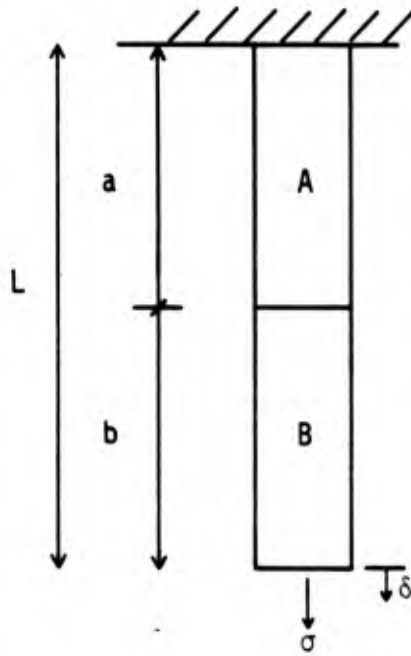
Figure C1. One-dimensional model problem.
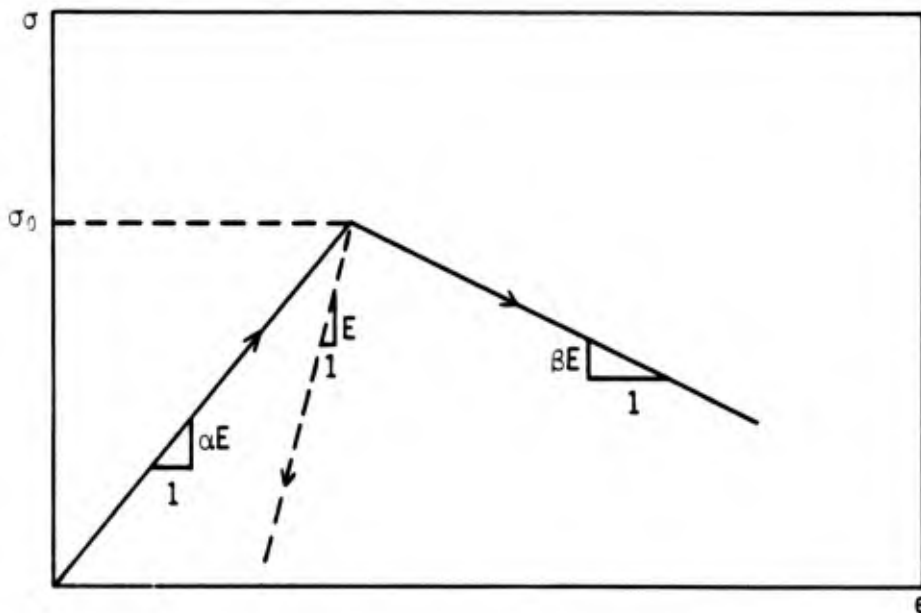
Figure C2. Constitutive relation for segments A and B.

78

There is a cogent argument that strain softening does not exist. It is the essence of damage theory (Krajcinovic, 1983) that a decrease in apparent stress occurs not by strain softening but by a reduction in effective area due to the coalescence of voids and microcracks. The viewpoint adopted here is that for an engineering approach, the choice of a procedure for providing a drop in nominal stress with strain can be based on convenience because a rigorous development of the two methods should provide the same results on a macroscopic basis. For the current development, the assumption of strain softening provides a suitable basis for deriving general results that would not change if an alternative approach were used.

For given values of strain in regions A and B, which are denoted by e_a and e_b, respectively, the corresponding elongations are

$$\delta_a = ae_a \qquad \delta_b = be_b \tag{1}$$

Then the elongation and the composite strain for the complete element are given by

$$\delta = \delta_a + \delta_b \qquad e = \delta/L \tag{2}$$

The composite constitutive equation is characterized by the relation between stress, σ, and strain, e, or equivalently, a P-δ curve.

For monotonically increasing stress from zero up to the limit stress, the composite constitutive equation is identical to the constitutive equation for either segment. However, the postlimit response is different. To obtain this part of the curve, suppose that e_b is given an increment, Δe_b. From equilibrium in segment B,

$$\Delta \sigma = -\beta E \Delta e_b \tag{3}$$

and the change in strain in segment A is

$$\Delta e_a = \frac{\Delta \sigma}{E} = -\beta \Delta e_b \tag{4}$$

79

It follows from Eq. 2 that the increment in total strain is

$$\Delta e = \frac{(b - \beta a)}{L} \Delta e_b \tag{5}$$

The result of substituting Eq. 3 in Eq. 5 is

$$\Delta \sigma = -\eta E \Delta e \tag{6}$$

where

$$\eta = \frac{\beta L}{b(1 + \beta) - \beta L} \tag{7}$$

The composite, or smeared, constitutive relation is shown schematically in Figure 3. For $0 < \eta < \infty$, conventional softening is displayed. The case of an infinite value of η corresponds to a vertical drop in stress, whereas the stress-strain curve displays a decrease in strain with a decrease in stress for negative values of η. The parameter α, which characterizes strain hardening, does not appear in the expression for η. As L increases, η approaches asymptotically the limiting value of -1.
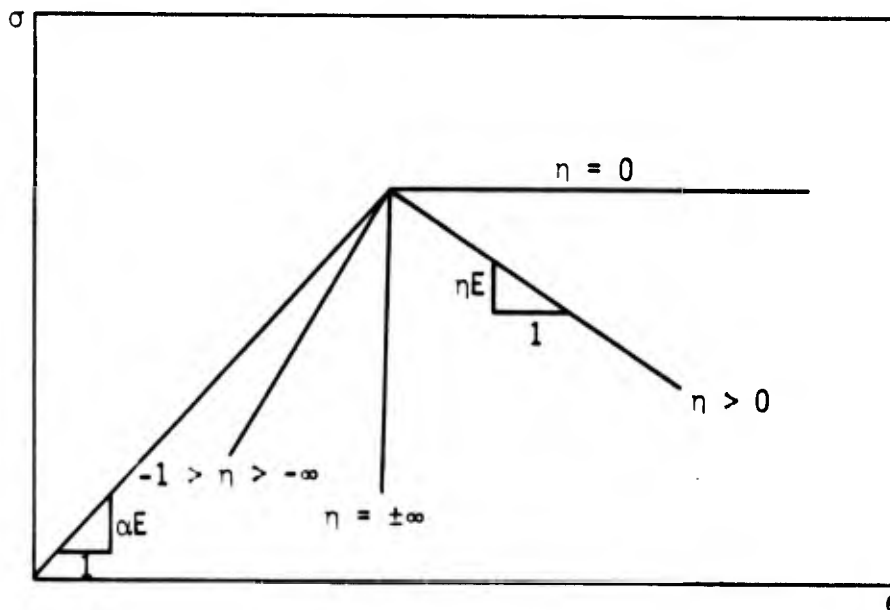
Figure C3. Composite constitutive relation.

IMPLICATIONS

Experimental data are often obtained with stress-prescribed devices, in which case failure occurs when the limit load is reached. For some devices, however, displacements are prescribed, in which case postlimit data can be obtained unless the case corresponding to negative values of n exists. If the model problem represents an element in a continuum, for example, then because of the basic indeterminacy of such a system, the situation is probably closer to a displacement or strain-controlled problem than to one of load or stress control.

If the loading condition can be represented adequately by increasing the strain monotonically, and if n is negative, then it is apparent from Figure 3 that it is impossible to follow the actual stress-strain curve. If an increment in load forces e to be larger than $e_0 = \sigma_0/\alpha E$, the result will be a snapdown to zero stress with a corresponding release of energy. Because loss of stability is often associated with failure, a condition of negative n is assumed to be undesirable. However, no matter how small a value (positive) of β is appropriate, Eq. 7 shows that n can be made negative for a sufficiently large value of L with b fixed. In a structural member context, the dependence of instability on the size of the structure is a manifestation of a size effect that has not been investigated extensively. For example, fracture can be used to justify the argument that strain softening is not observed in metals. However, an alternate interpretation for fracture can be given. The phenomenon of crack growth occurs in such a small zone compared to the length of the specimen that the terms involving L in Eq. 7 dominate, and n is negative. In other words, fracture is usually an unstable process because of the size of the specimen, not because strain softening does not exist. In fact, since crack widening has been controlled for concrete (Shah and Gopalaratnam, 1984), it would be interesting to know whether one could obtain a similar result for metals by using a sufficiently small specimen.

An energy interpretation is apparent. Once softening occurs, the energy dissipated in region B must be provided from region A and from any work added by an external agency. The situation defined by $n = \mp\infty$ is the critical case in which region A can provide enough energy to match that dissipated in region B with no additional work, a case corresponding to $\Delta e = 0$.

81

In many finite-element codes that use explicit time integration, the total strain increment is fixed at each time step. Many algorithms incorporate the conventional softening identified with $\eta > 0$, but almost none incorporate the possibility associated with $\eta < 0$. From Eq. 7, the need for the latter case can be averted by selecting the element size, L, such that

$$0 < L < L^* \equiv \frac{b(1 + \beta)}{\beta} \qquad (8)$$

It is assumed, of course, that b is known.

If the element dimension is chosen to be b, which would probably be too small for practical applications, then $a = 0$ and $\eta = \beta$; i.e., the original constitutive equation for a segment could be used. The choice of an even smaller element would necessitate the use of a composite constitutive relation with $\eta < \beta$. The reason is that softening would concentrate in an area defined by the element size, and to take this fact into account, a smaller value of η would be required so that the correct amount of energy dissipation could be obtained.

The primary problem is that the use of elements larger than L* is desirable. Therefore, a constitutive equation that incorporates a negative value of η is required. To the authors' knowledge, such an algorithm has not been developed. This feature should not be difficult to incorporate, because plasticity algorithms automatically incorporate an elastic unload feature. In the postpeak regime, which is not unloading because energy is being dissipated, a pseudoelastic behavior could be incorporated as a three-dimensional representation of the case corresponding to negative η. Simultaneously, the limit surface must contract to exclude any path that involves an increase in stress.

INITIAL IMPERFECTIONS

So far, the development for the model problem indicates a size effect based on the softening feature of an element, but there is no implication that the apparent failure or fracture stress varies with the size of the structural member. To show that there may be a size effect for the failure stress as well, consider the case in which $L \gg b$, so that η is close to (slightly less

than) -1. The situation is illustrated in Figure 4 with $n_1 < n_2 < n_3 \leq -1$. The fact that the pre- and postlimit equilibrium states can be close suggests that the response of the structural member will be sensitive to initial imperfections or loading disturbances. Rather than being geometrical in nature, the imperfections of concern here are those associated with variations in stiffness, αE, as the structure is loaded. Suppose such variations are bounded on one side by the dotted line in Figure 4, where the imperfection is characterized by the strain parameter, ε. Then, for strain-prescribed loading, it is possible for a snap-down response to occur at stress values of σ_1, σ_2, and σ_3 for softening conditions characterized by n_1, n_2, and n_3, respectively. To be specific, if $n = n_2$ and the load increases from point A to point C, then the possibility of reaching an alternative equilibrium state exists at $\sigma = \sigma_2$, and snap-down from point D is feasible.

The presence of initial imperfections provides the rationale for a potential size effect on the limit stress (or limit load) that can be exhibited by a structural member. As the size of the element increases, the softening parameter approaches -1, and the probability of snap-down at a stress less than the ultimate stress becomes greater.

Geometrical arguments based on Figure 4 can be used to show that the failure stress, in the presence of imperfections, is

$$\sigma_F = \sigma_0 \qquad\qquad n > 0$$

$$\sigma_F = \sigma_0 - \frac{\varepsilon \alpha E}{1 + \alpha/n} \qquad n < -1 \tag{9}$$

For brittle materials, modeled by a value of α close to unity, the failure stress is sensitive to imperfections as exhibited through ε; whereas for ductile materials, modeled by small values of α, the decrease in the failure stress from σ_0 is not as abrupt. The idealized postpeak response, as reflected through n in Eq. 7, does not depend on α, whereas a consideration of initial imperfections shows that strain hardening, as exhibited by values of α less than one, is an important characteristic.

A plot of failure stress as a function of L/b is shown in Figure 5. For strain-controlled loading, no reduction in failure stress occurs if the
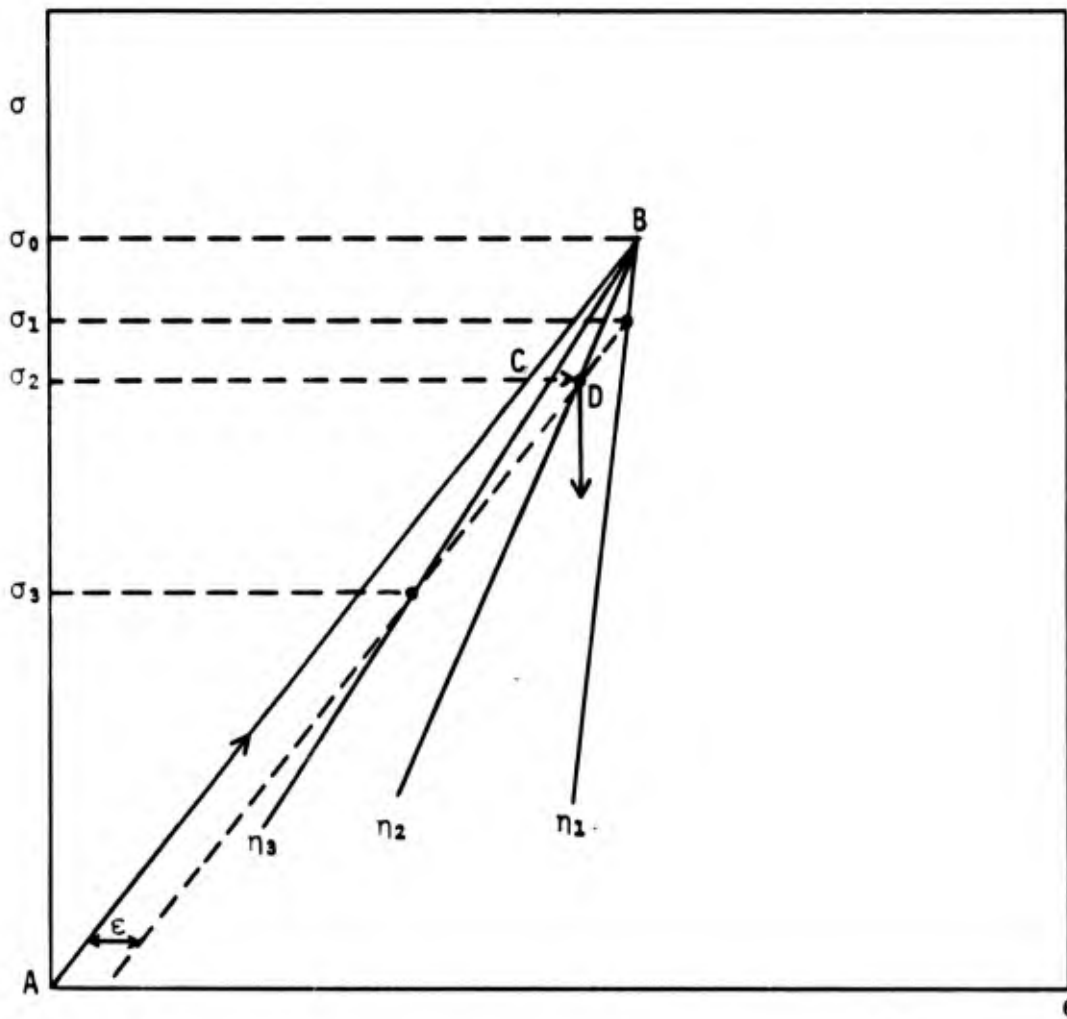
Figure C4.   The effect of an initial imperfection on a stable equilibrium state.
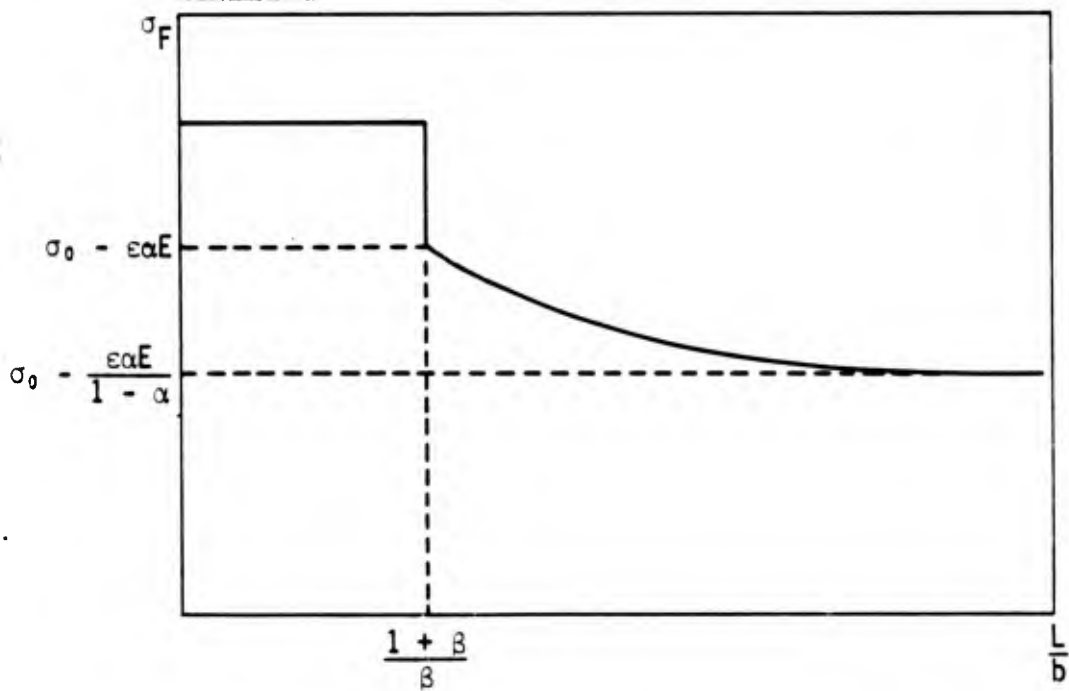
Figure C5.   Failure stress as a function of element length.

84

structural element is small enough. When L/b reaches the critical value of $(1 + \beta)/\beta$, the failure stress decreases sharply. The magnitude of the jump depends on the degree of inelasticity in the loading part of the stress-strain curve. With a further increase in structural size, or a decrease in the size of the region localization, the failure stress asymptotically approaches a limiting value, which also depends on the parameter α. In fact, if α is close to one, the limiting value can be zero for large values of L/b. This disturbing aspect was pointed out by Bazant (1984) in connection with the cracking of beams.

These results must be ameliorated to a certain extent because neither total strain nor a stress-controlled loading condition describes a typical problem. Instead, a stable postpeak response may be any line with a slope of $-m$, where $0 \leq m < \infty$, so that an additional regime of instability exists for values of n between m and ∞ as shown in Figure 6. Except for a change in some of the details, the basic concepts outlined previously are still valid, and the matter will not be pursued further.
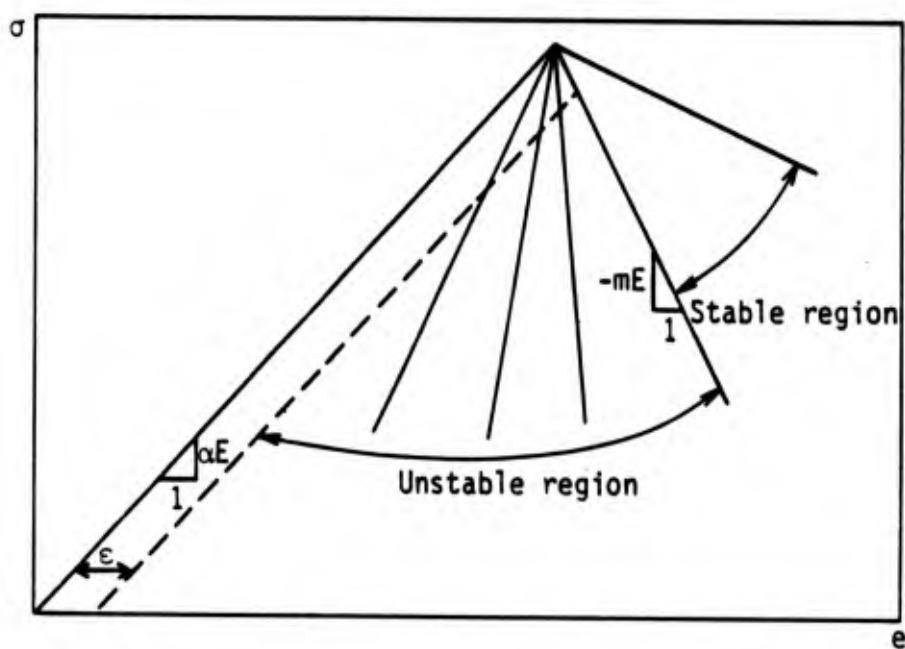
Figure C6.   Reduction in failure stress for initial imperfections
on a spring-loaded element.

A NONLOCAL CONSTITUTIVE MODEL

The existence of a localized region with strains much larger than those in the adjacent region implies that the strain gradient must be large. For cases in which softening and localization have been observed carefully, the region of localization does not remain fixed in size; instead, it expands monotonically with deformation. One approach is to postulate that a characteristic dimension of localization depends on the material (Bazant, 1984) and perhaps on the postpeak stress (Shah and Gopalaratnam, 1984). The disadvantage of this approach is that a separate procedure for handling softening must be established for numerical computations. On the other hand, an alternate approach involving an assumption on the constitutive equation might provide equivalent results, but with the advantage that the softening mechanism would be a consequence of the loading path. As a result, existing numerical algorithms could be used with a minimal degree of modification.

To explore the potential usefulness of a nonlocal constitutive equation, a modified form of the relation shown in Figure 2 is used. It is assumed that the peak stress, σ_p, is a function of strain gradient rather than being the constant, σ_0. If the following simple relation is assumed,

$$\sigma_p = \sigma_0 \ (1 - g|e_{,x}|)$$

$$e_p = \frac{\sigma_p}{\alpha E} \tag{10}$$

in which x is the spatial variable, then the constitutive equation can be represented by the sketch shown in Figure 7. The result of such an assumption is to force the localization away from the point of initiation, allowing the degree of expansion of the softening region to be governed by the material parameter g, which has the dimension of length. Thus, the approach introduces through the constitutive equation a length parameter that should ultimately be relatable to the microstructure of the material.
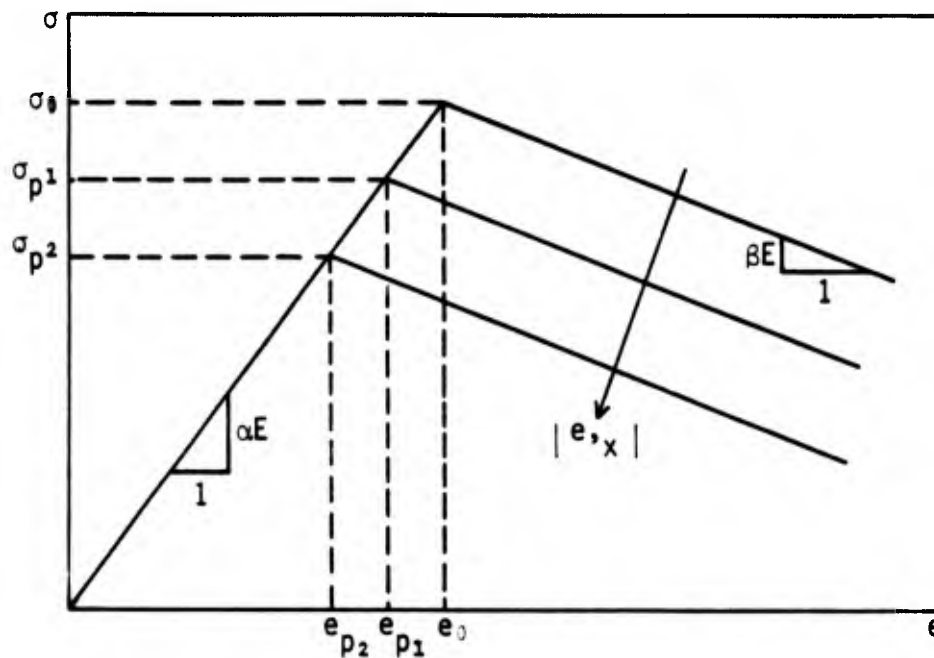
Figure C7.   Nonlocal constitutive relation.

To show the effect of g on the response of a bar, consider a case in which a bar under uniaxial stress is loaded such that the strain in the softening region is increased monotonically. For the case of $E = 5$, $\alpha = 0.8$, $\beta = 0.1$, $g = 150$, and $\sigma_0 = 1$, the evolution of strain distribution is shown in Figure 8. Initially, the strain is uniform. Once the peak stress is reached, however, at a point chosen arbitrarily to be $x = 0$, a portion of the bar will continue to elongate, while elastic retraction will cause the remainder of the bar to shrink. The region of continued extension is the localized softening region, which develops in the smooth manner shown in Figure 8.

Strain distributions for a fixed value of stress are shown in Figure 9 for various values of g. An increase in g corresponds to a widening of the softening region; thus, if softening is very localized, which occurs with cracking, for example, then a small value of g should be used.
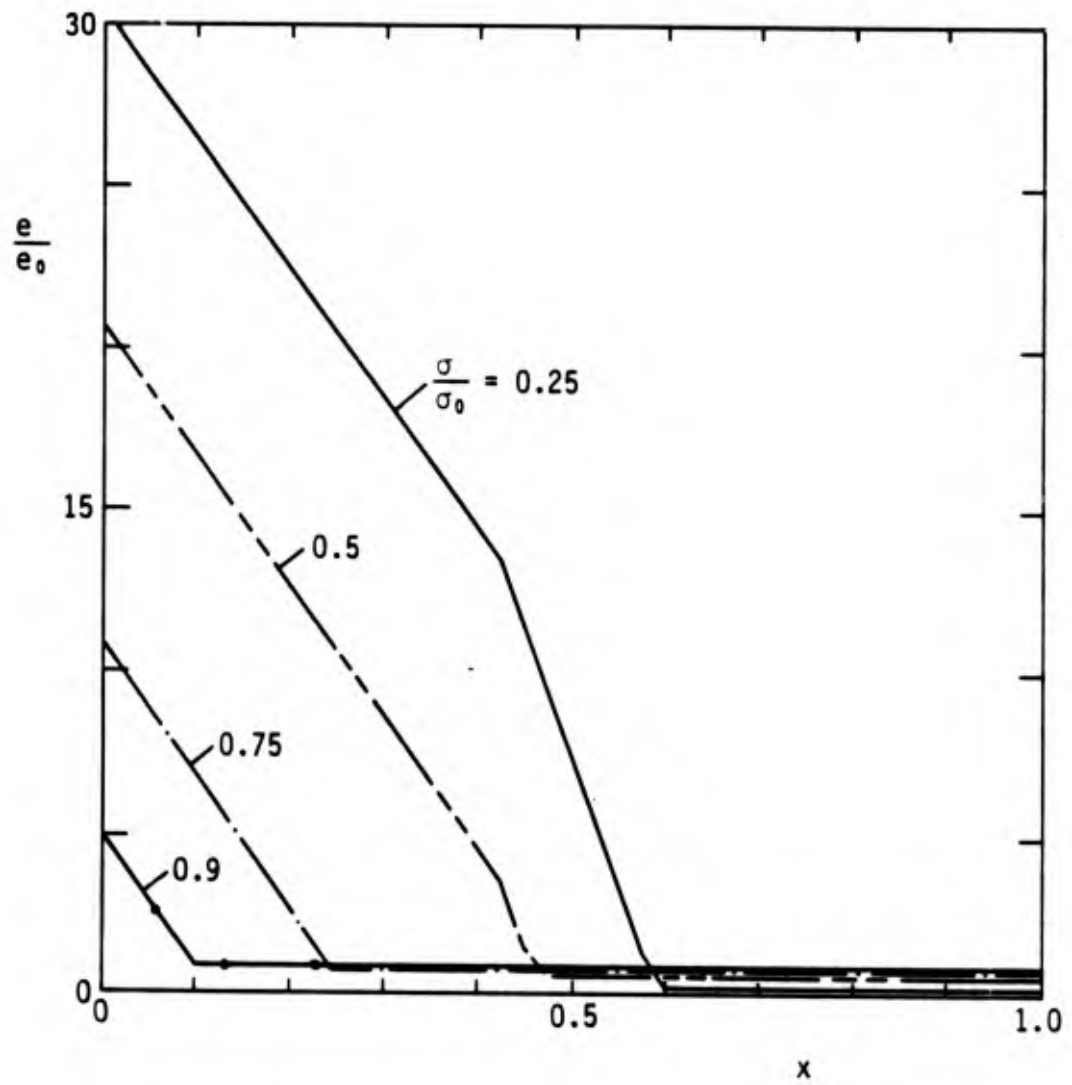
Figure C8. Evolution of strain distribution.
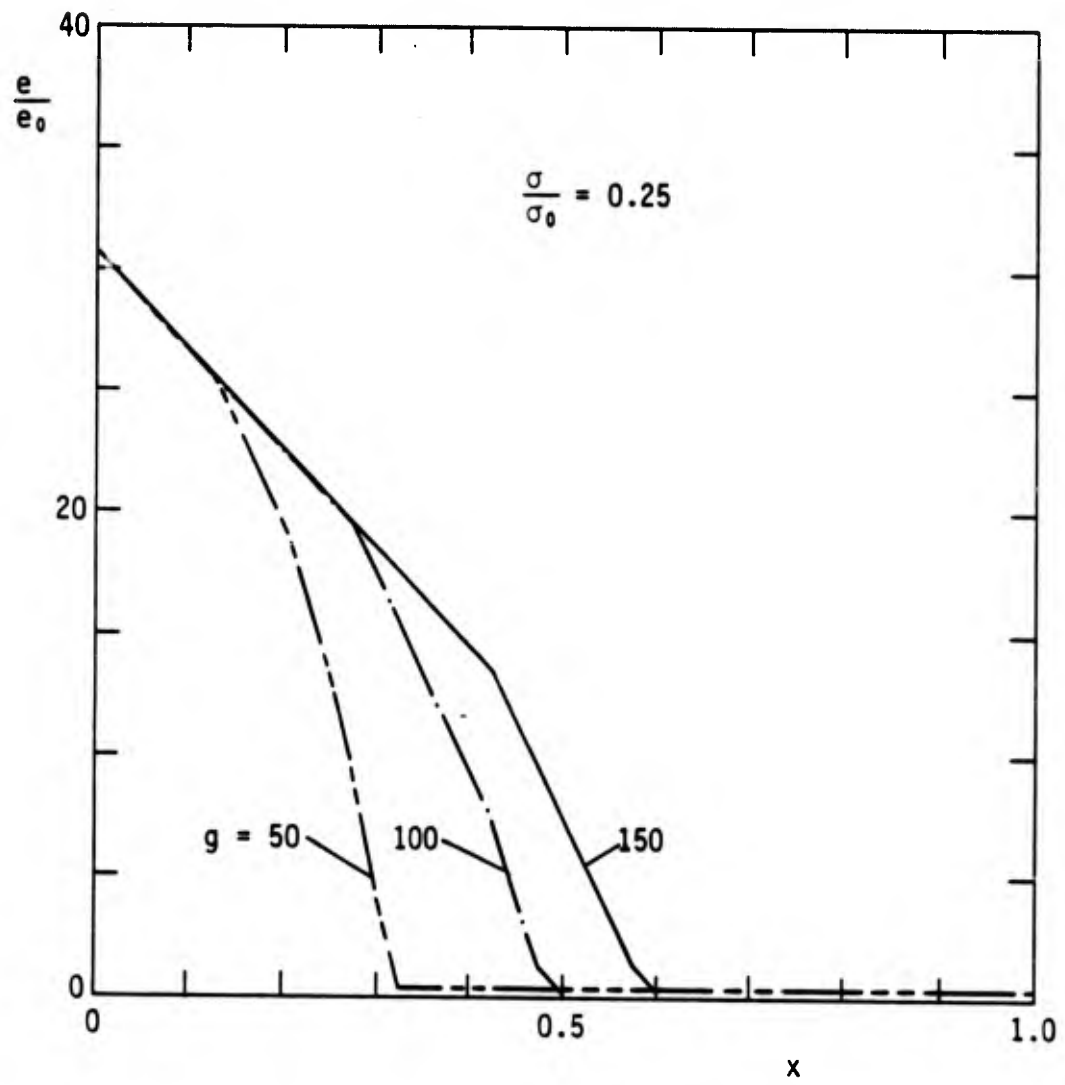
Figure C9.   Strain distributions for
a fixed value of stress.

89

For a length of one unit, the stress-deflection relation is shown in Figure 10. Again, a smooth behavior in g is shown, even to the extent that an abrupt drop in stress can be displayed as a routine result of the constitutive relation. All softening curves would be steeper if a longer segment had been chosen.

The effect of element size is shown in Figure 11, in which convergence is displayed. Except for the case of an element length of L/10, the results agree to acceptable engineering accuracy.

Shah and Gopalaratnam (1984) performed tensile tests on concrete under carefully controlled loading conditions, using refined measuring techniques. Their suggestion that the hardening part of the stress-strain curve should be nonlinear was adopted, but linear softening in strain and a linear decay in peak stress with strain gradient were retained. Specifically, the following relations were used:

$$\sigma_p = \sigma_0 \left(1 - g|e,_x|\right)$$

$$\sigma = \sigma_p \left[1 - \left(1 - \frac{e}{e_p}\right)^n\right] \qquad 0 \le e < e_p$$

$$\sigma = \sigma_p[1 - \beta'(e - e_p)] \qquad e \ge e_p \qquad (11)$$

where

$$n = 1.18$$
$$\beta' = 2.03 \times 10^{-10}$$
$$\sigma_p = 531 \ \text{lb/in}^2$$
$$g = 7.67 \times 10^{-6} \ \text{in}$$

The stress deflection relation for a gage length of 3.25 in is shown in Figure 12. Experimental data, the predictions of Shah and Gopalaratnam based on an alternate approach, and the results of Eq. 11 are plotted. Except for the latest phase of the softening phenomenon, the essential feature has been captured in a very simple nonlocal constitutive relation.

90
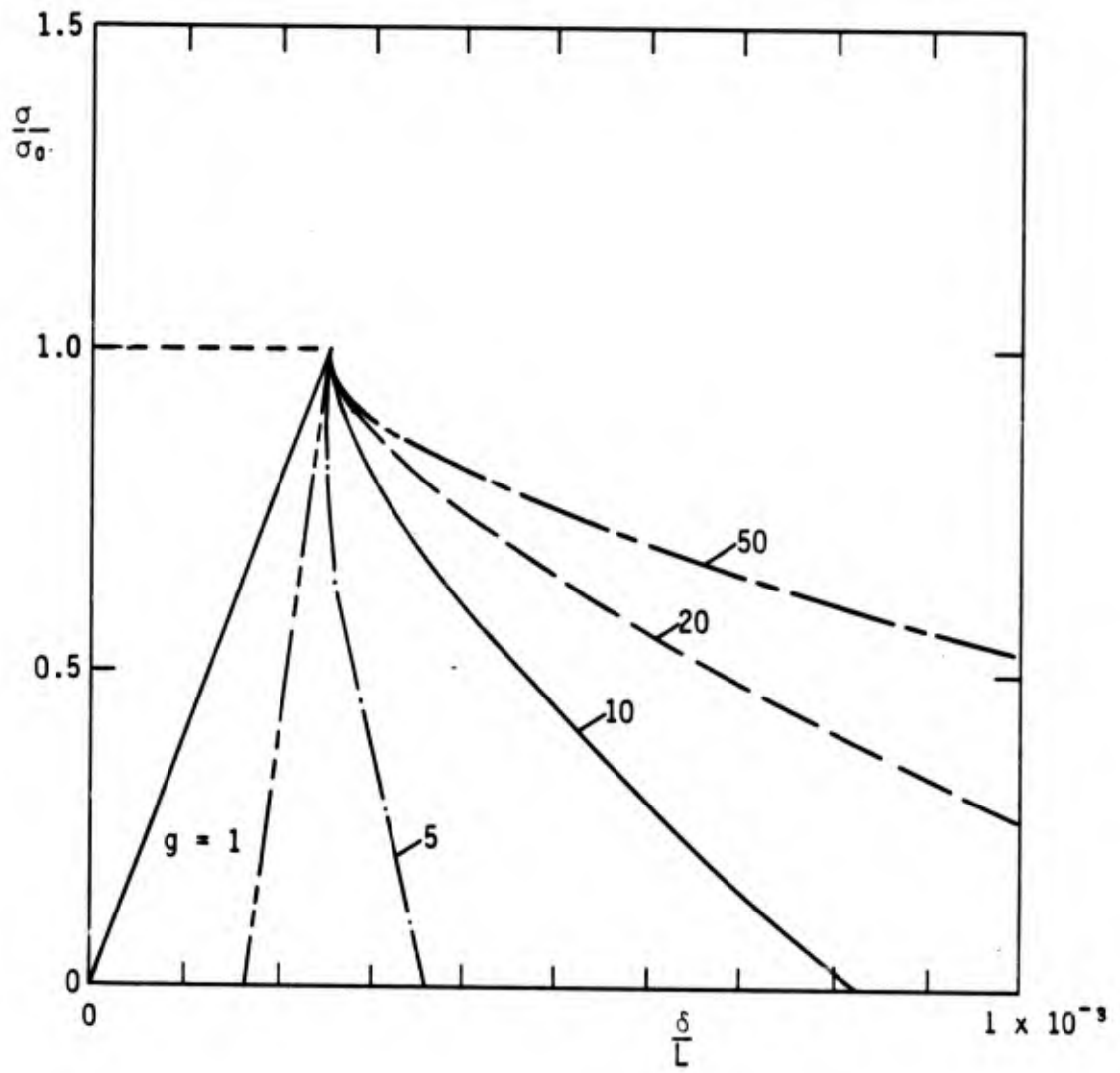
Figure C10. Stress-deflection relation for
a length of one unit.
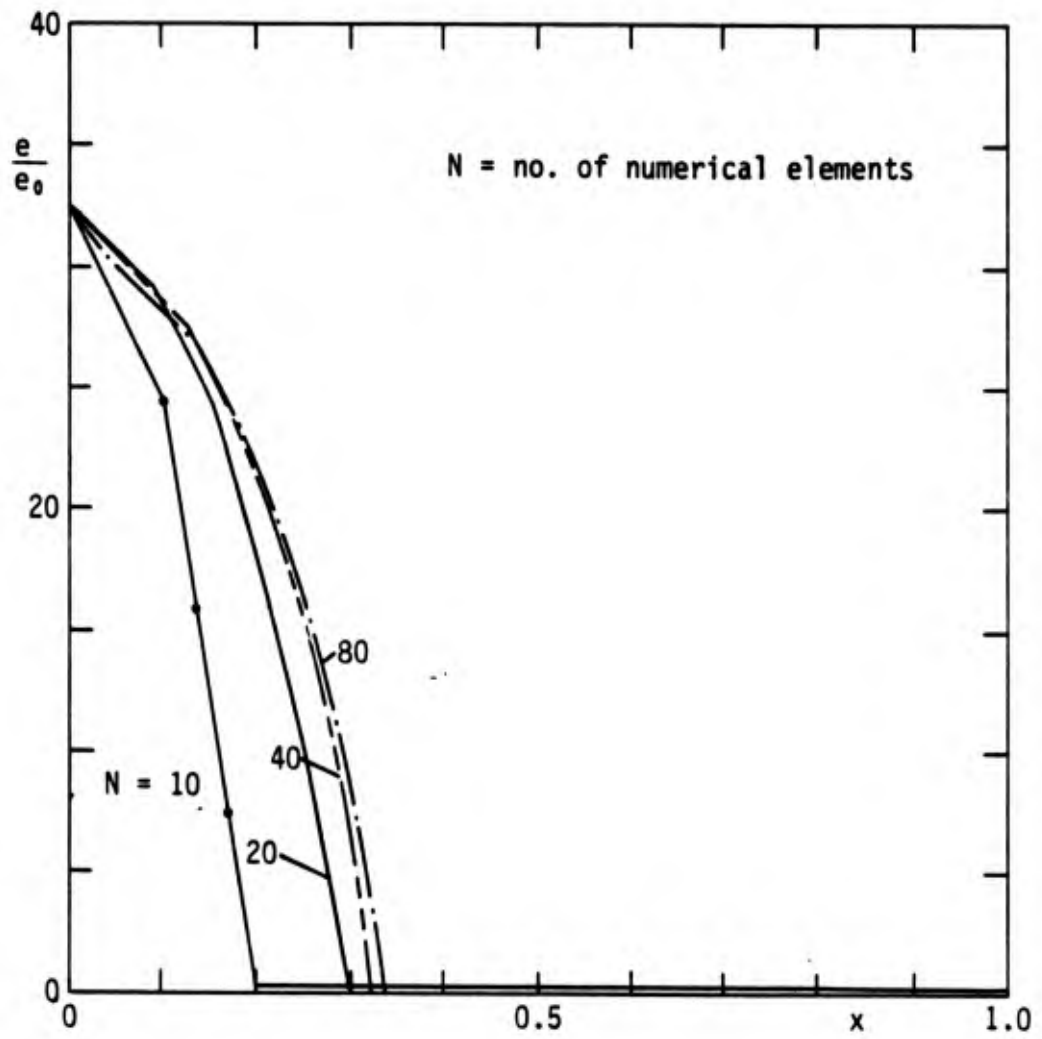
Figure C11. Effect of element size in which
convergence is shown.
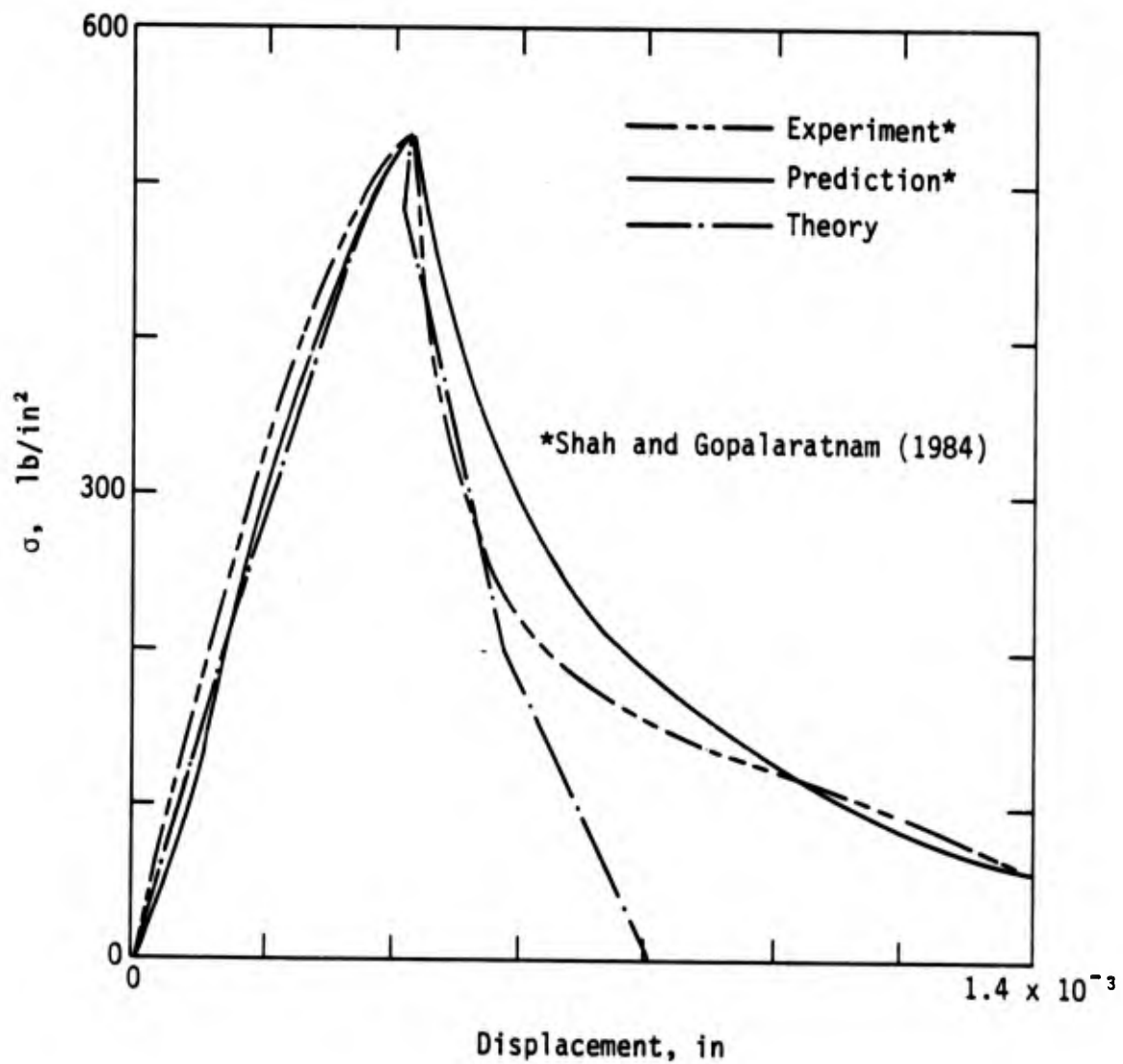
Figure C12. Stress-deflection relation for a gage length of 3.25 in.

The size of the predicted softening zone at the state of zero stress is 0.12 in, which is considerably larger than the measured crack width. The difference between theoretical and experimental values may be due to the existence of a softening region outside the crack zone.

CONCLUSIONS

With the use of an elementary model problem, the significance of both strain softening and the size of the softening region has been demonstrated. If the structural member is large enough, the assumption of strain softening can lead to unstable equilibrium states, even if the problem is one of strain- or displacement-controlled loading. The existence of unstable equilibrium states near stable equilibrium states implies that such a structure may be sensitive to initial imperfections in stiffness. Consequently, the failure load may be less than the load associated with the nominal peak stress. That there is a size effect is indicated by the dependency of the drop in failure load on the geometry of the structural member.

The results are useful for suggesting appropriate choices of finite elements and smeared constitutive models. They also demonstrate that existing constitutive algorithms should be modified to take into account the existence of a wider class of equilibrium states.

An approach for predicting both softening and the region of localization is to assume that the constitutive equation is nonlocal. Preliminary comparisons between theoretical and experimental data associated with the cracking of concrete indicate that the method is feasible and that a generalization to three dimensions might be useful.

ACKNOWLEDGEMENT

REFERENCES

Bazant, Z. P., 1976, "Instability, Ductility, and Size Effect in Strain-Softening Concrete," ASCE Journal of the Engineering Mechanics Division, EM2, pp. 331-334.

Bazant, Z. P., 1984, "Size Effect in Blunt Fracture: Concrete, Rock, Metal," ASCE Journal of Engineering Mechanics, Vol. 110(4), pp. 518-535.

Bazant, Z. P., and Chang, T. P., 1984, "Instability of Nonlocal Continuum and Strain Averaging," ASCE Journal of Engineering Mechanics, Vol. 110(10), pp. 1441-1450.

Crisfield, M. A., 1982, "Local Instabilities in the Nonlinear Analysis of Reinforced Concrete Beams and Slabs," Proceedings of the Institution for Civil Engineers, Vol. 73(12), pp. 135-145.

Krajcinovic, D., 1983, "Constitutive Equations for Damaging Materials," ASME Journal of Applied Mechanics, Vol. 50, pp. 355-360.

Pietruszczak, St., and Mroz, Z., 1981, "Finite Element Analysis of Deformation of Strain-Softening Materials," International Journal of Numerical Methods in Engineering, Vol. 17, pp. 327-334.

Prevost, J. H., 1984, "Localization of Deformation in Elastic-Plastic Solids," International Journal for Numerical and Analytical Methods in Geomechanics, Vol. 8, pp. 187-196.

Rudnicki, J. W., and Rice, J. R., 1975, "Conditions for the Localization of Deformation in Pressure-Sensitive Dilatant Materials," Journal of the Mechanics and Physics of Solids, Vol. 23, pp. 371-394.

Shah, S. P., and Gopalaratnam, V. S., 1984, Softening Response of Plain Concrete in Direct Tension, The Technological Institute, Northwestern University, Evanston, Illinois 60201.

Vermeer, P. A., 1982, "A Simple Shear-Band Analysis Using Compliances," _International Union of Theoretical and Applied Mechanics, Proceedings of the Symposium on Deformation and Failure of Granular Materials_, Delft, The Netherlands, 31 August-3 September, edited by P. A. Vermeer and H. J. Luger, published by A. A. Balkema, Rotterdam.

Willam, K. J., 1984, _Experimental and Computational Aspects of Concrete Fracture_, Invited Paper, International Conference on Computer-Aided Analysis and Design of Concrete Structures, Split, Yugoslavia, September 17-21.

DARPA
ATTN: TECH LIB
1400 WILSON BLVD
ARLINGTON, VA 22209

DIR, FEMA
DIRECTOR FOR RESEARCH
1725 I ST NW
WASHINGTON DC 20472

DEFENSE TECHNICAL INFORMATION CENTER
ATTN: DDA
CAMERON STATION
ALEXANDRIA, VA 22314

DIR, DEFENSE INTELLIGENCE AGENCY
ATTN: DB-4C
WASHINGTON, DC 20301

DEFENSE NUCLEAR AGENCY
ATTN: SPSS
WASHINGTON, DC 20305

COMMANDER, FIELD COMMAND DNA
ATTN: FCTK
KIRTLAND AFB, NM 87115

DIRECTOR, CONSTRUCTION ENGINEERING
  RESEARCH LABORATORY
ATTN: CERL-SL
P.O. BOX 4005
CHAMPAIGN, IL 61820

CHIEF OF ENGINEERS, DOA
ATTN: DAEN-MCE-D
PULASKI BLDG
WASHINGTON DC 20314

DIRECTOR, US ARMY ENGR WATERWAYS
  EXPERIMENT STATION
ATTN: DR SAM KISER
P.O. BOX 631
VICKSBURG, MS 39180

DIRECTOR, US ARMY ENGR WATERWAYS
  EXPERIMENT STATION
ATTN: MR C.D. NORMAN
P.O. BOX 631
VICKSBURG, MS 39180

OFFICER-IN-CHARGE
  CIVIL ENGINEERING LABORATORY
ATTN: MR BOB MURTHA
NAVAL CONSTRUCTION BATALLION CENTER
PORT HUENEME, CA 93043

COMMANDER, U.S. NAVAL OCEAN SYSTEMS
  CENTER
CODE 9431, R.H. CHALMERS
SAN DIEGO, CA 92152

DAVID TAYLOR NAVAL SHIPS R&D CENTER
UNDERWATER EXPLOSIVE RESEARCH DIVISION
ATTN: RAY WALKER
PORTSMITH, VA 23709

NAVAL SEA SYSTEMS COMMAND
- CODE 55X1
WASHINGTON, DC 20362

COMMANDER, NAVAL WEAPONS CENTER
ATTN: CODE 3665, W.N. JONES
CHINA LAKE, CA 93555

AF OFFICE OF SCIENTIFIC RESEARCH
ATTN: LT COL HOKANSON
BOLLING AFB
WASHINGTON DC 20332

AIR FORCE WEAPONS LABORATORY, AFSC
ATTN: SUL
KIRTLAND AFB, NM 87117-6008

AIR FORCE WEAPONS LABORATORY, AFSC
ATTN: HO
KIRTLAND AFB, NM 87117-6008

AIR FORCE WEAPONS LABORATORY, AFSC
ATTN: NTED
KIRTLAND AFB, NM 87117-6008

AIR FORCE WEAPONS LABORATORY, AFSC
ATTN: NTESR
KIRTLAND AFB, NM 87117-6008

AIR FORCE WEAPONS LABORATORY, AFSC
ATTN: NTESG
KIRTLAND AFB, NM 87117-6008

AIR FORCE WEAPONS LABORATORY, AFSC
ATTN: NTESE
KIRTLAND AFB, NM 87117-6008

COMMANDER, FOREIGN TECHNOLOGY DIV,
  AFSC
ATTN: SDBF (MR S. SPRING)
WRIGHT-PATTERSON AFB, OH 45433

.IQ USAF/RD
ATTN: RDPM
WASHINGTON DC 20330

BALLISTIC MISSILE OFFICE
ATTN: ENSN
NORTON AFB, CA 92409

BALLISTIC MISSILE OFFICE
ATTN: PPH
NORTON AFB, CA 92409

LAWRENCE LIVERMORE NATL LABORATORY
ATTN: TECH INFO DEPT L-3
P.O. BOX 808
LIVERMORE, CA 94550

LOS ALAMOS NATL LABORATORY
ATTN: TECH LIB
P.O. BOX 1663
LOS ALAMOS, NM 87545

SANDIA NATIONAL LABORATORIES
ATTN: DR TOM BACA
P.O. BOX 5800
ALBUQUERQUE, NM 87115

DEPARTMENT OF ENERGY
U.S. ENERGY RSCH AND DEV ADMIN
ALBUQUERQUE OPERATIONS OFFICE
ATTN: DOC CON FOR TECH LIB
P.O. BOX 5400
ALBUQUERQUE, NM 87115

DEPARTMENT OF ENERGY
U.S. ENERGY RSCH AND DEV ADMIN
NEVADA OPERATIONS OFFICE
ATTN: DOC CON FOR TECH LIB
P.O. BOX 14100
LAS VEGAS, NV 89114

CENTRAL INTELLIGENCE AGENCY
DSWR/OSD/BMB
ATTN: JOE ZECOSKI
WASHINGTON DC 20505

DEPT OF THE INTERIOR
BUREAU OF MINES
ATTN: TECH LIB
BLDG 20 DENVER FEDERAL CENTER
DENVER, CO 80225

DEPT OF THE INTERIOR
U.S. GEOLOGICAL SURVEY
ATTN: G. BRADY
345 MIDDLETON RD
MENLO PARK, CA 94025

- AEROSPACE CORPORATION
ATTN: L. SELZER
P.O. BOX 92957
LOS ANGELES, CA 90009

AEROSPACE CORPORATION
ATTN: DR J. CRAWFORD
P.O. BOX 92957
LOS ANGELES, CA 90009

BDM CORP
ATTN: MR H.T. WEBSTER
1801 RANDOLPH ROAD SE
ALBUQUERQUE, NM 87106

BOEING COMPANY
ATTN: B. DRYDAHL
P.O. BOX 3999, MAIL STOP 17-04
SEATTLE, WA

CAL RSCH AND TECH
ATTN: Y. MARVIN ITO
6269 VARIEL AVE
WOODLAND HILLS, CA 91367

ELECTRIC POWER RESEARCH INSTITUTE
ATTN: GEORGE SLITER
3412 HILLVIEW AVE
PALO ALTO, CA 94303

ACTA, INC.
PLAZA DE RINA, SUITE 101
24430 HAWTHORNE BLVD
ATTN: DR COLLINS
TORRANCE, CA 90505

KAMAN SCIENCE CORPORATION
ATTN: J.R. BETZ
P.O. BOX 7463
COLORADO SPRINGS, CO 80933

LOCKHEED MISSILES AND SPACE CO
ATTN: P. STERN
P.O. BOX 504
SUNNYVALE, CA 94008

JACK BENJAMIN & ASSOCIATES
444 CASTRO STREET, SUITE 501
ATTN: DR McCANN
MOUNTAIN VIEW, CA 94041

JAMES E. BECK & ASSOCIATES
4216 LOS PALOS AVE
PALO ALTO, CA 94306

CALIFORNIA RESEARCH & TECHNOLOGY, INC
ATTN: DR ERIC J. RINEHART
1900 RANDOLPH RD SE, SUITE B
ALBUQUERQUE, NM 87106

UNIVERSITY OF ILLINOIS
CE BLDG, DR W.J. HALL
208 N. ROMINE ST
URBANA, IL 61801

UNIVERSITY OF WASHINGTON
DEPT OF CIVIL ENGINEERING
ATTN: PROFESSOR NEIL HAWKINS
SEATTLE, WA 98195

R&D ASSOCIATES
ATTN: JOHN LEWIS
P.O. BOX 9695
MARINE DEL REY, CA 90291

RAND CORPORATION
ATTN: TECH LIBRARY
1700 MAIN ST
SANTA MONICA, CA 90406

STANFORD UNIVERSITY
JOHN BLUME EARTHQUAKE ENGINEERING CTR
ATTN: H. KRAWINKLER
STANDFORD, CA 94305

NORTHWESTERN UNIVERSITY
DEPT OF CIVIL ENGINEERING
ATTN: PROF BELYTSCKO
EVANSTON, IL 60205

WASHINGTON STATE UNIVERSITY
DEPT OF CIVIL ENGINEERING
ATTN: PROF SORENSEN
PULLMAN, WA 99164

UNIVERSITY OF COLORADO
DEPT OF CIVIL ENGINEERING
ATTN: K. GERSTLE
BOULDER, CO 80302

UNIVERSITY OF NEW MEXICO
DEPT OF MECHANICAL ENGRG
ATTN: PROF SCHREYER
ALBUQUERQUE, NM 87131

UNIVERSITY OF MINNESOTA
DEPT OF CIVIL/MINERAL ENGRG
ATTN: PROF KRAUTHAMMER
MINNEAPOLIS, MN 55455

UNIVERSITY OF FLORIDA
GRADUATE ENGINEERING CENTER
DR C.A. ROSS
P.O. BOX 1918
EGLIN AFB, FLORIDA 32542-0918

SCIENCE APPLICATIONS, INC
ATTN: HOWARD PRATT
P.O. BOX 2351
LA JOLLA, CA 92038

SCIENCE APPLICATIONS, INC.
ATTN: G. BINNINGER
2111 EISENHOWER AVE, SUITE 205
ALEXANDRIA, VA 22314

SOUTHWEST RESEARCH INSTITUTE
ATTN: BRUCE MORRIS
P.O. RAWER 28510
SAN ANTONIO, TX 78284

SRI INTERNATIONAL
ATTN: DR COTTON
333 RAVENSWOOD AVE
MENLO PARK, CA 94025

S-CUBED
ATTN: G. HEGEMIER
P.O. BOX 1620
LA JOLLA, CA 92038

TRW SYSTEM GROUP
ATTN: W. LIPNER
ONE SPACE PARK
BLDG 134/9851
REDONDO BEACH, CA 90278

TRW SYSTEMS GROUP
SAN BERNARDINO OPERATIONS
ATTN: PETER K. DAJ 527/712
P.O. BOX 1310
SAN BERNARDINO, CA 92402

UNIVERSITY OF NEW MEXICO/NMERI
BOX 25, UNIVERSITY STATION
ALBUQUERQUE, NM 87131

WEIDLINGER ASSOC
ATTN: MELVIN L. BARON
333 SEVENTH AVE
NEW YORK, NY 10001

WEIDLINGER ASSOCIATES
ATTN: H. LEVINE
620 HANSEN WAY, SUITE 100
PALO ALTO, CA 94304

WEIDLINGER ASSOCIATES
620 HANSEN WAY, SUITE 100
ATTN: F.S. WONG
PALO ALTO, CA 94304-1069

APPLIED RESEARCH ASSOC INC
ATTN: DOUG MERKLE
2101 SAN PEDRO NE
SUITE A
ALBUQUERQUE, NM 87110

AIR FORCE ARMAMENT DEVELOPMENT AND
  TEST CENTER
ATTN: TECHNICAL LIBRARY
EGLIN AFB, FL 32542

AIR FORCE ENGINEERING AND SERVICES
  CENTER
ATTN: RD
TYNDALL AFB, FL 32403

AUL (LDE)
MAXWELL AFB, AL 36112

HQ, AIR FORCE SYSTEMS COMMAND
ATTN: DLWM
ANDREWS AFB
WASHINGTON, DC 20334

AFWL/NTES/DR ROSS
OFFICIAL RECORD COPY